A FUNDAMENTAL STUDY OF BIO-ETHANOL COMBUSTION UNDER SI AND CI ENGINE CONDITIONS

MR. RONNACHART MUNSIN

A THESIS SUBMITTED IN PARTIAL FULFILLMENT
OF THE REQUIREMENTS FOR
THE DEGREE OF DOCTOR OF ENGINEERING (MECHANICAL ENGINEERING)
FACULTY OF ENGINEERING
KING MONGKUT'S UNIVERSITY OF TECHNOLOGY THONBURI
2014

A Fundamental Study of Bio-Ethanol Combustion under SI and CI Engine Conditions

Mr. Ronnachart Munsin M.Eng. (Mechanical Engineering)

A Thesis Submitted in Partial Fulfillment of the Requirements for
the Degree of Doctor of Engineering (Mechanical Engineering)
Faculty of Engineering
King Mongkut's University of Technology Thonburi
2014

Thesis Committee

…… Chairman of Thesis Committee
(Assoc. Prof. Somchai Chanchaona, Ph.D.)

…… Member and Thesis advisor
(Prof. Sumrerng Jugjai, D.Eng.)

…… Member and Thesis Co-advisor
(Asst. Prof. Yossapong Laoonual, Ph.D.)

…… Member
(Lect. Worawarong Rakreungdet, Ph.D.)

…… Member
(Prof. Hidenori Kosaka, D.Eng.)

หัวข้อวิทยานิพนธ์	การศึกษาขั้นพื้นฐานของการเผาไหม้ของไบโอเอทานอลภายใต้สภาวะเครื่องยนต์จุดระเบิดด้วยประกายไฟและจุดระเบิดแบบอัด
หน่วยกิต	36
ผู้เขียน	นายรณชาติ มั่นศิลป์
อาจารย์ที่ปรึกษา	ศ. ดร.สำเริง จักรใจ
	ผศ. ดร.ยศพงษ์ ลออนวล
หลักสูตร	วิศวกรรมศาสตรดุษฎีบัณฑิต
สาขาวิชา	วิศวกรรมเครื่องกล
ภาควิชา	วิศวกรรมเครื่องกล
คณะ	วิศวกรรมศาสตร์
ปีการศึกษา	2557

บทคัดย่อ

วิทยานิพนธ์นี้ศึกษาการเผาไหม้ของไบโอเอทานอลภายใต้สภาวะเครื่องยนต์ทั้งสองประเภทได้แก่ เครื่องยนต์จุดระเบิดด้วยประกายไฟและเครื่องยนต์จุดระเบิดแบบอัด สำหรับเครื่องยนต์จุดระเบิดด้วยประกายไฟ ไบโอเอทานอลที่มีน้ำผสมอยู่ 20% ถึง 40%โดยปริมาตร ถูกใช้เป็นเชื้อเพลิง ผลการศึกษาพบว่า ไบโอเอทานอลที่มีน้ำผสมอยู่ถึง 40% สามารถใช้ในเครื่องยนต์จุดระเบิดด้วยประกายไฟได้ การเพิ่มสัดส่วนของน้ำทำให้ประสิทธิภาพโดยรวม และ ออกไซด์ของไนโตรเจนลดลง ในขณะที่อัตราการสิ้นเปลืองเชื้อเพลิงจำเพาะ ไฮโดรคาร์บอน คาร์บอนไดออกไซด์ ฟอร์มัลดีไฮด์ และอะเซตัลดีไฮด์เพิ่มขึ้น และควรมีเครื่องฟอกไอเสียเชิงเร่งปฏิกิริยาเพื่อควบคุมค่ามลพิษ

สำหรับการเผาไหม้ภายใต้สภาวะเครื่องยนต์จุดระเบิดแบบอัด ไบโอเอทานอลที่ผสมสารช่วยจุดระเบิดถูกใช้เป็นเชื้อเพลิง สารช่วยจุดระเบิดที่ใช้คือ สารเติมแต่งเชิงพาณิชย์ กลีเซอรอลเอโทซิเลท 1% 3% 5% โดยน้ำหนัก ไบโอดีเซลและไดเอทิลอีเทอร์ 5% โดยน้ำหนัก ห้องเผาไหม้จำลองถูกออกแบบและสร้างขึ้นเพื่อใช้ศึกษาการเผาไหม้ในสภาวะเครื่องยนต์จุดระเบิดแบบอัด ภาพถ่ายของเปลวไฟถูกทำการศึกษาในเครื่องอัดและขยายตัวอย่างรวดเร็ว ผลการศึกษาพบว่า สารช่วยจุดระเบิดทำให้คุณลักษณะการฉีดเปลี่ยนไป ควรมีการปรับระยะเวลาในการฉีดเชื้อเพลิงเพื่อให้ค่าพลังงานเข้าไปคงที่ เวลาล่าช้าในการจุดระเบิด อัตราการเพิ่มขึ้นของความดันและอัตราการปลดปล่อยความร้อนของเอทานอลถูกปรับปรุงให้ดีขึ้นโดยกลีเซอรอลเอโทซิเลท 5% เช่นเดียวกับสารเติมแต่งเชิงพาณิชย์ ในขณะที่สารช่วยจุดระเบิดอื่นมีผลต่อการปรับปรุงน้อย โดยกลีเซอรอลเอโทซิเลท 5% และสารเติมแต่งเชิงพาณิชย์ มีผลกระทบต่อการเปลี่ยนแปลงอุณหภูมิเปลวไฟ KL factor และเขม่าเพียงเล็กน้อย

คำสำคัญ : เครื่องยนต์จุดระเบิดด้วยประกายไฟ / เครื่องยนต์จุดระเบิดแบบอัด / ไบโอเอทานอล / สารช่วยจุดระเบิด

Thesis Title	A Fundamental Study of Bio-Ethanol Combustion under SI and CI Engine Conditions
Thesis Credits	36
Candidate	Mr. Ronnachart Munsin
Thesis Advisors	Prof. Dr. Sumrerng Jugjai
	Asst. Prof. Dr. Yossapong Laoonual
Program	Doctor of Engineering
Field of Study	Mechanical Engineering
Department	Mechanical Engineering
Faculty	Engineering
Academic Year	2014

Abstract

This study investigates bio-ethanol combustion under the conditions of two engines, i.e. SI and CI engines. For the SI engine, bio-ethanol with water content of 20% to 40%v is used as fuel. The results show that bio-ethanol with water content up to 40% can be used as fuel in the SI engine. Increasing the water content in bio-ethanol decreased the overall efficiency and NO_x, while BSFC, HC, CO, formaldehyde and acetaldehyde increased. A catalytic converter is required to meet the emission regulation.

For the combustion under CI engine conditions, bio-ethanol with ignition improvers is used as fuel. Ignition improvers used are commercial additive; 1%w, 3%w and 5%w glycerol ethoxylate; 5%w biodiesel; and 5%w diethyl ether. An in-house constant volume combustion chamber (CVCC) is designed and built to use for the combustion study under CI engine conditions. A rapid compression and expansion machine (RCEM) also use to study flame visualization. The results show that the ignition improvers change injection characteristics of bio-ethanol. Adjusting injection duration is required to maintain the constant energy input. Ignition delay, rate of pressure rise and heat release of bio-ethanol are significantly improved by 5%w glycerol ethoxylate as same as the commercial additive, while the other improvers are slightly effective. The effect of 5% glycerol ethoxylate and the commercial additive on the change in flame temperature, KL factor and the measured soot emission are minor.

Keywords: Bio-ethanol/ CI Engine/ Ignition Improvers/ SI Engine

ACKNOWLEDGEMENTS

I would like to express my special appreciation and thanks to my supervisors, Prof. Dr. Sumrerng Jugjai and Asst. Prof. Dr. Yossapong Laoonual who have given me the opportunity to pursue this research. They always inspire and give the invaluable advices and supports. I would like to sincerely thank to Prof. Hidenori Kosaka who has given a chance to perform the experiment in his laboratory. I have learned many things under his kind guidance during I spent my special time in Tokyo Institute of Technology. The sincere gratitude is expressed to Assoc. Prof. Dr. Somchai Chanchaona who is one of my idols. Thanks for his encouragement, suggestion, time and providing SAE journals. Dr. Worawarong Rakreungdet is acknowledged for his pieces of sugestion and time.

My financial support from the Office of Higher Education Commission and the Thailand Research Fund through the Royal Golden Jubilee Ph.D. Program (Grant No. PHD/0083/2551) is gratefully acknowledged.

Dr. Nuwong Chollacoop who is a researcher at MTEC and his staff are acknowlegded for fuel property test.

I would like to thank Mr. Rubchai Jensraku, Mr. Nawee Nuntapap, Mr. Kitthi Iampremjit, Mr. Ob Nilaphai, Mr. Pithayodom Kanboa, Mr. Puwadol Kaewkamjan, Mr. Veerapol Sae-Wang, Mr. Sitthiborn Chiawtada, Mr. Reywat Aramsiriwat, Mr. Rachen Chumuang, Mr. Athimate Charatsuksawat, Dr. Wasan Yoksenakul, Dr. Apinun Namket, Dr. Piyatida Trinuluk, Dr. Peerawat and Dr. Penyarat Saisirirat, Dr. Usa Makmoon, other CERL members, a technical staff of the department of mechanical engineering, Mr. Prathan Srichai and Asst. Prof. Dr. Chanawat Nitatwichit for their helps and friendship. My special thanks are expressed to one of my best friends, Mr. Masataka Matsuki, for his hospitalities and supports during I was in Tokyo.

Finally, I would like to thank my family for their understanding and supports, especially Mr. Apichard, Mrs. Pongpayom, Mr.Anucha, Mrs. Duangkamon, Ms. Kamala, Ms. Nutcha and Mrs. Nuthicha Munsin; Ms. Siriporn Angkananupong and Ms. Hui-Ju Sae Chua.

CONTENTS

PAGE

PAGE

PAGE

LIST OF TABLES

LIST OF FIGURES

FIGURE **PAGE**

FIGURE **PAGE**

FIGURE **PAGE**

FIGURE **PAGE**

NOMENCLATURE

T_1	=	Initial gas temperature at BDC (K)
T_2	=	Compressed gas temperature at TDC (K)
P_1	=	Initial gas pressure at BDC (Pa)
P_2	=	Compressed gas pressure at TDC (Pa)
n	=	Polytropic index (1.35 for real air, Heywood, 1988)
V_1	=	Volume at BDC (m^3)
V_2	=	Volume at TDC (m^3)
CR	=	Compression ratio
X	=	Spray penetration (m)
R	=	Spray width (m)
C	=	Flow coefficient
ρ_a	=	Air density (kg/m^3)
ρ_f	=	Fuel density (kg/m^3)
ΔP_{inj}	=	Different pressure between injection and chamber pressure (N/m^2)
t	=	Time after injection (s)
d_N	=	Nozzle diameter (m)
θ	=	Spray angle (degree)
σ	=	Hoop stress (MPa)
P_{cy}	=	Pressure exerted on the wall (MPa)
a	=	Inner cylinder radius (m)
b	=	Outer cylinder radius (m)
τ	=	Shearing stress (MPa)
σ_b	=	Bending stress (MPa)
a	=	Inner radius of quartz (m)
P_{cy}	=	Pressure exerted on the surface of quartz (MPa)
A	=	Surface area (m^2)
L	=	Quartz thickness (m)
σ_B	=	Bearing stress (MPa)
b	=	Outer radius of quartz (m)
T_{bulk}	=	Bulk gas temperature of combustion products (K)
T_{int}	=	Initial temperature of the unburned premixed charge (K)

P_{bulk}	=	Bulk gas pressure of combustible gas (N/m^2)
P_{int}	=	Initial pressure of the unburned premixed charge (N/m^2)
M	=	Ratio of molecular weights of the combustion products and the premixed charge
$\frac{dm}{dt}$	=	Mass flow rate (kg/s)
ρ_f	=	Fuel density (kg/m^3)
V	=	Chamber volume (m^3)
K	=	Modulus of compressibility (Pa)
$\frac{dP}{dt}$	=	Rate of pressure changed in chamber (Pa)
$\dot{m}_f$	=	Measured mass flow rate (kg/s)
$\dot{m}_{th}$	=	Theoretical mass flow rate (kg/s)
τ	=	Ignition delay (ms)
T	=	Ambient gas temperature (K)
[ ]	=	Substance concentration (mol/cc)
$\frac{dQ}{dt}$	=	Heat release rate (J/s)
V	=	In-cylinder volume (m^3)
P	=	In-cylinder pressure (Pa)
γ	=	Specific heat ratio
t	=	Time (s)
ε	=	Emissivity
λ	=	Wavelength (nm)
K	=	Absorption coefficient
L	=	Path length
A	=	An empirical constant equal to 1.39 in the visible spectrum
T	=	True temperature of the flame (K)
T_a	=	Apparent temperature of the flame (K)
$I_{(\lambda,T)}$	=	Monochromatic radiant intensity
C_1,C_2	=	First and second Planck constant

CHAPTER 1
INTRODUCTION

1.1 Rationale

Nowadays, the global society is facing two crises, i.e. energy and environment crises. It is impossible to expand the global oil production, because the resources are limited. The international energy agency (IEA) (2013) showed that the world oil supply decreases, while oil consumption increases annually as shown in Figure 1.1. With growing rate of oil demand, the imbalance leads to oil scarce resulting in high cost and insecurity. In addition, growing fossil oil demand plays an important role in CO_2 emissions which directly contribute to climate change. Anthropogenic climate change (climate change due to originating in human activity) is primarily caused by the combustion of fossil fuels. Annual CO_2 emissions from fuel combustion dramatically increased from 1971 about of 100% in 2011 (IEA, 2013) shown in Figure 1.2. This is a critically worldwide challenge. The countries must take urgent action to drastically reduce CO_2 emissions in order to reduce the dramatic change of climate.

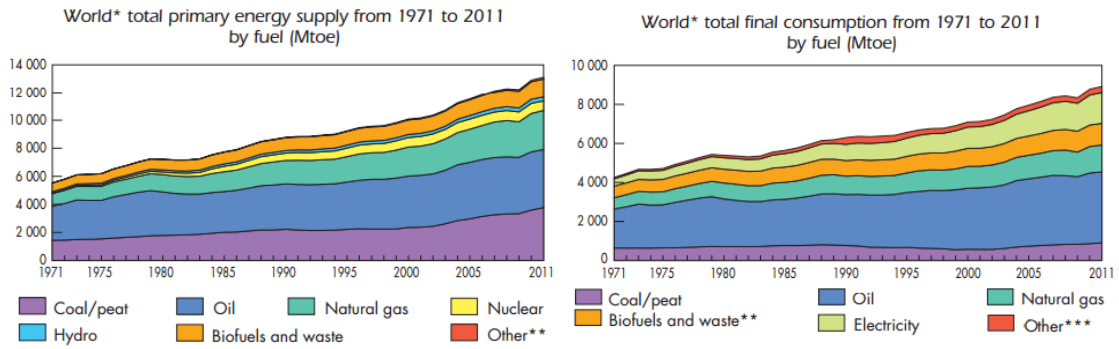

(a) Total energy supply (b) Total energy demand

Figure 1.1 World total energy supply and demand by fuel (IEA, 2013).

The BLUE Map/shifts scenario, including modal shift (using public transportation), vehicle efficiency improvement and alternative fuels, play significant roles in cutting greenhouse gas emissions as shown in Figure 1.3 (IEA, 2010). The BLUE Map/shifts scenariocan reduce CO_2 emissions in 2050 approximately 3 Gt of CO_2 equivalent

compared to the Baseline scenario (old scenario that follows the reference scenario to 2030 outlined in the World Energy Outlook 2009, and then extends it to 2050. It assumes governments introduce no new energy and climate policies) and nearly 6 Gt of CO_2 equivalent compared to the High Baseline scenario (It assumes a higher growth in passenger light-duty vehicle ownership in the developing world and faster growth in vehicle travel and freight transport, especially trucking).

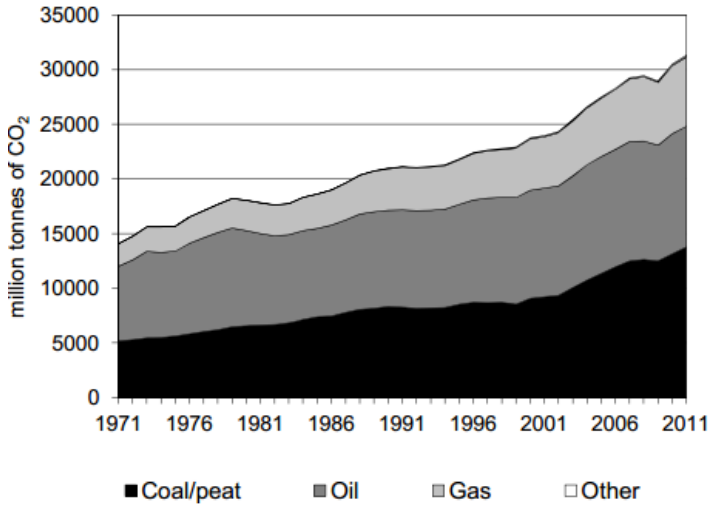

Figure 1.2 World CO_2 emissions by fuel (IEA, 2013).

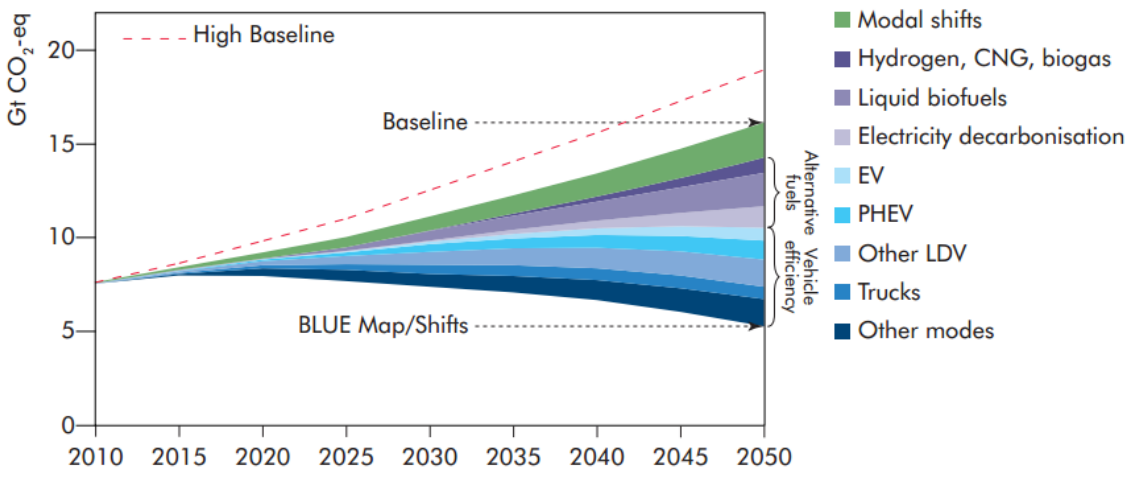

Figure 1.3 Sources of greenhouse-gas emissions reduction, transport sector (IEA, 2010).

In Thailand, the energy consumption in transport sector is also facing serious challenges by the oil and environment crises. Current energy consumption of Thailand shows that diesel consumption is twice as much of gasoline as shown in Figure 1.4. It is clear that energy consumption in Thai transport sector is dominated by the use of diesel and gasoline. Thai government realized that the alternative energy is required to meet energy demand in transport sector and substantially reducing associated greenhouse gas emissions. Corresponding to IEA analyses, biofuels may have to play an important role to make significant reductions in CO_2 emissions, and reduce dependence on crude oil at costs similar to those of gasoline and diesel in the medium-term. (IEA, 2014). Biofuels are included in the alternative energy development plan (AEDP: 2012-2021) by the Ministry of Energy of Thailand as shown in Figure 1.5. The objective of this plan is to promote the use of new and renewable energy at 25% of total energy consumption leading to energy security and low-carbon society by 2021.

The biofuel targets used for transportation sector were set for bioethanol, biodiesel and alternative diesel-replacement fuel consumptions of 9, 7.2 and 3 million liters/day (ML/day), respectively. Corresponding to the BEST project, bioethanol is well suited as an important part of the future fuel mix that can be used as petroleum oil substitute for both SI and CI engine in different ways, represented in Figure 1.6 (Fenton and Carlsson, 2009).

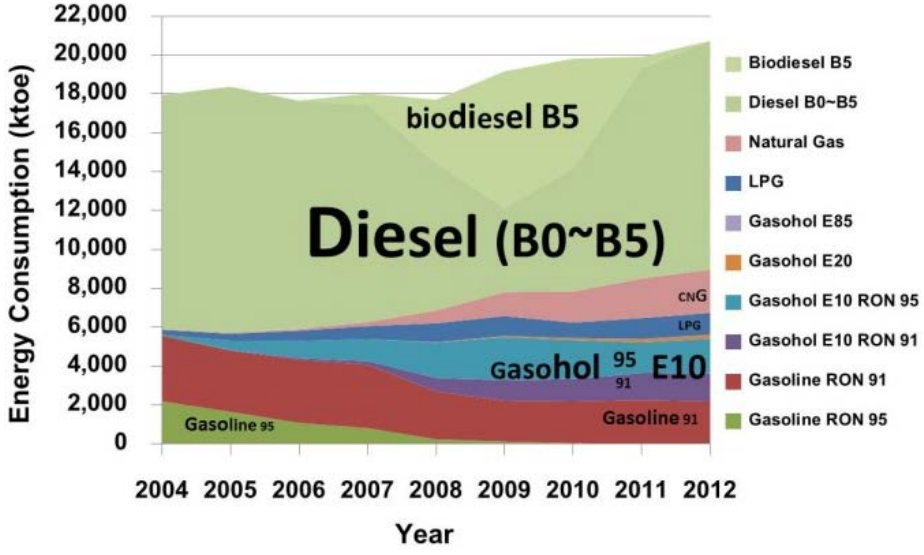

Figure 1.4 Energy consumption in Thai transportation sector.

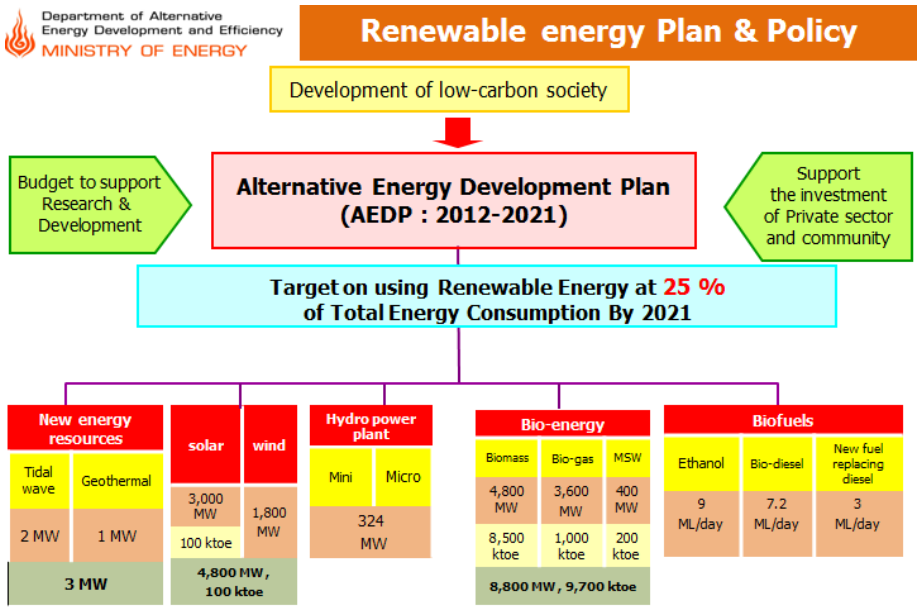

Figure 1.5 Alternative energy development plan 2012-2021 adapted from Ministry of Energy (DEDE, 2012; Vongsoasup, 2014).

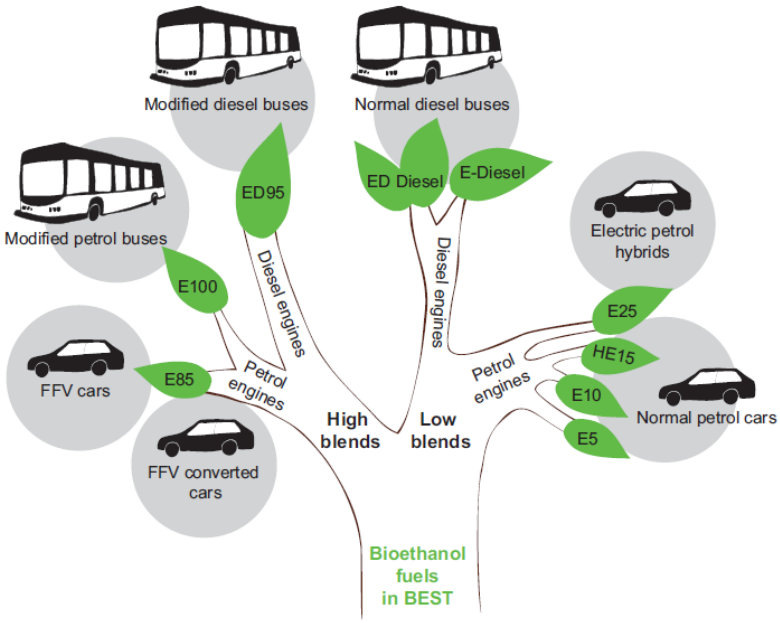

Figure 1.6 The “bioethanol tree” illustrates the fuels that were tested in the BEST project. (Fenton and Carlsson, 2009).

Various blends of ethanol in gasoline, i.e. gasohol, (10%, 20% and 85%) are used for SI engines. in order to achieve the target for ethanol consumption in AEDP 2012-2021, while ED95, which stands for 95% hydrous ethanol and 5% ignition improver additive, is used as one of the alternative diesel-replacement fuel for CI engines beside

the others such as jatropha oil, algae, fatty acid ethyl ester (FAEE), diesohol, bio-hydrogenated diesel (BHD) and biomass-to-liquid (BTL) (Chollacoop, et al., 2013) for achieving the target for 3 ML/d the alternative diesel-replacement fuel consumption by 2021. To promote the use of ED95, the demonstration project of Thailand's first ethanol bus was launched in 2010-2011 for public transportation (Laoonual, 2013; Nilaphai, et al., 2012; Chollacoop, et al., 2013). The ethanol bus showed insignificant difference of performance and fuel economy compared with ethanol bus used in other countries as well as lower emissions than diesel (Laoonual, 2013).

However, the use of bioethanol is critically limited from cost competitiveness. For SI engines, the standard specification for fuel ethanol (ASTM D 5798-99) allows a maximum water content of 1% by weight in ethanol (National Renewable Energy Laboratory and the National Ethanol Vehicle Coalition, 2006), which requires additional cost and energy for the removal of water from hydrous ethanol. Most of the energy consumption for distillation of ethanol occurs in distilling above 85 percent ethanol. Above 90 percent ethanol, the energy gain drops drastically, and the distillation energy input approaches the ethanol energy output if the azeotrope in which the composition of mixture cannot be changed by simple distillation is approached (Ladisch and Dyck, 1979). The high cost of production is a drawback for ethanol from an economic point of view to be competitive. Cost saving can be achieved through the use of hydrous ethanol with water content. Therefore, the direct use of hydrous ethanol with some water in engines is considered an option to improve the cost of ethanol production.

For CI engines, ED95 is also limited from cost competitiveness compared to the conventional diesel. So far, the Swedish company SEKAB is the only one to produce additive for the ethanol used in CI engine (Moreira, et al., 2013). Chollacoop, et al. (2013) suggested that the compatible ignition improvers, which can domestically produce in Thailand, with similar ignition characteristics as the original one from Sweden should be investigated. In addition, little is known about ignition characteristics use in ethanol CI engine.With the environmental, technical and economic perspectives, there are still gaps of the use of bioethanol in both SI and CI engines.

1.2 Objectives and Thesis Outline

To cover the main issue of bioethanol used in the SI and CI engines. The objectives for this research study are the following:

- The first objective is to investigate the use of bioethanol with high water content up to 40% by volume in a small SI engine equipped with a generator set.
- The second objective is to design and develop a constant volume combustion chamber (CVCC) for simulating CI engine-like conditions.
- The last is to study bioethanol combustion under CI engine-like conditions.

With these objectives, a deeper understanding of bioethanol combustion in SI and CI engines can be obtained. It could be used to facilitate control of the engine combustion and achieve higher engine performance and a wide range of engine operation.

There are five chapters in this report. In this chapter, the general background and motivation are clarified. This introduction has presented the background of this research. The thesis is structured on the following way:

Chapter 2 presents the effects of water content up to 40% by volume in ethanol on engine performance and emissions of a small SI engine in order to explore the feasibility of using hydrous ethanol with high water content as fuel for SI engine.

Chapter 3 describes the systematic design for constant volume combustion chamber (CVCC) with pre-combustion technique that use to simulate CI engine-like conditions for fundamental study of spray and combustion. The CVCC can be operated under different parameters, e.g. injection pressure, in-chamber pressure and temperature, fuel type to identify their influence on combustion characteristics.

Once the CVCC was built, the combustion of hydrous ethanol with ignition improvers was carried out under CI engine-like conditions to extend the possibility of using hydrous ethanol as fuel for CI engine in Chapter 4. In addition, the rapid compression and expansion machine (RCEM) is used to study the combustion characteristics and flame visualization of hydrous ethanol. Some results are then compared with the results in CVCC under the similar conditions.

Chapter 5 summarizes all the work, and suggestions are included to continue the similar research works in the future.

CHAPTER 2

PERFORMANCE AND EMISSIONS OF A SMALL SI ENGINE GENERATOR SET FUELLED BY HYDROUS ETHANOL WITH HIGH WATER CONTENTS UP TO 40%

2.1 Introduction

Today, the electricity power generation system is mostly based on the centralized power station model whereby the power sources are typically generated from the combustion of conventional fuels, e.g. coal, petroleum oil, and natural gas; as well as from nuclear energy. The installation of a centralized system has become difficult, however, because of safety and environmental concerns; while the use of renewable energy for power generation has become compelling due to concerns about global warming.

The distributed generation system is a small to medium size power generation unit (200W to 20 MW, depending on the generation technology (Pepermans, et al., 2005)) that can be connected directly to the distribution network or on the customer side, increasing the security of the electricity supply and standby capacity for peak demand. It can also be used as a stand-alone power generator for remote and rural areas or emergency cases.

The spark ignition (SI) engine generator is widely used for distributed generation. The development of the SI engine during the last decade to achieve both engine efficiency and stringent emissions limits, especially greenhouse gas emissions, has advanced in two ways. One is on the engine side, with improvements such as combustion control and direct injection spark ignition engine (Li, et al., 2010; Turner, et al., 2011). The other is on the fuel side by using ethanol, with its many advantages, e.g. the potential to reduce greenhouse gas emissions and increasing of energy security by diversifying energy supply sources. The use of anhydrous or hydrous ethanol in the SI engine used in distributed generation is a potential sustainable solution for the countries where ethanol can be produced locally, e.g. Brazil, China, India and Thailand (OECD-FAO, 2011).

During the past few decades, ethanol has played an important role as an octane booster for gasoline, replacing MTBE (da Silva, 2005; Magnusson and Nielsson, 2011). There have been many studies of pure ethanol and blending ethanol with gasoline in a dedicated SI engine, as reviewed in Niven (2005) and Jeuland, et al. (2004). They concluded that ethanol has a higher octane number and higher latent heat than gasoline, so that the thermal efficiency of engines can be increased by using a higher compression ratio. Ethanol also has a higher flame speed and lower combustion temperature that reduce the heat loss to cylinder walls, thus enhancing thermal efficiency (Costa and Sodre, 2009). Maximum engine power and maximum torque output are increased by 5.4% and 1.9% respectively (Li, et al. 2003). In comparison with typical gasoline, the use of gasoline-ethanol blends or gasohol and ethanol can substantially reduce CO and HC emissions by 30% to 60% and up to 40%, respectively (Costa and Sodre, 2009; Li, et al. 2003; Chen, 2009; Agarwal, 2006). Previous study of NOx emission of gasohol, however, was found to be lower by 30% (Chen, 2009) and also higher by 50 % (Agarwal, 2006). Carbonyls are also generated from ethanol combustion, i.e. formaldehyde and acetaldehyde, which are mainly produced from partial oxidation (Magnusson and Nielsson, 2011; Magnusson, et al. 2002). Formaldehyde and acetaldehyde levels depend on engine load, ethanol content (Agarwal, 2006) and oxygen concentration (Poulopoulos, 2001). Aldehyde formation is most severe at low temperatures. Any aldehydes and ketones appearing in exhaust gases are formed in the engine and exhaust system (Wagner and Wyszyhki, 1996). Formaldehyde and acetaldehyde have been classified by the EPA as group B1 and B2, which are probable medium and low human carcinogenic hazards, respectively (U.S. Environmental Protection Agency, 2007). The use of ethanol-gasoline blends has been observed to increase acetaldehyde emissions markedly by 100% to 200% (Niven, 2005; He, et al., 2002) and in some cases by up to 700% (Niven, 2005). Formaldehyde emissions have also been found to increase by 15% to 50% (Magnusson, et al., 2003). In addition, formaldehyde and acetaldehyde contribute to the formation of nitric acid, peroxyacetyl nitrate (PAN), other smog components, and ground-level ozone by photochemical reactions with ultraviolet from the sun. However, formaldehyde and acetaldehyde can be reduced by 71% and 75%, respectively (Haupt, et al., 2004), using a catalytic converter. Some of the reactions in a catalytic converter are summarized as follows (Kašpar, et al., 2003).

Oxidation	$2CO + O_2 \rightarrow 2CO_2$
	$HC + O_2 \rightarrow CO_2 + H_2O$
Reduction/three-way	$2CO + 2NO \rightarrow 2CO_2 + N_2$
	$HC + NO \rightarrow CO_2 + H_2O + N_2$
	$2H_2 + 2NO \rightarrow 2H_2O + N_2$
Water gas shift (WGS)	$CO + H_2O \rightarrow CO_2 + H_2$
Steam reforming	$HC + H_2O \rightarrow CO_2 + H_2$

The literature cited over 60 reactions among 31 species (Chatterjee, et al., 2001; Koop and Deutschmann, 2009).

The standard specification for fuel ethanol for automotive spark-ignition engines (ASTM D 5798-99) allows a maximum water content of 1% by weight in ethanol (National renewable energy laboratory, 2006), which requires additional cost and energy for the removal of water from hydrous ethanol. Most of the energy consumption for the distillation of ethanol occurs in distilling above 85 percent ethanol. Above 90 percent ethanol, the energy gain drops drastically, and the distillation energy input approaches the ethanol energy output if the azeotrope (in which the composition of the mixture cannot be changed by simple distillation) is approached (Ladisch and Dyck, 1979). This report agrees with Shapouri, et al. (1995; 2003), who studied details of the energy balance of ethanol. They reported that the energy for water removal is 37% of total output energy (ethanol and co-productions, i.e. corn gluten and oil). The energy for water removal includes energy of distillation (23%) and dehydration (14%). Martinez-Frias, et al. (2007) also report that for the direct utilization of ethanol with a 35% by volume water content, the cost of water separation is only 3% of the output energy (ethanol and co-products), while producing pure ethanol uses 37% of the output energy. Furthermore, the net energy gain improves from 21% to 55% of the output energy. Details of the combustion mechanism of pure ethanol were shown in Marinov (1999), in which the mechanism of hydrous ethanol is expected to be similar.

The high cost of anhydrous ethanol production is a drawback from an economic point of view. Energy savings can be achieved through the use of hydrous ethanol with high water content that can be produced in the community with the simple distillation method. Therefore, the direct use of hydrous ethanol in engines is considered an option

to improve the energy balance of ethanol production. Many research programs (Clemente, et al., 2001; Olberding, et al., 2009) are currently being undertaken on this subject, aiming at reducing the use of petroleum fuel, improving engine efficiency, and optimizing fuel composition for the transport sector.

Clemente, et al. (2001) reported on the development of an engine running on hydrous ethanol (93% by volume ethanol). They concluded that the peak torque and peak power of an SI engine are improved by 9% and 14% respectively, with the engine operating on hydrous ethanol, compared with gasohol, i.e. 78% by volume gasoline blended with 22% by volume anhydrous ethanol; but the specific fuel consumption is increased by 35%. For the comparison of emissions, CO from ethanol combustion is lower than that of gasohol by 41%, while NO_x, HC and aldehyde from ethanol are higher than those of gasohol by 14%, 56% and 58%, respectively. However, all emissions are below the permitted level.

Olberding, et al. (2009) studied the engine performance and emissions of a transit van, which used a catalytic igniter that requires less activation energy than spark plugs, using hydrous ethanol with 30% water content by volume (Eh70). The results showed that the efficiencies of ethanol-water fuel are considerably higher than those of gasoline. An ethanol lean fuel-air mixture operation also showed a slightly higher efficiency than a stoichiometric fuel-air mixture operation, at the same operating conditions over the entire load and speed range. In comparison with gasoline, the use of hydrous ethanol has indicated substantial increases in HC emission. CO from hydrous ethanol combustion at lean and stoichiometric conditions is reduced because of the water-gas shift mechanism (a chemical reaction where CO reacts with water vapor to form H_2 and CO_2). NO_x is decreased significantly at most operating points.

The direct utilization of hydrous ethanol with high water content is achieved not only in SI engines, but also in homogeneous charge compression ignition (HCCI) engines (Martinez-Frias, et al., 2007; Mack, et al., 2009). Brake thermal efficiency is increased to 38.7%, and NO_x is 1.6 ppm when using hydrous ethanol with 35% water content by volume in an HCCI engine (Martinez-Frias, et al., 2007). Stable HCCI engine operation was obtained for fuels containing up to 40% water content by volume (Mack, et al., 2009). HC and CO emissions tend to increase because of incomplete conversion of

hydrous ethanol fuel to combustion products, while NO_x slightly increases with increased water concentration.

The objective of this study was to investigate the effects of high water content up to 40% by volume in ethanol and effects of generator loads on engine performance and emissions of a small SI engine equipped with a generator set in order to explore the feasibility of using hydrous ethanol with high water content as fuel for a small SI engine for a generator. Brake specific fuel consumption, overall efficiency, regulated emissions, i.e. HC, CO and NO_x, and aldehyde emission were evaluated.

2.2 Experimental Setup

In this section, the experimental apparatus and conditions are shown.

2.2.1 Experimental Apparatus

The experiments were carried out on a SI engine equipped with 5.5 kW rated power generator set. The schematic diagram of the apparatus is shown in Figure 2.1 (a). The SI engine was modified to provide optimized operating conditions for hydrous ethanol. The fuel injection system was controlled by an electronic control unit (ECU), which could adjust the amount of fuel and ignition timing. The injector was typical of the ethanol injectors used in Brazil. Technical specifications of the modified engine are described in Table 2.1.

Fuel consumption was recorded by a continuous fuel flow meter, Ono Sokki model FM-2500. The intake air pressure was measured by a digital manometer, Sokken model PZ-77, which was located between the air filter and the throttle valve. K-type thermocouples (not shown) were used to measure the temperatures of the intake air, spark plug, engine oil, exhaust gases and catalytic converter. The equivalence ratio was measured by the oxygen sensor. A pressure transducer was used to detect the ignition timing at the minimum advance for best torque (MBT). The test procedures were adapted from California Exhaust Emission Test Procedures for Small Off-Road Engines. In this study, the generator was connected to a heater which provided the load instead of a dynamometer. The engine was operated for sufficient time to achieve thermal stability, which was checked by the temperatures of the spark plug, engine oil and exhaust. The regulated emissions, which are CO, HC and NO_x, were measured from

the exhaust pipe before and after the catalytic converter, when engine speed and load had reached the required state. The schematic diagram of exhaust gas sampling for aldehyde analysis is shown in Figure 2.1 (b). For aldehyde measurement, the procedures for sampling followed the California Air Resource Board (CARB) Method No. 1004. For each sample the exhaust gas was trapped by a Dinitrophenylhydrazine (DNPH) cartridge with exhaust gas flow rate of 150 ml/min for five minutes. The sampled material was dissolved from the cartridges with 5 ml of acetonitrile. The solution in acetonitrile 50 µl was analyzed by high performance liquid chromatography (HPLC), using Shimadzu UV-HPLC wavelength of 365 nm. An HPLC grade liquid solvent of 60% acetonitrile and 40% water was used with a flow rate of 1 ml/min to carry solutes (aldehydes and other substances) to the chromatographic column for separation of aldehydes and other substances.

2.2.2 Experimental Conditions

In this study, the ignition timing was kept constant at the minimum advance for best torque (MBT) detected by the pressure transducer. The effect of varying water content in hydrous ethanol on ignition timing is insignificant, but different water contents have an effect on the rate of combustion after the onset of ignition (Cherry, et al., 1992).The equivalence ratio for all conditions was kept constant at stoichiometric air-fuel ratios for each fuel (i.e. ϕ=1), because results are difficult to compare if the equivalence ratio is not constant (Schifter, et al., 2011). For hydrous ethanol preparation, the mixing of ethanol and water does not require any special processes, because ethanol can absorb water readily (Olberding, et al., 2005).

The experiment had two parts for two different purposes as shown in Table 2. In the first part, effect of generator loads on engine performances with ethanol with 5% by volume water content (Eh95) at constant engine speed of 3600 rpm was investigated under conditions. For the engine loads, the term of electric power generated from a generator is suitable to represent the output as same as the work of Lee, et al. (2011) who studied the performance and emission from generator set and Leclercq, et al. (2003) who studied the control of a flywheel energy storage system associated with wind and diesel generators, because the propose of this work is to explore the possibility of using hydrous ethanol with high water content for a small SI engine

generator set. In addition, a small SI engine was typically equipped with generator for all time. However, the BMEPs of engine for generator can be calculated from the estimated generator efficiency (i.e. 62.5%) and are shown in Table 2.2. These generator loads were same condition as the small SI engine tested under the California exhaust emission standards and test procedures for 2005 and later small off-road engines (State of California Air Resources Board, 2005). Then the average emission values were compared with EPA model limit years 2007 to 2010, and model year 2011(U.S. Environmental Protection Agency, 2010). The second part was to determine the effect of the fuel water content from 20% to 40% by volume (Eh80 to Eh60) on engine performance at constant engine speed of 3300 rpm and generator output of 4 kW. In addition, the effects of the use of hydrous ethanol on materials, lubricant and fuel system are observed during and after the experiments.

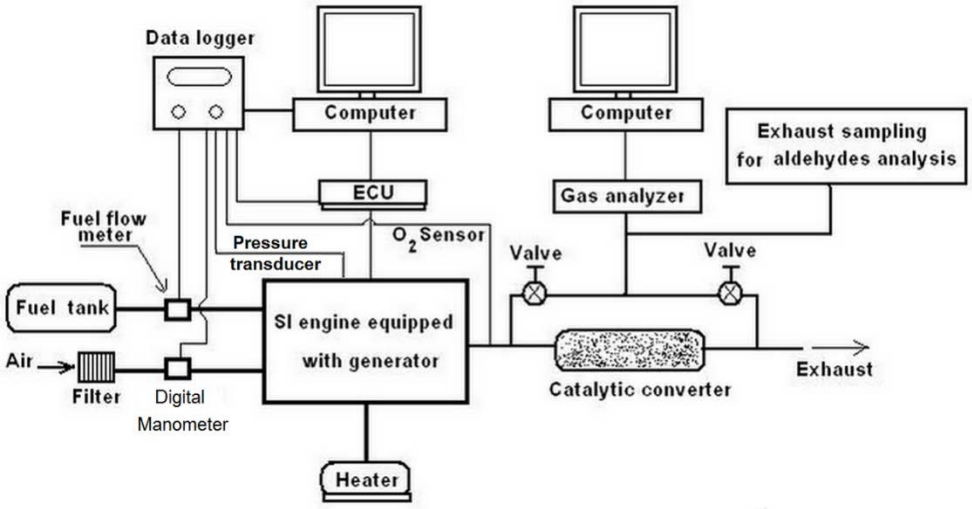

(a) Schematic diagram of the experimental apparatus

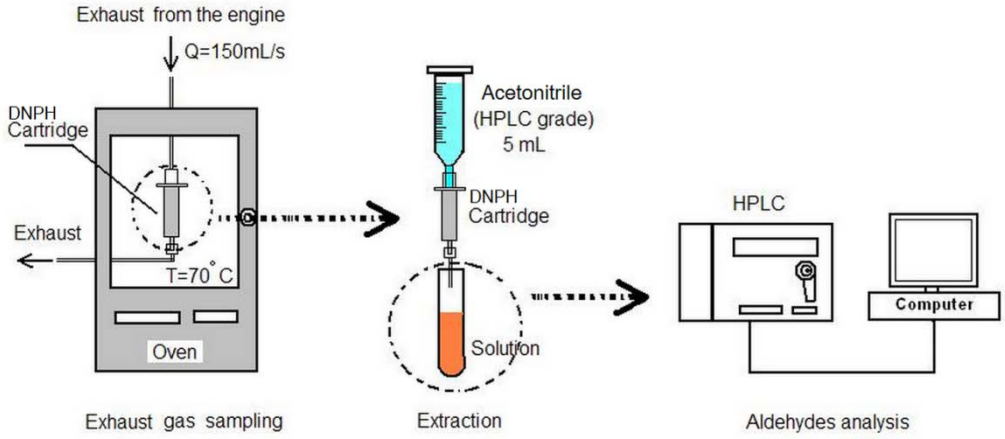

(b) Schematic diagram of exhaust gas sampling for aldehyde analysis

Figure 2.1 Experimental setup for the study of performance and emissions of a small SI engine fuelled bioethanol with water content.

Table 2.1 Specifications of modified engine and generator

Parameter	Description
Modified engine	
Engine type	4-stroke, overhead valve, single cylinder
Displacement (cm^3)	389.2
Bore x Stroke (mm)	88x64
Compression ratio	10.2:1 (original 8:1)
Engine speed (rpm)	2400-3600
Rated power (kW)	8.8
Cooling system	Forced air
Fuel supply	Electrical fuel injection (original carburetor)
Generator	
Generator type	AC output
Rated voltage (V)	120/240
Rated frequency (Hz)	60
Rated ampere (A)	45.8/22.9
Rated output (kW)	5.5

Table 2.2 Test conditions

First part: different generator loads tested	
Generator loads (kW) (% of rated power)	0, 0.55, 1.38, 2.75, 4.13 and 5.5 (0, 10, 25, 50, 75 and 100)
Estimated BMEP (bar)	0, 0.75, 1.89, 3.77, 5.66 and 7.54
Engine speed (rpm) at rated power	3600
Equivalence ratio (ϕ)	1
Fuel	Hydrous ethanol (Eh95, ethanol 95% by volume and water 5% by volume)
Second part: different water contents tested	
Generator load (kW) (% of rated power)	4 (72)
Estimated BMEP (bar)	5.48
Engine speed (rpm)	3300
Equivalence ratio (ϕ)	1
Fuels	Eh80, Eh75, Eh70, Eh65 and Eh60
Water contents (% by volume)	20, 25, 30, 35 and 40

2.3 Results and Discussions

2.3.1 Effect of Generator Loads

Figure 2.2 shows effect of load on BSFC and overall efficiency using Eh95. By increasing the generator load from 10% to 100%, overall efficiency increased by 18%, while BSFC decreased by about 76 %.

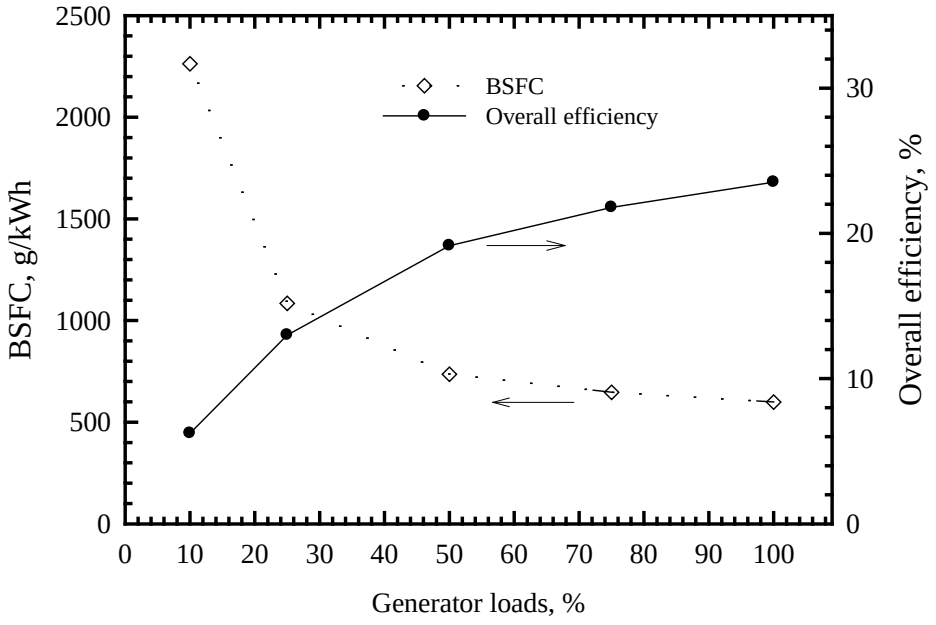

Figure 2.2 Effect of load on BSFC and overall efficiency using Eh95.

Figure 2.3 shows the corresponding emissions of CO, HC, HCHO, CH_3CHO and NO_x with 95% confidence limits from the engine using Eh95. As the generator load increased from 10% to 100%, carbon monoxide, hydrocarbon, formaldehyde and acetaldehyde emissions before the catalytic converter decreased by about 76%, 63%, 40% and 49% respectively, while oxide of nitrogen shows conversely. It is thought that the higher cylinder temperatures as indicated by the higher spark plug temperature at higher loads enhance the degree of combustion, which reduces the carbon monoxide, hydrocarbon and aldehydes but increases oxide of nitrogen. The catalytic converter reduced the amount of carbon monoxide, hydrocarbon, formaldehyde, acetaldehyde and oxide of nitrogen in the emissions by 78% to 94%,23% to 61%, 14% to 30%, 80% to 90%, and 29% to 65%, respectively. These results are similar to those of Haupt, et al. (2004),who found that acetaldehyde and formaldehyde emissions were abated by a catalytic converter.

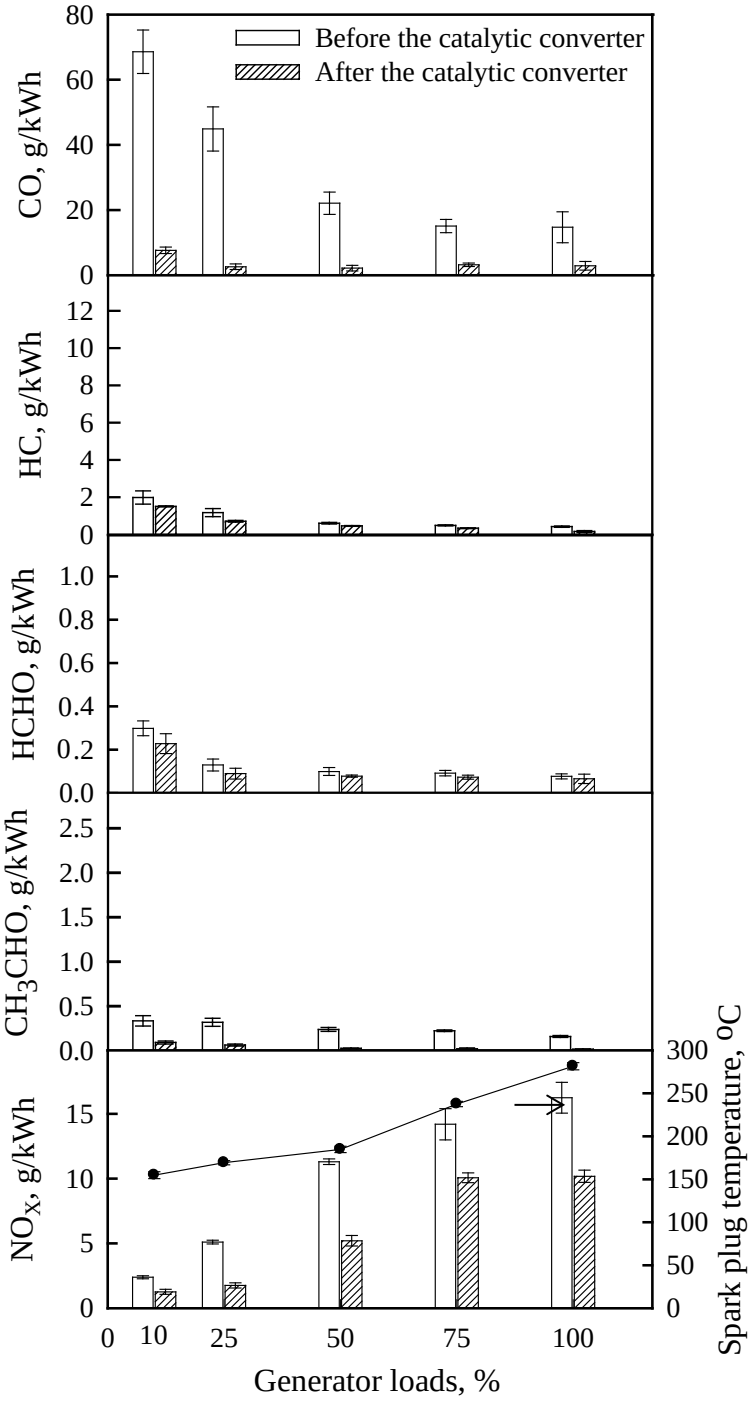

Figure 2.3 The corresponding emissions of CO, HC, HCHO, CH_3CHO and NO_x from the engine using Eh95.

Figure 2.4 shows comparison between the amounts of regulated emission gases with the EPA limit using Eh95. CO emissions (both before and after the catalytic converter) from Eh95 are substantially lower than the EPA limit. The low level of CO can be attributed to the ethanol molecule has a low carbon content, and the laminar

flame speed of ethanol is different from that of gasoline (Hara and Tanoue, 2006). These low levels of CO are similar to those of Jeuland, et al. (2004) and Costa and Sodre (2009). The values of $HC+NO_x$ emissions both before and after the catalytic converter were low enough to meet the EPA limit model year 2007 to 2010. But $HC+NO_x$ emissions before the catalytic converter were above the EPA limit model year 2011, while $HC+NO_x$ emissions after the catalytic converter were below the limit. The results show that the catalytic converter can reduce CO, and $HC+NO_x$ emissions by 80% and 50%, respectively.

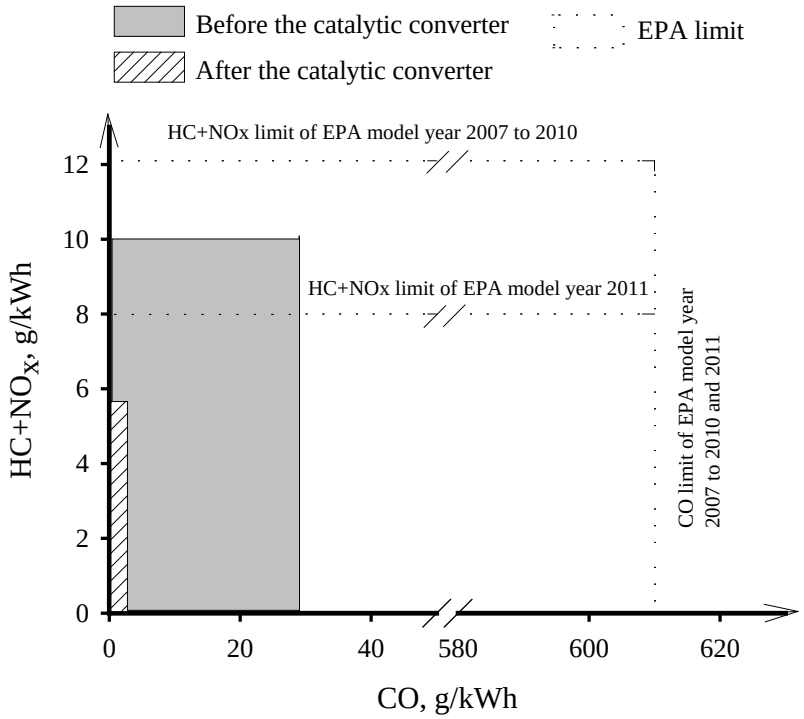

Figure 2.4 Comparison between the amounts of regulated emission gases with the EPA limit using Eh95.

2.3.2 Effect of Water Content in Ethanol

Figure 2.5 shows effect of water content on BSFC and overall efficiency at constant load. Increasing water content from 20% to 40% by volume (Eh80-Eh60) increased BSFC by about 75%, because heating value per mass of hydrous ethanol is reduced with higher water content. Overall efficiency gradually decreased by 5% as water content increased from 20% to 40 % by volume because of longer combustion duration. As combustion duration increases, the peak pressure occurs later in the expansion stroke and reduces the expansion work transfer from the cylinder gasses to the piston (Schifter,

et al., 2011). In addition, some energy from the combustion of hydrous ethanol is lost to vaporization of the incompletely vaporized water present in the charge mixture (Mack, et al., 2009). However, in a compromise between the energy gain in ethanol production and the decreased overall efficiency due to increasing the water content, the use of hydrous ethanol with high water contents between 20% and 40% by volume in a small SI engine generator, at constant engine speed and load, could achieve the goals of energy sustainability and economy of ethanol production.

Figure 2.6 shows the difference of BSFC with and without considering water. The results show that BSFC with no considering water are lower than that of BSFC with water for all tests. BSFC without considering water increase with increasing of water content as same as BSFC with water, but BSFC without considering water has a smaller gradient.

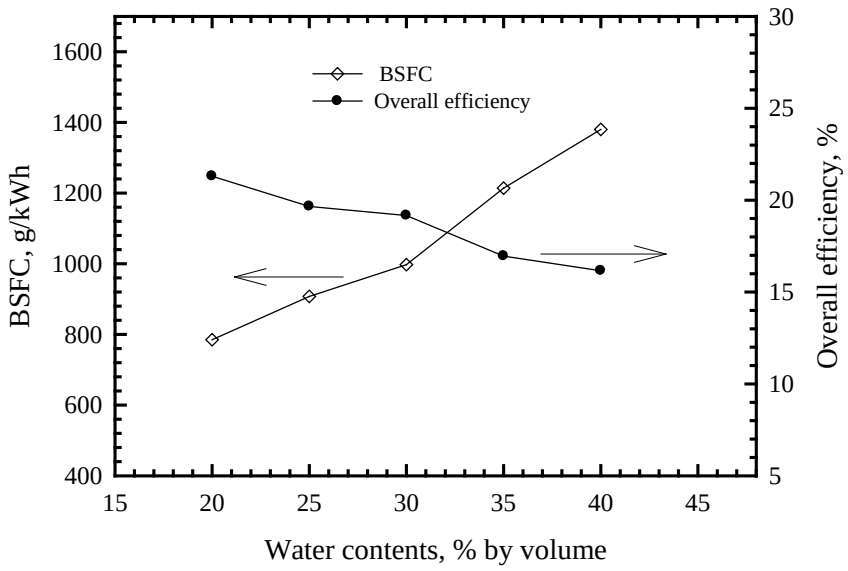

Figure 2.5 Effect of water content on BSFC and overall efficiency.

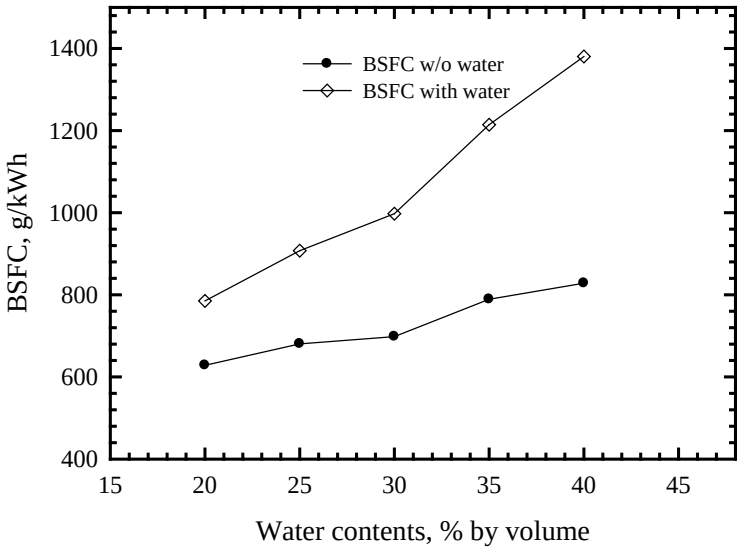

Figure 2.6 The difference of BSFC with and without considering water.

Figure 2.7 illustrated the corresponding emissions of CO, HC, HCHO, CH_3CHO and NO_x from the combustion of hydrous ethanol with various water contents. The addition of water from 20% to 40% by volume (Eh80 to Eh60) results in incomplete combustion with increases in CO, HC and aldehyde emissions. In comparison between the emissions from the use of Eh80 to Eh60, CO, HC, HCHO and CH_3CHO emissions increased by about 58%, 267%, 150% and 275% respectively (before the catalytic converter). The trends of formaldehyde and acetaldehyde emission are similar to HC. It is believed that the ambient temperature in the combustion chamber might be sufficient for partial oxidation, but not enough for complete combustion (Wagner, et al., 1996). Formaldehyde emission initially decreased as water content increased from 20% to 25% by volume (Eh80 to Eh75). Nevertheless, formaldehyde levels increased as water content increased beyond 30% by volume (Eh70). Acetaldehyde emissions monotonically increased with water content. As with hydrocarbon, the quenching effect causes incomplete combustion and formation of formaldehyde and acetaldehyde. NO_x emissions decrease by approximately 80%. This result agrees with Chen, et al. (2011). It is believed that the combustion temperature as indicated by the spark plug temperature is decreased by the quenching effect of the water vapor. The lower temperatures of combustion affect the thermal NO_x generation mechanisms. The results also show that the catalytic converter substantially reduced CO, HC HCHO, CH_3CHO and NO_x emissions by 75% to 89%, 10% to 32%, 8% to 35%, 28% to 44%, and 32% to 50%, respectively. In comparison to the EPA limit as shown in Figure 2.8, the values of

$HC+NO_x$ emissions at constant load (72% of rated power) before the catalytic converter for hydrous ethanol with water content up to 40% by volume (Eh60) can meet the EPA limit model year 2007 to 2010. But such $HC+NO_x$ emissions were above the EPA limit model year 2011. However, $HC+NO_x$ emissions after the catalytic converter were below the limit. CO emissions (both before and after the catalytic converter) from hydrous ethanol with water content up to 40% by volume (Eh60) are substantially lower than both the EPA limit.

2.3.3 The Effect of the Use of Hydrous Ethanol on Engine Operation

In this study, the hydrous ethanol engine for a generator was operated over 100 hours, including setup and experimental time. The engine for the generator operated normally during such time. However, there were some negative effects observed which were caused by the use of hydrous ethanol on materials, lubricant and the fuel system. It will be necessary in the future to discuss both medium and long term effects of using hydrous ethanol on engine operation.

The increase of engine wear leading to shorter durability is expected as the drawback of the use of hydrous ethanol with high water content in engine operation, at both medium and long terms. Engine oil deterioration and oxidation of parts were noticed in this study. The use of hydrous ethanol provided a higher level of water contaminant in the lubricant, which formed oil-water micro emulsions that reduced the lubricity. Hence, an increase of water content in ethanol may increase the possibility of water contamination in the lubricant, leading to lubricity failure. In this study, oil-water micro emulsions can be easily detected by lubricant color change after a few tests. This result is similar to the study of Boons, et al. (2008). With this issue, the lubricant must be changed frequently.

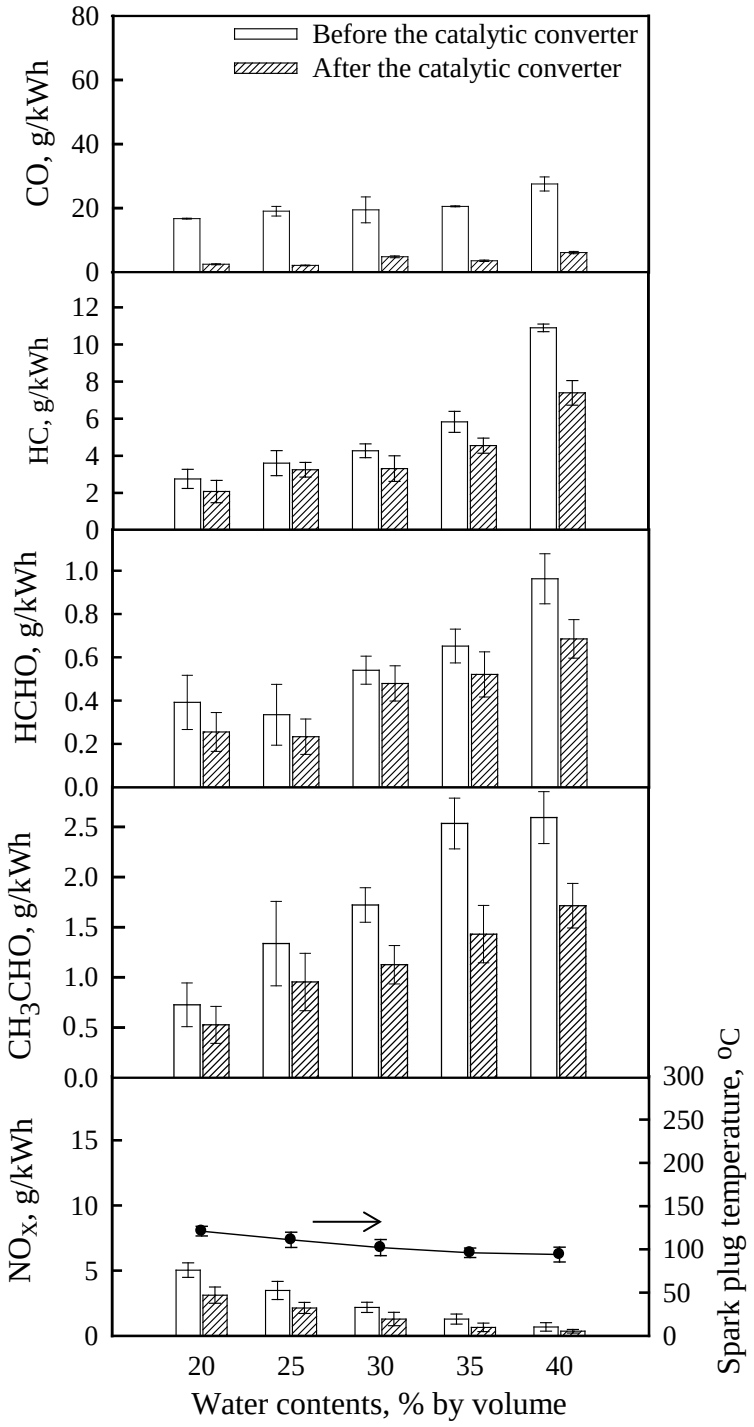

Figure 2.7 The corresponding emissions of CO, HC, HCHO, CH_3CHO and NO_x from the engine using hydrous ethanol with various water contents.

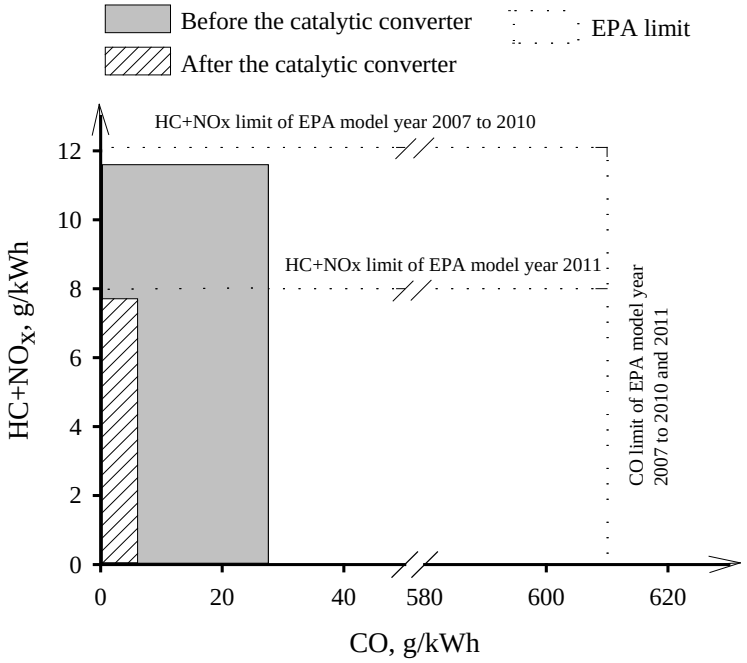

Figure 2.8 Comparison between the amounts of regulated emission gases with the EPA limit using Eh60.

The oxidation of engine parts was observed after stopping the engine operation for several days. Because ethanol can be oxidized into acetic acid, it enhances corrosion and chemical attack on the metals. Furthermore, the presence of high water content in ethanol increases ion concentrations that make hydrous ethanol much more aggressive than anhydrous ethanol (Jeuland, et al., 2004). Therefore, oxidation of engine parts is an important issue with regard to the use of hydrous ethanol with high water content.

A leak in the fuel hose occurred during the experiment, which was an effect of an ethanol chemical reaction with the fuel hose material, because swelling and weakening of rubber take place when ethanol is absorbed into it. The oxygen content in the ethanol can break the carbon-carbon double bounds of rubber (Jeuland, et al., 2004), leading to a leak or fuel system failure that will cause improper operation of the engine.

Unfortunately, the effects of using hydrous ethanol on engine operation in the medium and long terms are not yet included in the scope of this study. In the future, it will be interesting to overcome the disadvantages of the use of hydrous ethanol with improvements based on further investigation of engine wear, engine durability, visual investigation of several critical engine components, engine oil and fuel filter clogging, engine oil contamination, engine oil change frequency, and material and lubricant

compatibility. These will make them suitable for widespread use and improve the energy balance of ethanol production.

2.4 Summary

- Using ethanol with 5% water content (Eh95) in the SI engine at a constant speed of 3600 rpm and with stoichiometric air-fuel ratio showed that increasing the load increased overall efficiency, while BSFC, HC, formaldehyde and acetaldehyde emissions were decreased. In addition, the regulated emissions after the catalytic converter, i.e. CO, and HC+NO_x, were lower than the EPA limit model year 2011; but before the catalytic converter, only CO was lower than the EPA limit, while HC+NO_x were higher than the EPA limits.

- At constant load (72% of rated power) and engine speed, increasing the water content of ethanol decreased the overall efficiency and NO_x emissions, while BSFC, HC, CO, formaldehyde and acetaldehyde emissions increased. HC+NO_x were in the EPA limit model year 2011; but before the catalytic converter, only CO was lower than the EPA limit. However, the increased emissions from increasing the water content were substantially reduced by the catalytic converter.

- The catalytic converter is recommended when hydrous ethanol is used for a small SI engine generator set because it reduced the regulated and unregulated emissions in all conditions tested.

- Hydrous ethanol with high water content (up to 40% by volume) can be used in a small SI engine generator, especially in remote and rural areas where ethanol can be produced locally. Nevertheless, to affirm that hydrous ethanol with high water content (up to 40% by volume) is suitable for SI engine generators, an assessment of the engine wear, engine durability, visual investigation of several critical engine components, engine oil and fuel filter clogging, engine oil contamination, engine oil change frequency, material and lubricant compatibility should be studied in the next step with more development and research.

CHAPTER 3
DESIGN OF CONSTANT VOLUME COMBUSTION CHAMBER (CVCC) WITH PRE-COMBUSTION TECHNIQUE FOR SIMULATION OF CI ENGINE CONDITIONS

3.1 Introduction

The development of the modern CI engines is driven by environmental concerns, oil crisis and engine efficiency. This can be achieved by using higher supercharging, exhaust gas recirculation (EGR), higher temperature of combustion chamber surfaces and the use of various kinds of fuels (Kobori and Kamimoto, 1995). When a number of engine technology and new fuels are applied, the observation of combustion phenomena is required, because it play an important role in engine efficiency and emissions. However, it is difficult to access optically in the practical engines. Therefore, several optical test rigs have been used, e.g., optical research engines, a rapid compression and expansion machine (RCEM), constant pressure flow rigs, and constant volume combustion chambers. The optical test rigs have the following features:

- The gas conditions at start of injection can be changed widely.
- Various optical diagnostics can be easily accessed.
- The effect of lubricating oil on emission is intentionally disregarded.
- Only a small amount of fuel is consumed that is suitable when testing expensive fuels produced on a laboratory basis.

The advantages and drawbacks for each test rig were well summarized from several works by Baert, et al. (2009). The operating range of the test rigs compared to diesel in-cylinder conditions is shown in Figure 3.1. In addition, the strengths and weaknesses of the different test devices are compared in Table 3.1. Among them, the operating range of constant volume pre-combustion cells (CVPC) or constant volume combustion chamber (CVCC) covers the full range of Figure. CVCC gives a much wider range of gas pressures and temperatures prior to injection. Variation of simulated compression ratio is easily achieved simply by varying the lean mixture composition.

Table 3.1 reveals that only optical research engine (ORE) shows the most similarity to the real CI engine situation, while constant pressure flow rigs (CPFR), constant volume hot cells (CVHC) and constant volume pre-combustion cell (CVPC) are more suited for the basic research of free spray combustion. However, no the optical test equipment gives the identical conditions of CI engines. Consequently, the most appropriate optical test rigs will depend on the context of the study.

Several previous works have given attention to the fundamental study of free spray combustion. Hence, the constant volume pre-combustion cell (CVPC) or constant volume combustion chamber (CVCC) with pre-combustion technique is considered, because it gives a wide operating range and large volume for free spray.

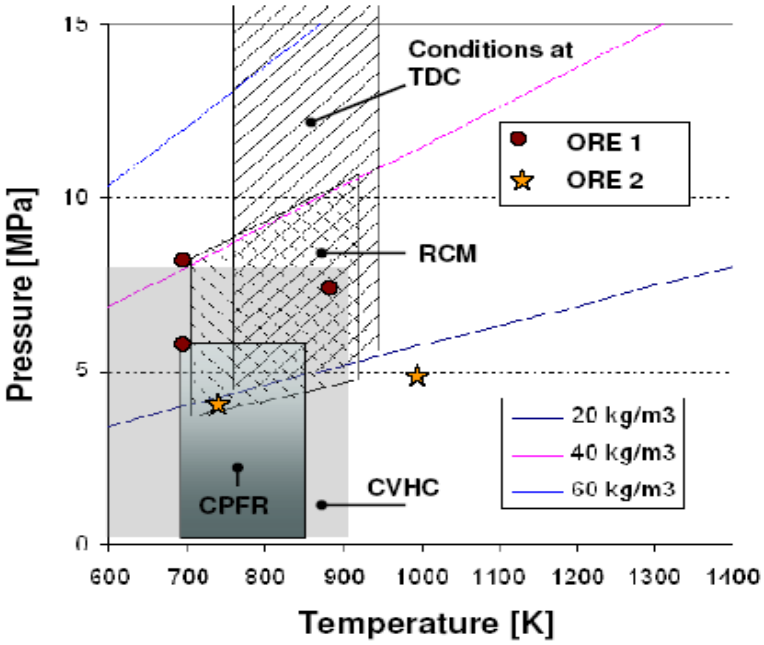

Figure 3.1 In-cylinder conditions prior to injection of CI engine compared to the operating range of different optical test rigs: optical research engines (ORE), rapid compression machines (RCM), constant pressure flow rigs (CPFR), constant volume hot cells (CVHC) and constant volume pre-combustion cells (CVPC) (Baert, et al., 2009).

Table 3.1 Quality attributes of different optical spray test rigs; optical research engines (ORE), rapid compression machines (RCM), rapid cycling machines (RCYM), constant pressure flow rigs (CPFR), constant volume hot cells (CVHC) and constant volume pre-combustion cell (CVPC) (Baert, et al., 2009).

Type of optical test rig	ORE	RCM	RCYM	CPFR	CVHC	CVPC
Optical accessibility	0	0	++	++	-	+
Similarity to the real engine situation	0	-	--	--	--	--
Free spray penetration distance	0	+	+	+++	++	++
Control on trapped gas p / T	0	+	0	++	++	++
Control on trapped gas composition (i.e. EGR)	0	-	0	+	++	+++
Flow field impact on combustion	--	-(-)	-	0	-	-
Test facility volume	0	+	0	0	++	++
Time to switch between operating conditions (i.e. T)	0	0	0	0	--	++
Time between tests [s] (*)	1	120-600	1	1-3	60	600

Note: mostly relative; 0= neutral, + better, - worse

Figure 3.2 shows the principle of a pre-combustion technique in order to generate a condition at start of injection in CI engines. The pressure history inside CVCC is used to explain . Initially, a lean premixed combustible gaseous mixture of acetylene (C_2H_2), O_2 and N_2, is filled into the CVCC at a certain pressure. Then, a spark plug ignites a gaseous mixture, resulting in a steep pressure rise, until complete combustion occur generating high pressure and temperature. Then, the pressure inside chamber is set to decrease as heat lose through the chamber wall to the surrounding. When pressure reaches to the target values that is the representative of CI engine condition, test fuel is injected by the injection system.

There are a number of recent works using a constant volume combustion chamber (CVCC) with pre-combustion technique for different purposes (Oren, et al., 1984; Baert, et al., 2009; Siebers and Edwards, 1987; Nguyen and Honnery, 2008; Nguyen, et al., 2010; Fujiomoto, et al., 2005) shown in Table 3.2. Most CVCC's were designed with a cylindrical shape with a diameter between 50-300 mm and width of 29-410 mm. Gas density, pressure and temperature are between 7-45 kg/m^3, 1-50 bar and 300-1200 K, respectively. Test fuels were injected with various nozzle types at different pressures in the range of 500-1800 bar.

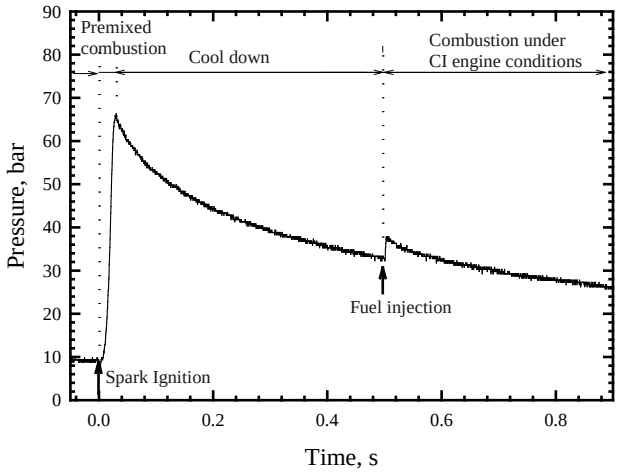

Figure 3.2 A principle of a pre-combustion technique.

However, a few information and detail of CVCC design were disclosed. Oren, et al., (1984) illustrated the best engineering practice in concept design, gas filling and CVCC operation. They state that the major difficulty in operating the constant volume combustion chamber is removing, cleaning and resealing the quartz windows. These processes have to be handled with extreme caution, because the windows are relatively expensive and easily damaged. Their CVCC do not include mixing fan. However, they have a mixing tank and using the tangential inlet to create homogeneous mixture as shown in Figure 3.3.

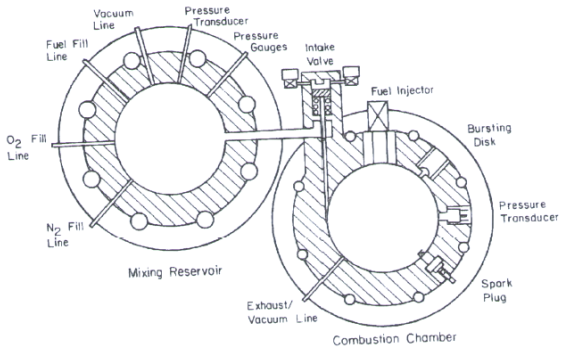

Figure 3.3 CVCC without mixing fan (Oren, et al., 1984).

Baert, et al., (2009) showed important design and operation considerations for a CVCC. One critical consideration noted is sealing deterioration. Finally, they showed examples of operating of CVCC and results of fuel spray characteristics. However, the systematic design of CVCC step by step is not shown in the previous works. Therefore, in this study, it is necessary to reveal the design method of CVCC, including chamber size calculation, strength analysis of chamber and effect of inlet on charge mixing.

Table 3.2 CVCC geometry and CI engine-like conditions using pre-combustion technique

Authors	Area of interest	Fuels	Chamber geometry			Test conditions			Injection conditions		
			ϕ (mm)	Depth (mm)	Volume (cm^3)	P_g (bar)	T_g (K)	ρ_g (kg/m^3)	Inj. Dur. (μs)	P_i (MPa)	Nozzle Type
Oren, et al. (1984)	Spray and combustion	D	101.6	44.5	361	55	n.a.	n.a.	n.a.	n.a.	n.a.
Baert, et al. (2009)	Spray and combustion	D	100	n.a.	n.a.	30	400-1100	25,32	n.a.	120	6 holes
Siebers and Edwards (1987)	Ignition and combustion	D,E	80	29	146	8-80	600-1600	n.a.	n.a.	n.a.	Pintle
Nguyen and Honnery (2008)	Ignition and combustion	D, BD, E	150	132	2332	25	1100	n.a.	5000	180	5 holes and single hole (0.2mm/hole)
Nguyen, et al. (2010)	Ignition	H_2, NG	80	30	150	30-50	700-1200	n.a.	n.a.	150	n.a.
Fujimoto, et al. (2005)	Soot behavior	D	70	26	100	45	700-1200	16.2	2700	74.5	Single hole (0.2 mm)

Note: D = Diesel, E = Ethanol, ME = Methanol, BD = Bio-diesel, H_2 = Hydrogen and NG = Natural gas

3.2 Design Criteria

3.2.1 In-Cylinder Gas Conditions of CI Engines at TDC

Design criteria are selected to cover the typical value of in-cylinder gas conditions at top dead center (TDC) of CI engines with CR 16-28. Pressure, temperature and density of at TDC of CI engines with CR 16-28 can be estimated by using polytropic process calculation as shown in equation (3.1).

$$\frac{T_1}{T_2} = \left(\frac{P_2}{P_1}\right)^{\left(\frac{n-1}{n}\right)} = \left(\frac{V_1}{V_2}\right)^{n-1} = (CR)^{n-1} \quad (3.1)$$

Where:

T_1	Initial gas temperature at BDC (K)
T_2	Compressed gas temperature at TDC (K)
P_1	Initial gas pressure at BDC (Pa)
P_2	Compressed gas pressure at TDC (Pa)
n	Polytropic index (1.35 for real air, Heywood, 1988)
V_1	Volume at BDC (m^3)
V_2	Volume at TDC (m^3)
CR	Compression ratio

Figure 3.4 shows surrounding gas condition at TDC obtained by polytropic process calculation. Gas pressure, temperature and density increased with increased compression ratio. Pressure, temperature and density at TDC are 40-90 bar, 800-960 K and 18-32 kg/m^3, respectively, for CR 16–28. Increasing compression ratio results in increase of surrounding gas pressure, temperature and density at TDC.

3.2.2 Injection and Fuels

CVCC is designed for the study of spray and combustion of test fuels, included the conventional diesel and alternative fuels, i.e. bioethanol and biodiesel. Nozzle hole diameter is a typical for common rail injector (0.1-0.2 mm). The injector with the maximum diameter-single hole nozzle (0.20 mm) will be used for design. Test fuels can be injected with high pressure up to 150 MPa by a typical common rail system.

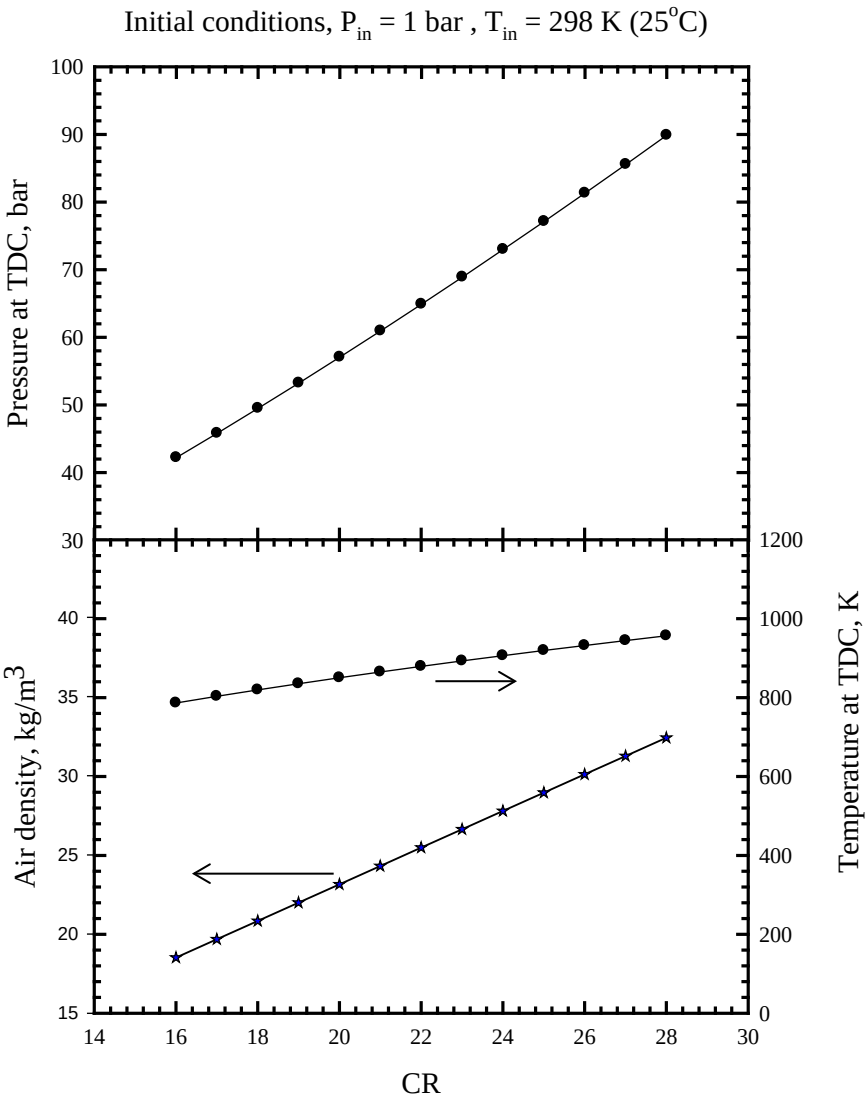

Figure 3.4 Surrounding gas condition at TDC obtained by polytropic process calculation with polytropic index (n) of 1.35.

3.2.3 Combustion Chamber Feature

Figure 3.5 shows the 3D sketch of CVCC. The main parts are cylindrical combustion chamber, quartz window, window case and holder. Combustion chamber and quartz window are directly contact with the high pressure gas mixture, which is considered an impact load because combustion occurs in short periods. Therefore, the combustion chamber and window are only considered for strength analysis.

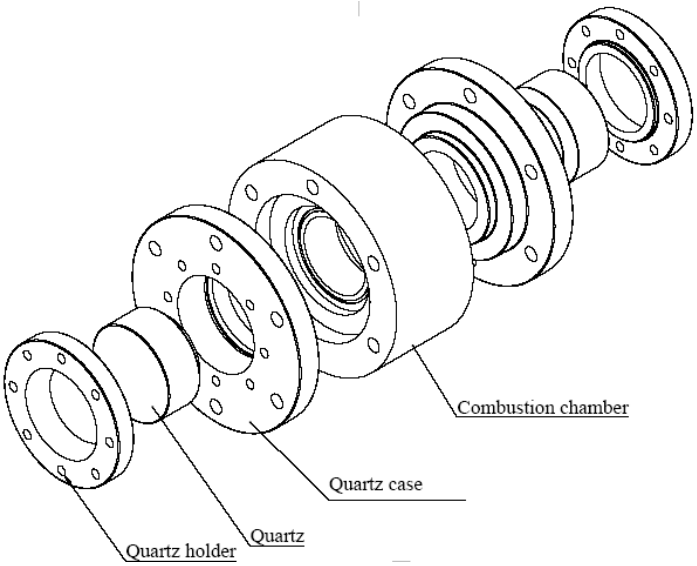

Figure 3.5 The sketch of main parts of CVCC.

3.3 Design Procedure

The procedure for design is shown in Figure 3.6. Starting design with justifying CVCC geometry and dimension by using spray characteristics of test fuels and strength analysis. Then, flow inside CVCC is analyzed to study the effect of inlet on charge mixing.

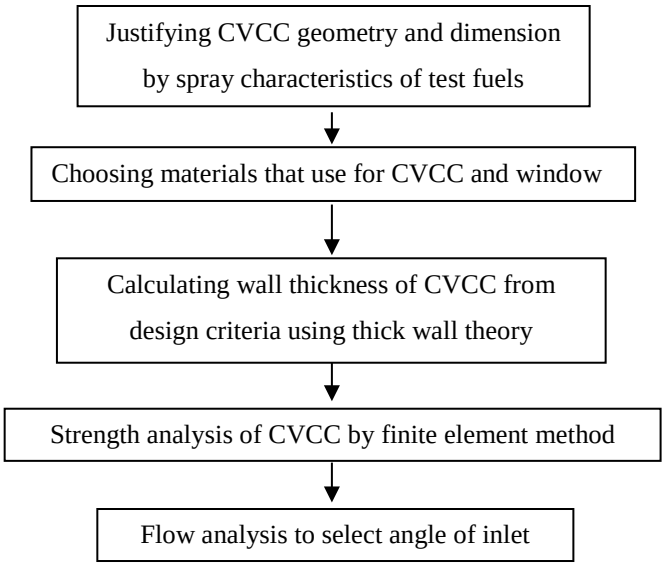

Figure 3.6 Design procedure.

3.3.1 Justifying of Combustion Chamber Size

Because combustion chamber geometry has effects on spray and combustion, the small volume combustion chamber results in impinging of spray on the chamber wall. This does not allow the study of free spray. Likewise, when a large volume of the chamber is used the small pressure rise occurred makes pressure analysis difficult. Therefore, the optimized size of the combustion chamber must be initially identified. Optimization of chamber size can be considered from fuel spray penetration and angle. As shown in design criateria, a single hole injector with hole diameter of 0.2 mm is selected to design. The single hole injector is located at the top of CVCC as shown in Figure 3.7.

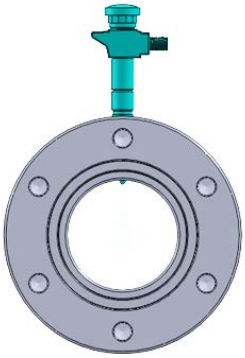

Figure 3.7 Injector position.

The optimization of chamber size, i.e. diameter and width, can be achieved from the free spray characteristic. To avoid impinging of spray on the chamber walls, the posible maximum fuel spray penetration and angle as shown in Figure 3.8 can be calculated from the surrounding gas conditions and fuel properties shown in Table 3.3 using equation (3.2) to equation (3.4) (Wakuri, et al., 1960). Fuels that will be used for test are diesel, ethanol and biodiesel. The maximum values of surrounding gas and injection conditions are selected for calculation to obtain the possible maximum spray characteristics. Injection pressure of 150 MPa, obtained by the common rail injection system, is used for calculation. The considered time after injection is chosen as 2.5 ms which is relative long for free spray, because the typical ignition delay of CI engine is in the range of 0.4 ms to 1 ms (Heywood, 1988). With this time, it is believed that the free spray will not impinge the combustion chamber wall during the study.

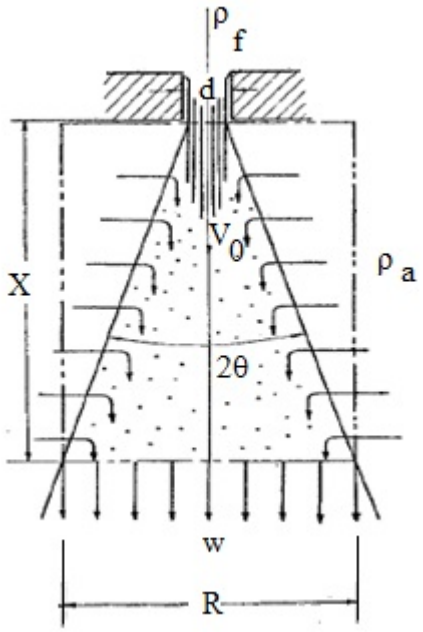

Figure 3.8 Spray penetration and angle (Wakuri, et al., 1960).

$$X = \left(\frac{2C\Delta P_{inj}}{\rho_a}\right)^{0.25} . \left(\frac{t.d_N}{tan\theta}\right)^{0.5} \quad (3.2)$$

$$tan\theta = 0.427 \left(\frac{\rho_a}{\rho_f}\right)^{0.325} \quad (3.3)$$

$$R = 2Xtan\theta \quad (3.4)$$

Where:

X	Spray penetration (m)
R	Spray width (m)
C	Flow coefficient
ρ_a	Air density (kg/m^3)
ρ_f	Fuel density (kg/m^3)
ΔP_{inj}	Different pressure between injection and chamber pressure (N/m^2)
t	Time after injection (s)
d_N	Nozzle diameter (m)
θ	Spray angle (degree)

Table 3.3 The surrounding gas conditions and fuel properties used for calculation of spray penetration and angle

Fuel	Ethanol	Diesel	Biodiesel
Fuel density (ρ_f) (kg/m^3)	785	848	881
Surounding gas	Air	Air	Air
Gas density (ρ_a) (kg/m^3)	18-32	18-32	18-32
Discharge coefficient of nozzle (C_d)	0.8	0.8	0.8
Injection pressure (P_{inj}, MPa)	150	150	150
Gas Pressure (P_g, MPa)	4	4	4
Pressure difference (d_P, MPa)	146	146	146
Time after injection (t, ms)	2.5	2.5	2.5
Nozzle diameter (dn, mm)	0.2	0.2	0.2

Figure 3.9 shows spray penetrations and angles calculated by the spray expression proposed by Wakuri, et al., (1960). The results show that the calculated spray penetrations and spray tip width for test fuels, i.e. ethanol, diesel and bio-diesel, decreased with increased surrounding gas density, while spray angle shows the contrary results. These results are similar to Heilig, et al. (2011) and Hu, et al. (2006). The differences in spray characteristics depend on fuel density. Biodiesel shows the longest spray penetration, i.e. approximately 100 mm, while ethanol shows the largest spray angle (17^o) and spray tip width (25 mm) at the calculated conditions. The possible maximum spray can be drawn as shown in Figure 3.10.

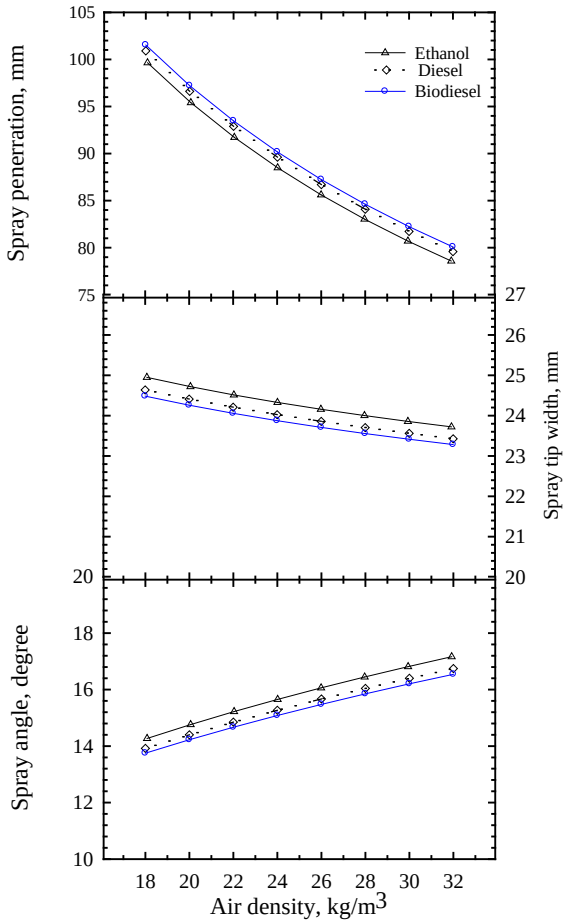

Figure 3.9 The spray characteristics of test fuels calculated by the expression of Wakuri, et al., (1960).

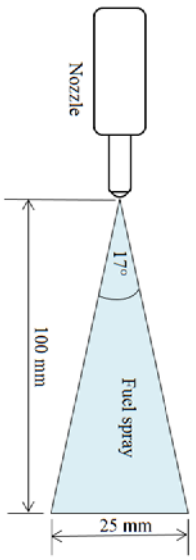

Figure 3.10 The possible maximum spray pattern for test fuels.

These spray characteristics are used to justify the size of the cylindrical-shaped combustion chamber. The diameter of the chamber depends on spray penetration, while the chamber width depends on spray tip width. The diameter and width of the cylindrical chamber should be equal or higher than the maximum spray penetration and tip width of fuels. For the width of chamber, it is double of the minimum required value to avoid fuel impinging on the wall. Therefore, in this work, the diameter and width of cylindrical combustion chamber are 100 mm and 45 mm, respectively, shown in Figure 3.11.

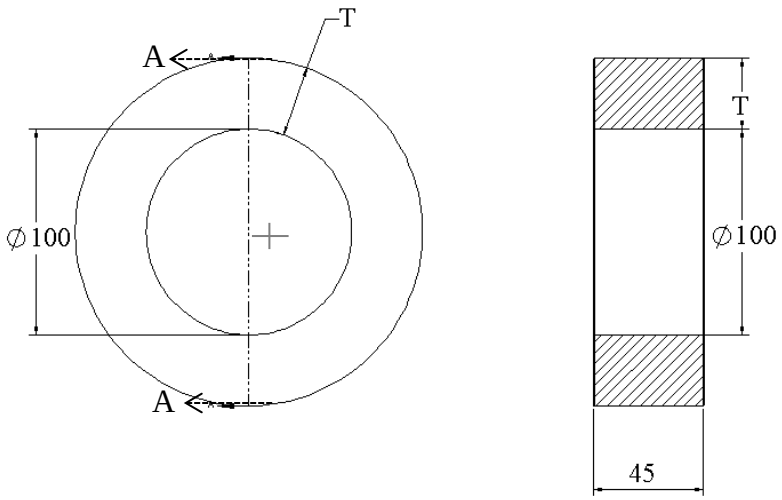

(a) Front view (b) Section view A-A

Figure 3.11 Simple geometry of combustion chamber.

3.3.2 Strength Analysis of Combustion Chamber

The optimum thickness of chamber and window is calculated by theory and computer simulation. Materials used for CVCC and window are stainless steel and quartz, respectively. Stainless steel is chosen for CVCC because of its high strength and anti-corrosion property. For the window, quartz is selected because it has very high strength and a wide range of light transmission. However, in this study quartz has not been installed with CVCC but it is studied for future development.

Circular cylindrical shape was selected for CVCC. With this geometry, the principle of thick wall pressure vessel can be applied (Mott, R.L., 2008). When pressure applied to the thick wall cylindrical vessel, there are three types of stress occurred in the material, i.e. hoop or tangential stress (σ_H), longitudinal stress (σ_L) and radial stress (σ_R), but hoop stress is the most critical stress. Therefore, only hoop stress is considered in calculation. For the calculation of window thickness, two stresses are considered: shearing stress and bending stress. Safety factor 12 is chosen for the combustion chamber and 15 for quartz window (Mott, R.L., 2008). Load on the combustion chamber wall and window is defined as pressure at 100 bar.

Calculation of wall thickness

When in-cylinder pressure applied to the chamber walls shown in Figure 3.12, there are three types of stress occurred in the material, i.e. hoop or tangential stress (σ_H), longitudinal stress (σ_L) and radial stress (σ_R).

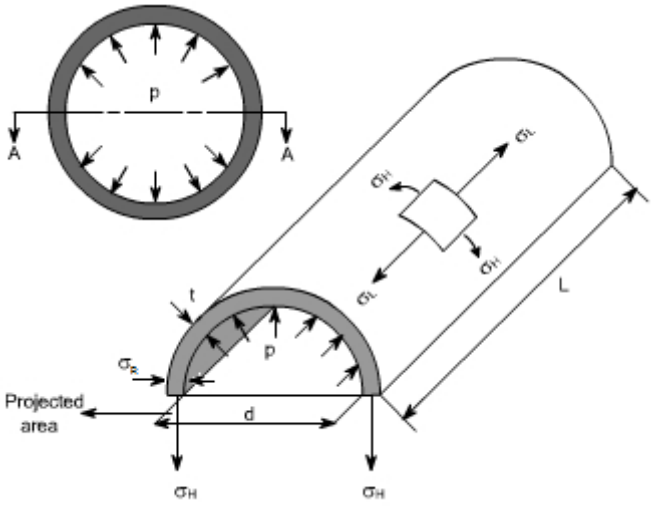

Figure 3.12 Stresses in thick wall vessel (Mott, R.L., 2008)

However, for calculation, only hoop stress is considered, because it is the most critical stress. The hoop stress of thick wall shown in equation (3.5) (Mott, R.L., 2008).

$$\sigma = \frac{P_{cy}(b^2+a^2)}{(b^2-a^2)} \tag{3.5}$$

Where:

σ	Hoop stress (MPa)
P_{cy}	Pressure exerted on the wall (MPa)
a	Inner cylinder radius (m)
b	Outer cylinder radius (m)

The material should be high strength and anti-corrosion materials. Therefore, stainless steel 304 is chosen. The details of material and data for calculation of wall thickness show in Table 3.4.

Table 3.4 The details of material and data for calculation of wall thickness.

Material properties	
Stainless steel 304	
Ultimate strength (S_u)	515 MPa
Design criteria	
Design stress for material that carry shock or impact loads (σ_d)	$\frac{S_u}{12} = \frac{515}{12}$=42.9 MPa
Maximum in-cylinder pressure (P_{cy})	10 MPa
Inner radius of cylinder (a)	50 mm
Outer radius of cylinder (b)	Calculated from equation 3.5

From given data, using equation (3.5), outer radius of cylinder (b) is 63.39 mm. The minimum wall thickness should be greater than 13.40 mm. However, there are the measurement devices and screws that will be connected to the CVCC. Therefore, the wall thickness of 60 mm is chosen to provide sufficient strength of CVCC connected with devices and screws.

Calculation of quartz window geometry

To find minimum quartz thickness that can carry load, there are four stresses involved, i.e. normal stress, bearing stress, shearing stress and bending stress when pressure applied to the quartz surface. Radius of the optical access area is selected as 47.5 mm. This area carry pressure load directly. The sketch of quartz window is shown in Figure 3.13. The details of material and data for calculation of window thickness shown in Table 3.5.

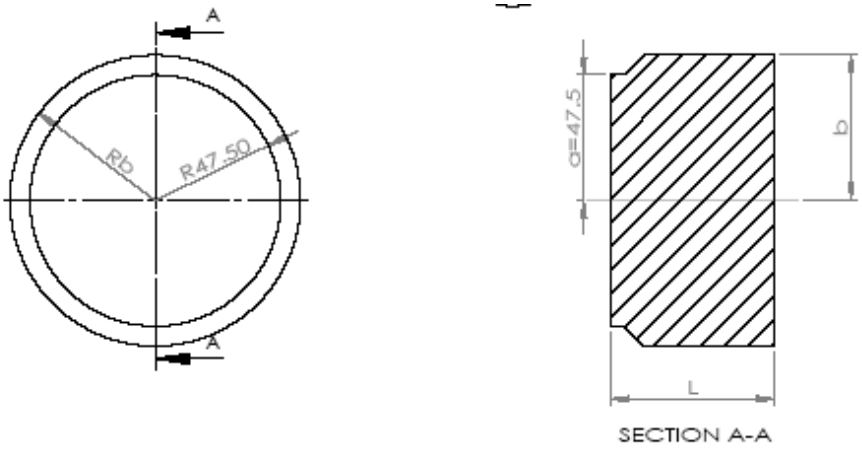

Figure 3.13 Sketch of quartz window.

Table 3.5 The details of material and data for calculation of window thickness.

Material properties	
Quartz	
Bending strength	94.3 MPa
Compression strength	1130 MPa
Tension strength	49 MPa
Design criteria	
Design shearing stress for material that carry shock or impact loads (τ_d)	$\frac{Tension\ strength}{12} = \frac{49}{12}$=4.1 MPa
Design bearing stress for material that carry shock or impact loads (σ_{Bd})	0.35 x Compression strength = 0.35 x 1130 = 395.5 MPa
Design normal stress for material that carry shock or impact loads (σ_{cd})	$\frac{Compression\ strength}{15}=\frac{1130}{15}$= 75 MPa
Design bending stress for material that carry shock or impact loads (σ_{bd})	$\frac{Bending\ strength}{20}=\frac{94.3}{20}$= 4.715 MPa
Maximum in-cylinder pressure (P_{cy})	10 MPa
Inner radius of quartz ($a=D_i/2$)	47.5 mm

(a) Finding quartz thickness

To find quartz thickness, two stresses are considered, i.e. shearing stress and bending stress. Shearing stress and bending stress can be found from the following equation,

Shearing stress $$\tau = \frac{P_{cy}\, a}{2L} \quad (3.6)$$

Bending stress $$\sigma_b = \frac{P_{cy}\, A}{4L^2} \quad (3.7)$$

Where

τ Shearing stress (MPa)

σ_b Bending stress (MPa)

a Inner radius of quartz (m)

P_{cy} Pressure exerted on the surface of quartz (MPa)

A Surface area (m^2) shown in Figure 3.14

L Quartz thickness (m) shown in Figure 3.14

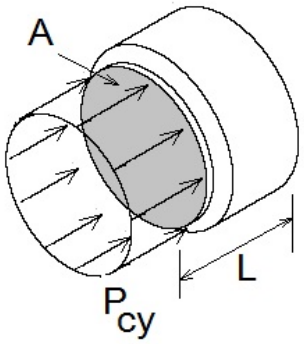

Figure 3.14 Window surface area and thickness of quartz.

From given data, the quartz thickness can be calculated. Using equation (3.6) to find thickness of quartz to resist shearing stress, the minimum thickness of quartz is 57.93 mm. To find the thickness of quartz to resist bending stress, equation (3.7) gives the required minimum thickness of quartz to carry bending stress is approximately 60 mm. Therefore, the required minimum quartz thickness should be greater than 60 mm.

(b) Finding outer radius of quartz (b)

From Figure 3.13, outer diameter (b) can be calculated from equation (3.8).

Bearing stress $$\sigma_B = \frac{P_{cy}\, a^2}{(b^2 - a^2)} \quad (3.8)$$

Where

σ_B Bearing stress (MPa)

b Outer radius of quartz (m)

From given data, using equation (3.8), the required minimum outer radius of quartz to resist bearing stress is 48.10 mm. Therefore, the required minimum outer radius should be greater than 48.10 mm.

Strength of material is also analyzed by the finite element method. The simple models of CVCC and quartz window are used to analyze. The model for simulation shows in Figure 3.15. The simple geometry of circular cylindrical vessel and window is initially analyzed. Results will be validated with theoretical calculation.

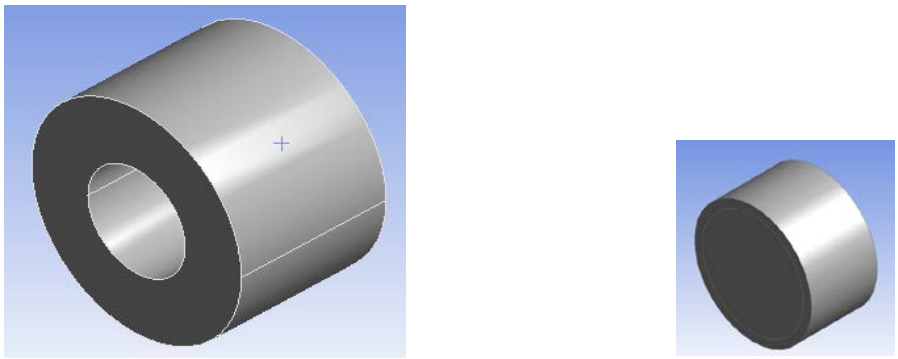

(a) CVCC (b) Quartz window

Figure 3.15 Simple models for simulation.

Figure 3.16 shows the model with mesh. The cubical elements are applied for simple geometry. The green area is the area where it carry load, i.e. pressure of 100 bar. The red dot is the support. With this support, results can be considered as similar to the theoretical calculation. Initially, grid independent study is performed to find the proper grid element for the simulation. Then the proper number of grid element is applied to all models. Boundary conditions for finding the optimum element are shown in Table 3.6. An example of stress distribution in material is shown in Figure 3.17.

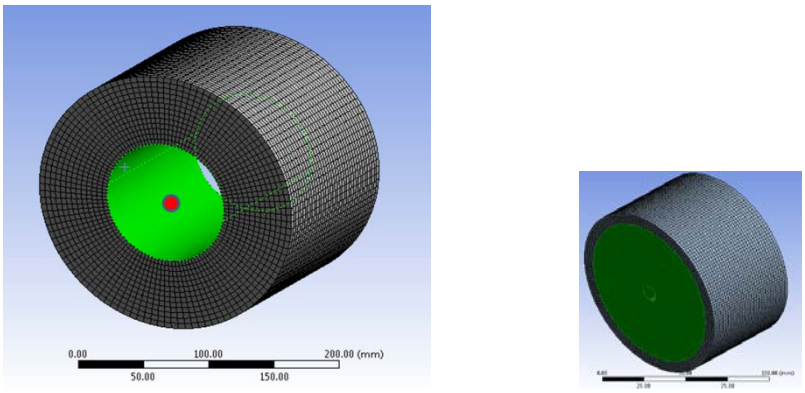

(a) CVCC (b) Quartz window

Figure 3.16 Simple models with mesh.

Table 3.6 Boundary conditions

CVCC	
Load	Pressure of 100 bar inside chamber
Support	Point
Type of element	Cubical element
Quartz window	
Load	Pressure of 100 bar at the surface
Support	Area
Type of element	Cubical element

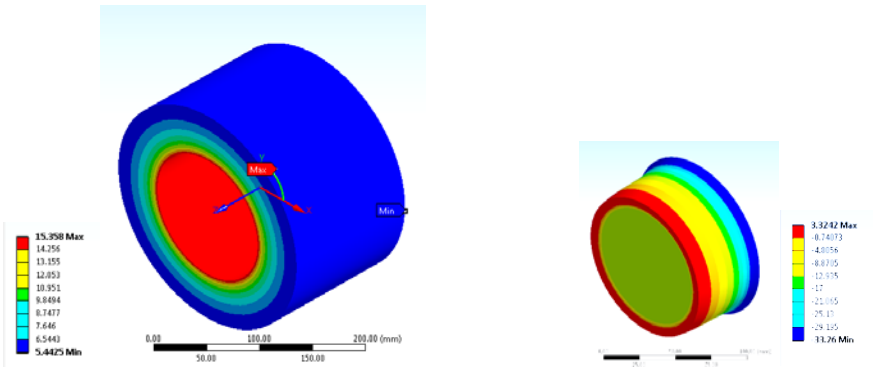

Figure 3.17 An example of stress distribution in CVCC and window.

Grid independent study for the chamber and window model was initially analyzed, shown in Figure 3.18 and Figure 3.19. The simulated maximum stresses at inner wall of the chamber and the edge of the quartz window are used to compare with those of the calculated maximum stresses. The proper numbers of elements for chamber and window model are about of 12000 and 90000, respectively.

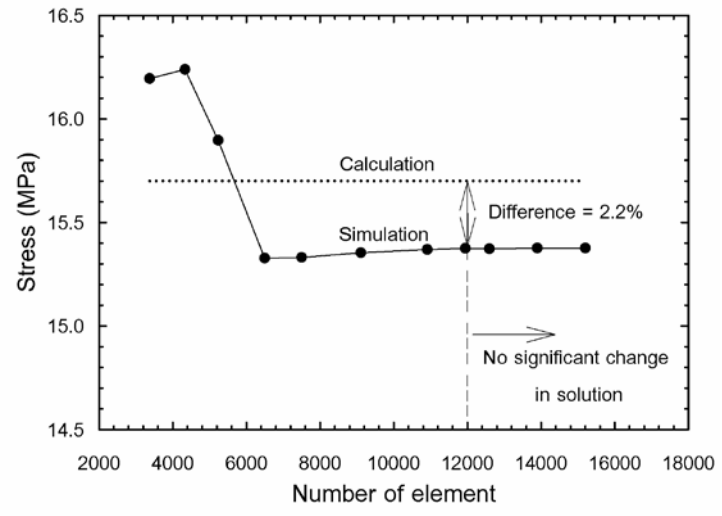

Figure 3.18 Grid independent study and validation for solution of combustion chamber at inside pressure of 100 bar.

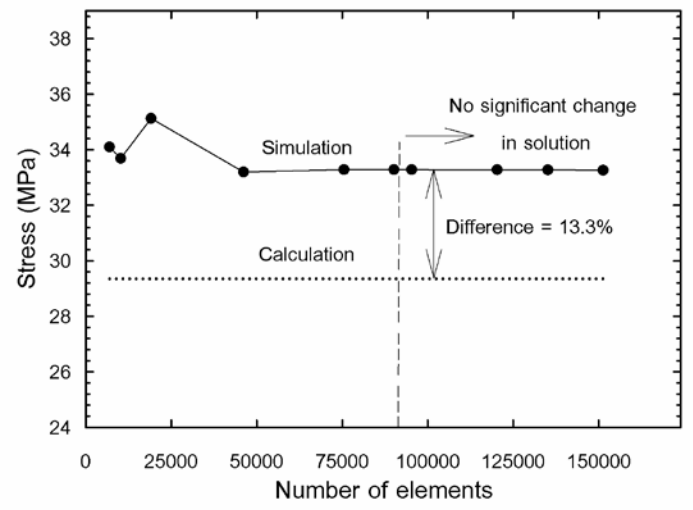

Figure 3.19 Grid independent study and validation for solution of quartz window at inside pressure of 100 bar.

The validation of the simulation results are also done by comparison with the calculation results shown in Table 3.7. The results illustrate that the differences between calculation and simulation of the maximum stress in CVCC and window are 2.2% and 13.3%, respectively. This difference will be cause of uncertainty in simulation results for the case studies.

Table 3.7 The differences between calculation and simulation results.

Part	Stress (MPa)		Difference (%)
	Calculation	Simulation	
CVCC	15.7	15.4	2.2
Window	28.5	33.5	13.3

The stress distribution on the combustion chamber and quartz window under pressure at 100 bar are shown in Figure 3.20 (a) and (b), respectively. To obtain the uniform and steady distribution on the walls, frictionless support is selected. The maximum stress in combustion chamber and quartz window are 47.2 and 36.3 MPa, respectively. The critical points are the edge of the small hole for combustion chamber and the edges for quartz window.

For the combustion chamber at critical point, safety factor is about 6.14, considered as half of the suggested value. However, the maximum stresses are far from the yield strengths of both materials. These material properties can be maintained during combustion because combustion with high temperature occurs in a very short time. Effect of temperature on safety factor of the CVCC is also analyzed. From Figure 3.21, it is clear that increasing temperature of CVCC decreases the safety factor, because increasing temperature of chamber results in decrease of the strength of material. However, the minimum safety factor is over 3.5 at chamber temperature of 500 K.

From strength analysis, it is assured that the CVCC and window can carry high pressure at design conditions. However, CVCC should be located in an explosion-protected room and operated from a distance (Baert, et al., 2009). The summary of CVCC and window geometry is shown in Table 3.8.

Table 3.8 The summary of CVCC and window geometry.

Constant volume combustion chamber	
Diameter, mm	100
Width, mm	45
Thickness, mm	60
Quartz window	
Diameter, mm	95
Thickness, mm	60

3.3.3 Effect of Inlet on Mixing of Pre-Charge

A mixing fan or stirrer can provides mixture homogeneity inside a combustion chamber, but there is a possibility of leakage along the shaft at high pressure. To avoid leakage along the shaft, the mixing fan is not included in the design. This is not a new concept for CVCC's as shown in previous works (Oren, et al., 1984; Fujiomoto, et al., 2005). However, gas inlet patterns that can enhance gas mixing are required to study in more detail. For this reason, four inlet patterns, illustrated in Figure 3.22, are studied by computational fluid dynamics (CFD) using AVL FIRE® software to obtain the proper inlet pattern for good mixing. Figure 3.23 shows the model for simulation. The example of mesh for case of tangential inlet is shown in Figure 3.24.

Table 3.9 shows initial and boundary conditions for computational fluid dynamics. Assumption used to simplify the model are following;

- Working fluid is the air.
- Air flow is considered as transient, turbulent and compressible flow.
- No slip wall condition is used for simulation.
- CVCC is treated as closed system and no leak of gas occurs in filling process.
- Ideal gas law is used for air.

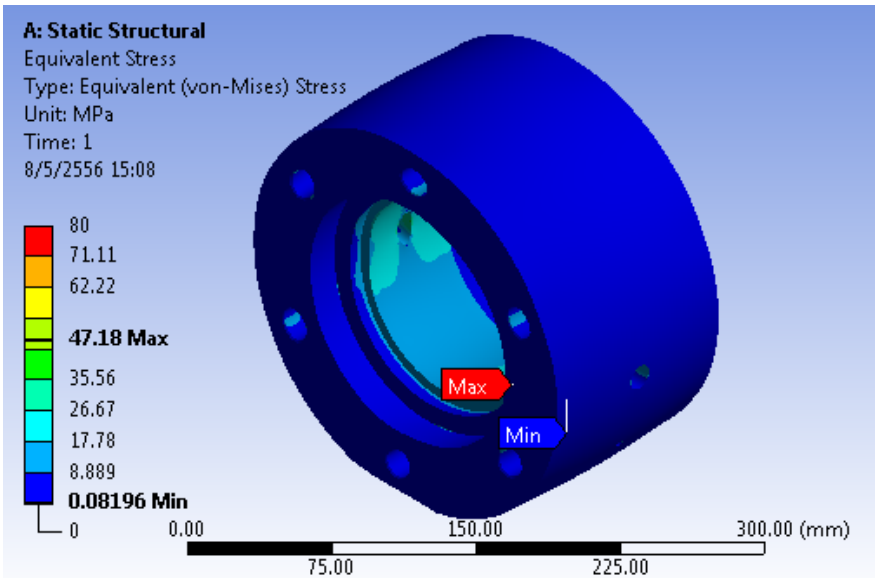

(a) Combustion chamber

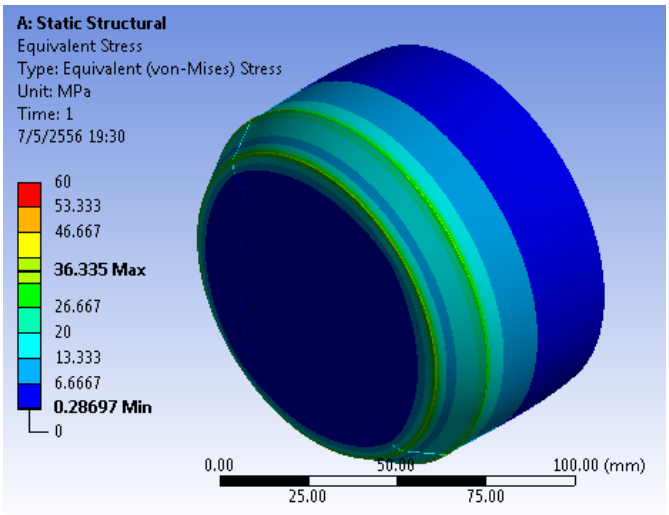

(b) Quartz window

Figure 3.20 Stress distribution on combustion chamber and quartz window under pressure of 100 bar.

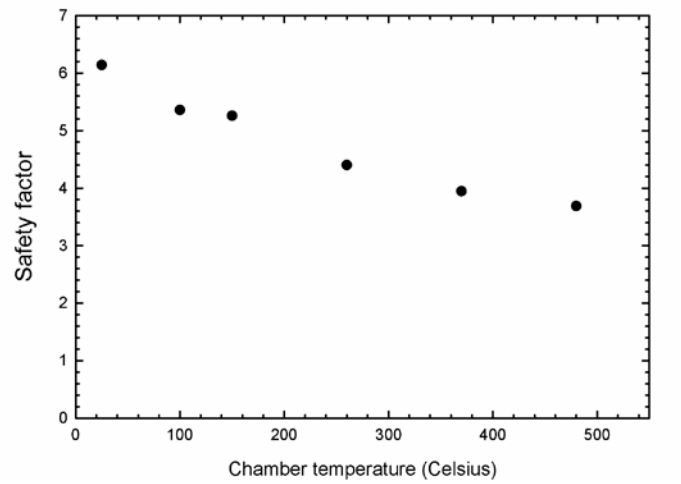

Figure 3.21 Effect of temperature on safety factor of combustion chamber.

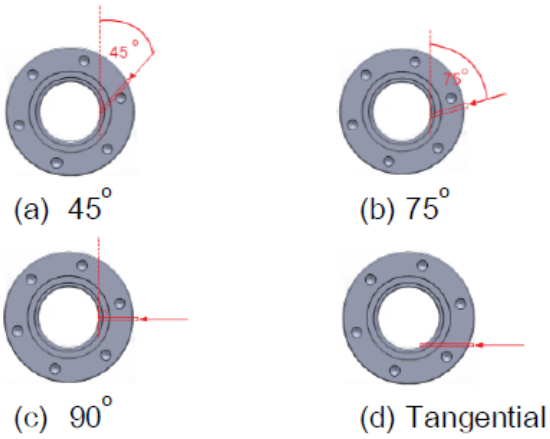

Figure 3.22 The models of CVCC for flow analysis.

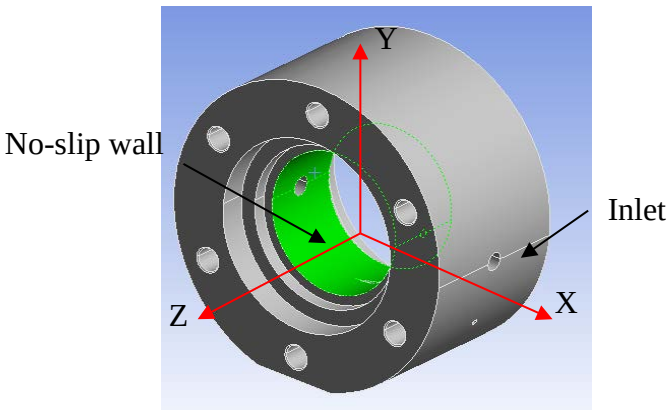

Figure 3.23 Model of chamber for CFD.

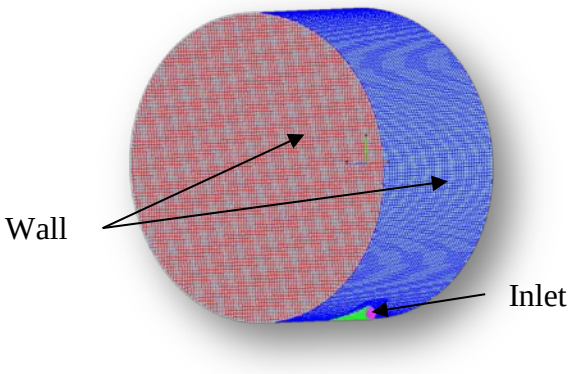

Figure 3.24 The example of Mesh for CVCC with tangential inlet.

Table 3.9 Initial and boundary conditions for computational fluid dynamics.

Initial conditions	
Pressure inside CVCC	P = 0 bar
No flow inside CVCC	U = 0, v = 0 and w = 0 m/s
Boundary conditions	
Wall temperature	T_w = 300K
Inlet pressure	P_{inlet} = 10 bar
Turbulent model - Turbulent kinetic energy - Turbulent dissipation rate	Standard k-ε K = 1 m^2/s^2 ε = 1 m^2/s^3

Due to the 3D model is simulated, it is quite difficult to analyze from 3D model. Therefore, it is better to illustrate the results in 2D plane. The results are broken down into 2D plane in axis z as shown in Figure 3.25.

Figure 3.26 shows total pressure inside the chamber in z axis at 0.1 s to 0.9 s after start of injection. Total pressure rises slower with time for the tangential inlet than other models. This means that individual gases injected inside CVCC with tangential inlet have more time to mix and become a homogeneous mixture. The velocity profiles are different for four inlets as shown in Figure 3.27. The tangential inlet shows the most uniformity of velocity inside the chamber compared with others.

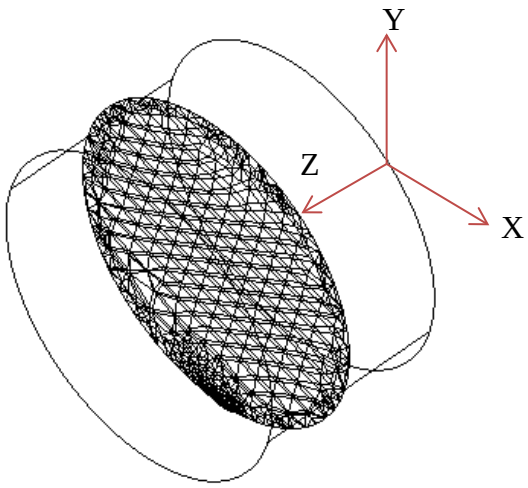

Figure 3.25 Plane for illustration of flow.

The turbulent kinetic energy is also higher at the centre for the tangential inlet than other models as observed from Figure 3.28, which suggests that the gaseous mixture inside is more homogeneous. From the simulation results, it is expected that CVCC model with tangential inlet is better than other models.

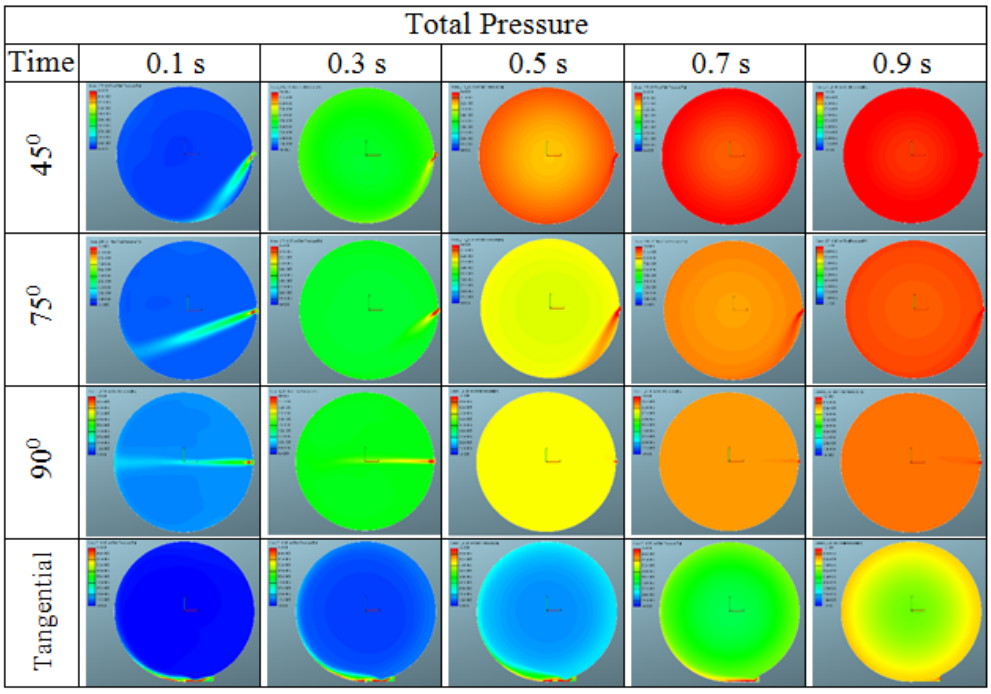

Figure 3.26 Total pressure inside CVCC with different injection angle at 0.1 s to 0.9 s after start of injection.

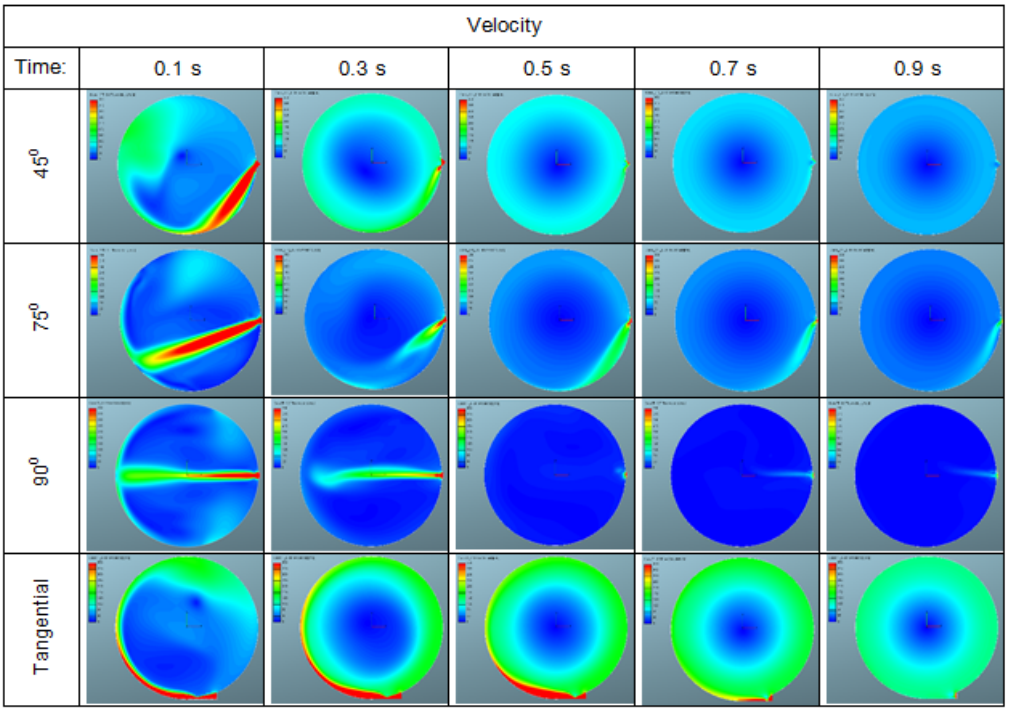

Figure 3.27 Velocity profile inside CVCC with different injection angle at 0.1 s to 0.9 s after start of injection.

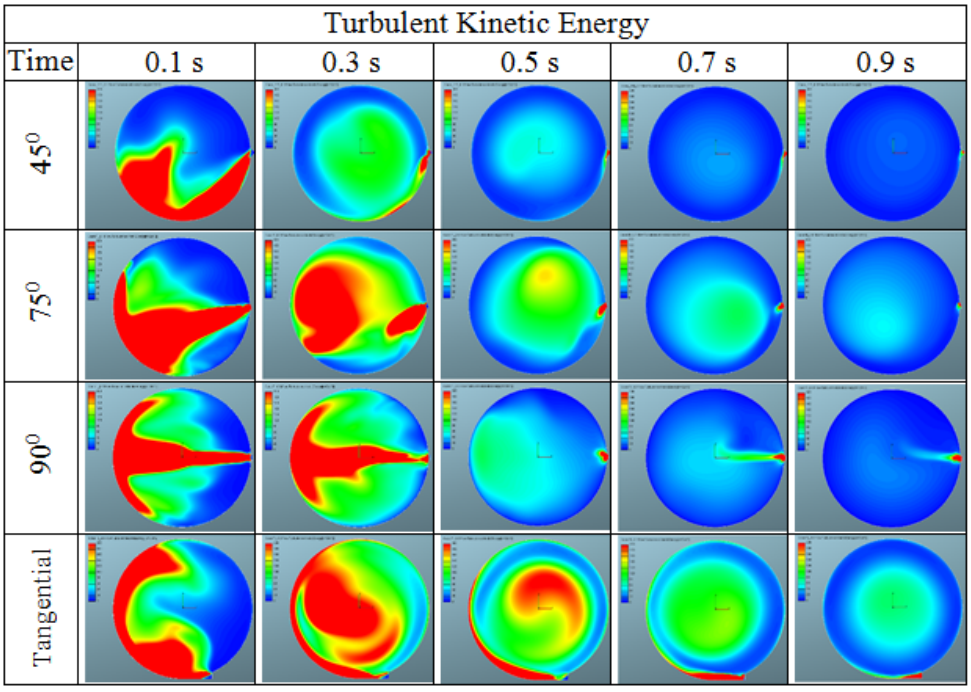

Figure 3.28 Turbulent kinetic energy for different injection angle at 0.1 s to 0.9 s after start of injection.

Figure 3.31 show mean turbulence kinetic energy distribution. The value of turbulent kinetic energy inside CVCC for each of injection angle of 45^{o}, 75^{o} and 90^{o} is higher than that of the tangential inlet initially after the start of injection. However, the value of turbulence kinetic energy for the tangential inlet is higher than that of other injection angle at time 0.4 s after the start of injection, which suggests that the gaseous mixture inside the CVCC with tangential inlet is more homogeneous. So, it is expected that CVCC model with tangential inlet is better than other models.

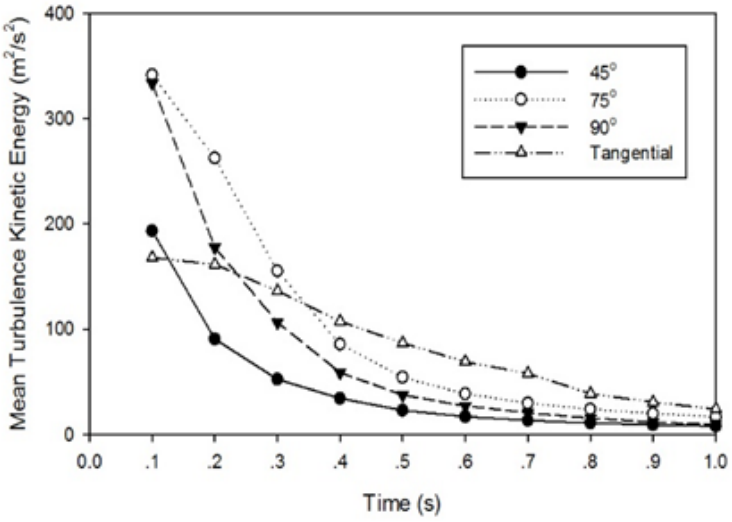

Figure 3.29 Mean turbulence kinetic energy distribution.

3.4 Constant Volume Combustion Chamber Geometry

From the systematic design, constant volume combustion chamber with tangential inlet for good mixing has been selected. From analysis of free spray and strength of materials, diameter and depth of cylindrical-shaped combustion chamber are selected as 100 mm and 45 mm, respectively, as shown in Figure 3.30. Full details of drawing are shown in Appendix A1.

Figure 3.31 shows an assembly of CVCC and miscellaneous devices, i.e. spark plug, static pressure transmitter, inlet and outlet valve.

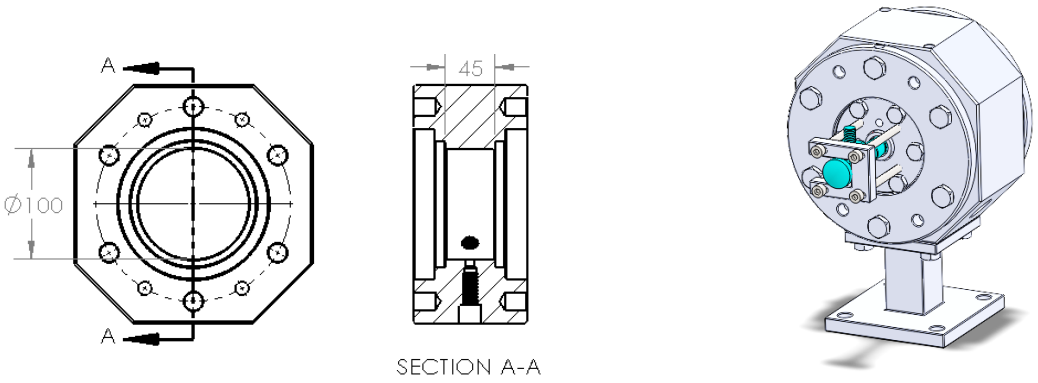

(a) CVCC diameter ans depth support

(b) CVCC with head and

Figure 3.30 Constant volume combustion chamber geometry.

3.5 Preliminary Test

3.5.1 Leak Test

The CVCC filled by nitrogen with high pressure of 70 bar was immersed in the water for 30 minutes. It was found that there is no leakage occurred during soak in water.

3.5.2 Strength Test

Hydraulic oil was used instead of gas. Oil pressure of 150 bar that is 1.5 time of design pressure is used to test the strength of CVCC for 30 minutes. Hydraulic oil was pressurized in CVCC by hand pump. Rupture disk was replaced by its dummy, because test pressure is higher than the limit of rupture disk. It was shown that CVCC can hold high pressure with no damage of material during and after tests.

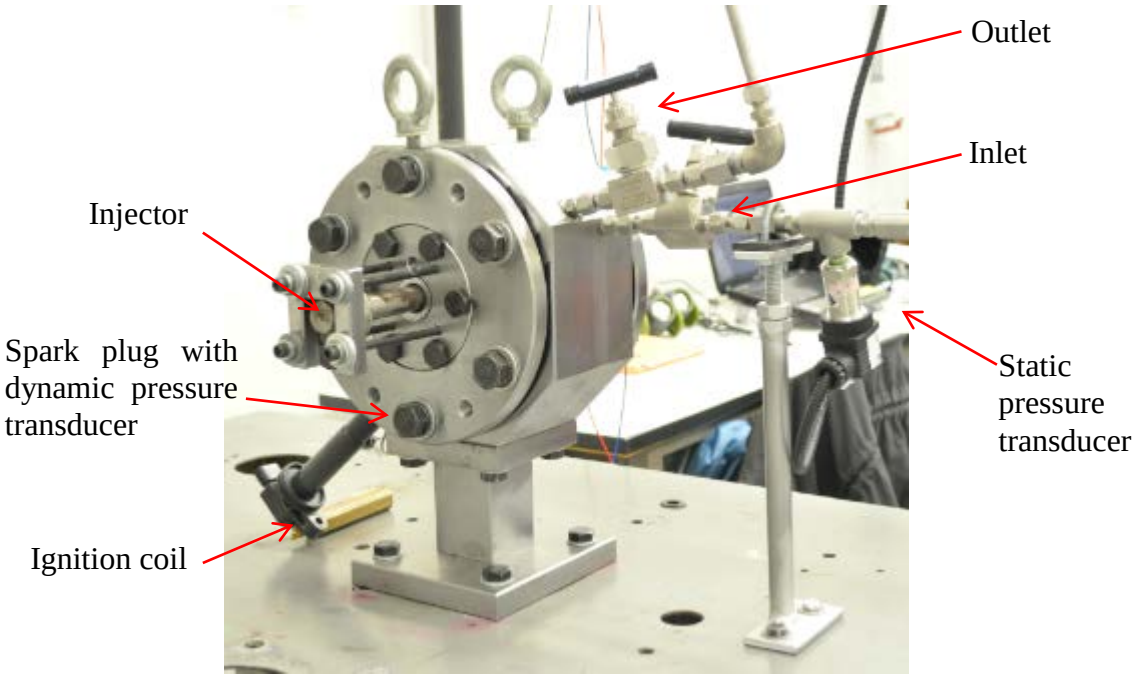

Figure 3.31 CVCC and miscellaneous devices.

3.5.3 Safety Device Test

Hydraulic oil was also used for testing explosion of rupture disk. Again, hydraulic oil was filled into CVCC equipped with the rupture disk by hand pump until the rupture disk burst. It was found that rupture disk will be broken at pressure of 110 bar. It is assured that this rupture disk can protect CVCC and other device from over pressure.

3.5.4 Pre-Combustion Test

Figure 3.32 shows a schematic diagram of a CVCC with pre-combustion technique consisting of injection system, ignition system, gas system, data acquisition and controller. The real setup for CVCC with pre-combustion technique are illustrated in the Figure 3.33.

Volume of CVCC is 353.4 cm^3 with diameter of 10 cm. Denso ignition coil was used for ignition system. Denso common rail system is also used. Injection pressure can be varied from 20-160 MPa. ADZ Nagano pressure transmitter Model-ADZ-SML-10.0 measuring in the range of -1 to 20 bar with accuracy 1% of full scale is used to measure static pressure during filling process. NI-DAQ is used for transferring and monitoring the static pressure to a computer. Dynamic pressure during combustion is measured by a piezoelectric pressure transducer Kistler model 6052C which is equipped with Kistler

spark plug model 6117B. Pressure data from Kistler model 6052C is monitored and recorded by a digital storage oscilloscope Tektronik model TDS2024C with maximum sampling rate 2GS/s on all channels. Wiring diagram of all devices is shown in Appendix A.2. In gas line, flame arrester is used to protect the gas cylinder in case of flash back. A rupture disk One-half 20 model-RD2-1.5M is used to limit the pressure inside the chamber. It will be exploded when inside pressure is over 110 bar. Swagelok needle valves are used for inlet and outlet. These valves can be used at high pressure and temperature up to 10000 psig (689 bar) and 850°F (454°C), respectively. Viton® or fluorocarbon O-ring is used for all sealing.

A lean combustible gas consisting of 5.1% C_2H_2, 33.75% O_2 and 61.7% N_2 at equivalence ratio (ϕ) 0.38 is used for making the diesel engine like-conditions by pre-combustion technique. With this technique, the high pressure and temperature products after pre-combustion are similar to the compressed air at TDC of diesel engine. Oxygen content is remained 21%mol after combustion (Baert, et al., 2009). The procedure for experiment shows below.

- CVCC is vacuumed by the vaccum pump.
- To avoid the explosion during filling process, acetylene (C_2H_2) is added first. Nitrogen is following. Finally, oxygen is added. The partial pressure of each gas is used for filling. Premixed charge compositions of C_2H_2, N_2 and O_2 are 5.1%, 33.2% and 61.7 % by volume, respectively. This composition results in 21% molar oxygen in its product after pre-combustion (Baert, et. al., 2009).
- After filling process, lean combustible gas is left for 2 minutes for mixing.
- When trigger button is pressd, the spark plug ignites the lean mixture to create the simulated compressed air in CI engine that has higher pressure and temperature. At desired condition, injector is energized to inject the test fuel resulting in combustion that is similar to CI engine combustion. The operating sequence is controlled by the micro controller with ARDUINO software. ARDUINO code is shown in Appendix A3. During combustion process, all data, i.e. trigger signal, injection signal and pressure inside CVCC, are recorded by the osciloscope.
- After combustion, exhaust valve is manually opened. Then nitrogen is used to purge the exhaust and flush spark plug.

To study combustion of ethanol under CI engine conditions, the required temperature to promote autoignition of hydrous ethanol without ignition improver is at least 900 K (Siebers and Edwards, 1987). This is the representative of polytropic compression with polytropic index (n) 1.35 from ambient conditions, i.e. air temperature of 25 ^{o}C and pressure of 1 atm, through compression ratios as high as 23:1. However, to obtain ignition delay and the rate of pressure rise during premixed combustion comparable with those for current diesel fuels when used in conventional diesel engines, in-cylinder temperatures of 1100 K is required for ethanol at injection (Siebers and Edwards, 1987). To achieve 1100 K at injection from ambient conditions using polytropic compression, the CI engine would require compression ratios in excess of 40:1, which is not practical in the typical CI engines. However, this condition is possible in CVCC with pre-combustion technique. Therefore, the target temperatures in this study are set as 900 and 1100 K. Preliminary test of pre-combustion of the lean combustible gas is required to provide the suitable time after pre-combustion for the target temperatures.

Figure 3.34 shows pressure history of 20 tests of lean combustible gas with initial absolute pressure of 9.35 bar. The initial pressure of 9.35 bar is selected to check repeability after a number of test shown in Appendix A.4. The results show that the variation of pressure trace is less than 4% during combustion duration.

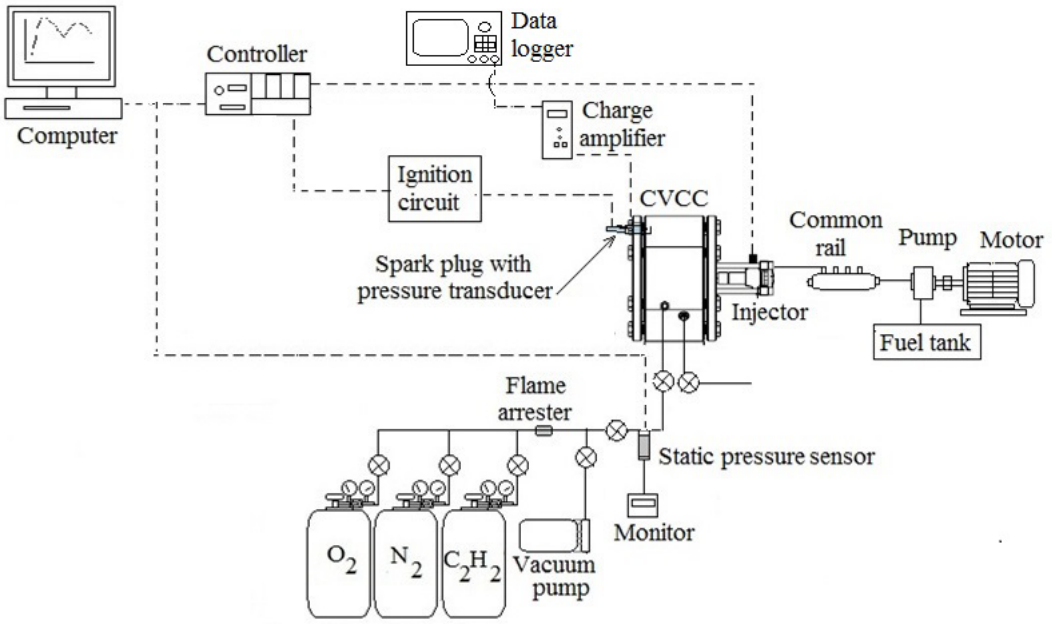

Figure 3.32 Schematic diagram of CVCC with pre-combustion technique.

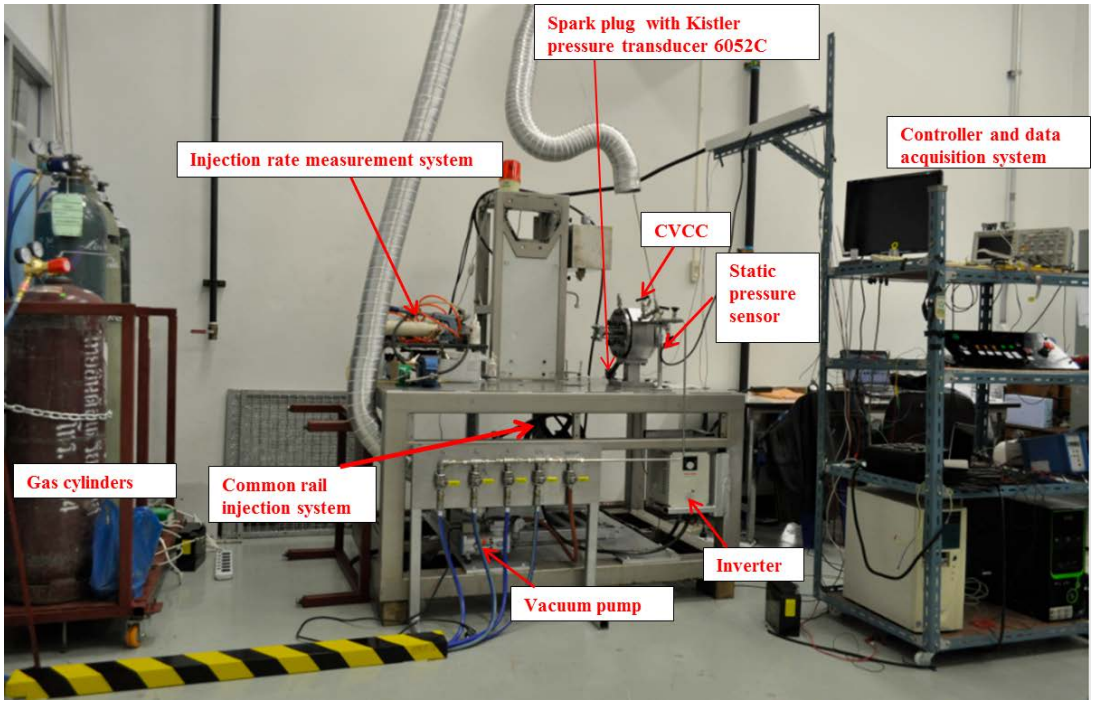

Figure 3.33 Experimental setup for the combustion study under CI engine conditions using CVCC with pre-combustion technique.

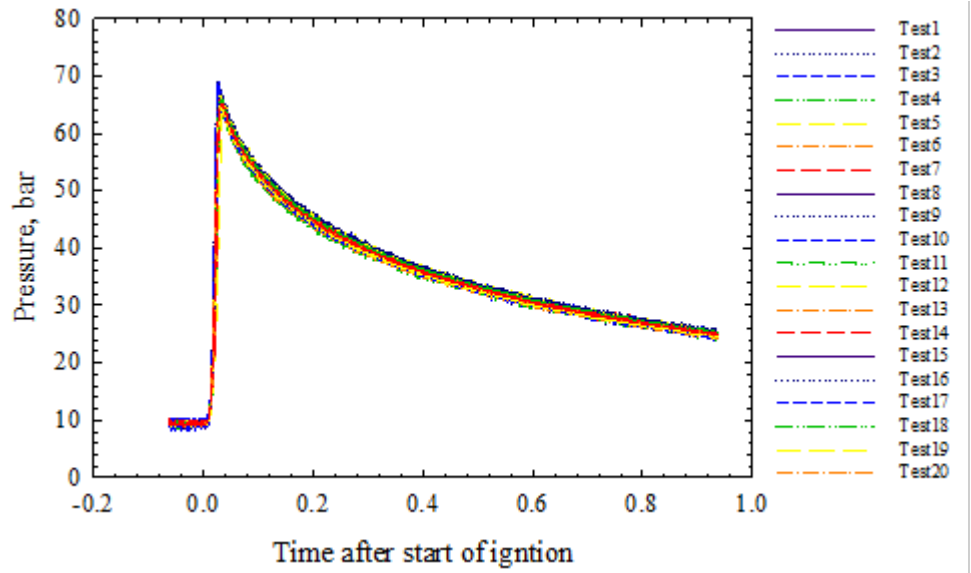

Figure 3.34 Pressure history of lean combustible gas at initial pressure of 9.35 bar.

Gas temperatures can be calculated from the pressures using the folowing assumptions.

- Complete combustion of lean mixture is assumed for pre-combustion. The chemical equation for complete combustion of lean mixture shown in Equation (3.9).

$$0.051C_2H_2 + 0.3375O_2 + 0.617N_2 \rightarrow 0.102CO_2 + 0.051H_2O + 0.617N_2 + 0.21O_2 \quad (3.9)$$

- Ideal gas is considered for the combustion products in CVCC as same as the previous works (Oren, et al., 1984; Baert, et al., 2009; Siebers and Edwards, 1987; Lee, et al., 2004; Nguyen and Honnery, 2008; Nguyen, et al., 2010; Fujiomoto, et al., 2005).The compressibility factor (Z) could be neglected in the range of interest, i.e. 900 to 1100K as shown in Appendix A.5.

With these assumptions, bulk gas temperature of combustion products, which depends on gas pressure and molecular weight, can be calculated by using equation (3.10).

$$T_{bulk} = T_{int}\frac{P_{bulk}}{P_{int}}\mathrm{M} \quad (3.10)$$

Where

T_{bulk} Bulk gas temperature of combustion products (K)

T_{int} Initial temperature of the unburned premixed charge (K)

P_{bulk} Bulk gas pressure of combustible gas (N/m^2)

P_{int} Initial pressure of the unburned premixed charge (N/m^2)

M Ratio of molecular weights of the combustion products and the premixed charge

Figure 3.35 shows the calculated temperature averaged from 20 tests using data from Figure 3.34. Burnt gas temperatures reach the target temperatures of 1100 and 900 K after start of ignition of 502 and 751 ms, respectively. These time will be used for programing fuel injection as shown in Appendix A.4.

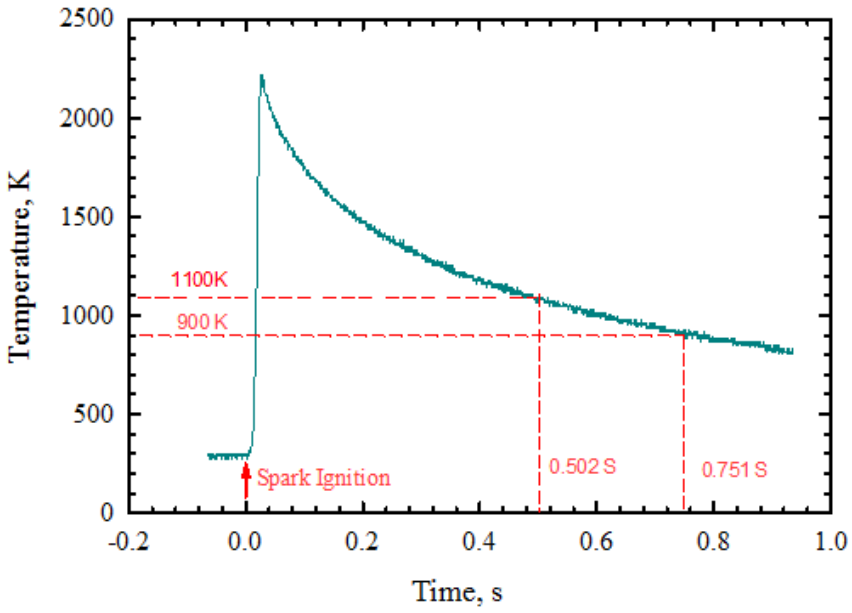

Figure 3.35 The average temperature of pre-combustion period from 20 tests at initial pressure of lean combustible gas of 9.35 bar (ϕ =0.38).

3.6 Summary

From the systematic design, the design criteria cover the typical value of CI engines with compression ratio 16-28 at high pressure of 100 bar. The summary of CVCC feature and target conditions for ethanol combustion study can be drawn in Table 3.10 and Table 3.11, respectively.

Table 3.10 Summary of CVCC feature.

Cylindrical CVCC with tangential inlet	
Diameter, mm	100
Width, mm	45
Thickness, mm	60
Quartz window	
Diameter, mm	95
Thickness, mm	61.7

Table 3.11 Summary of target condition for ethanol combustion study.

Gas temperature, K	Injection timing (time after trigger), ms
900	751
1100	502

CHAPTER 4
COMBUSTION CHARACTERISTICS OF HYDROUS ETHANOL WITH IGNITION IMPROVERS UNDER CI ENGINE CONDITIONS

4.1 Introduction

Ethanol can be used as fuel not only in spark ignition engines but also in diesel engines that obtain higher thermal efficiency. Ethanol fuelled diesel engine buses have been used for public transportation in Sweden since 1984 (Egeback, 1993), facilitating the development and years of continual improvement of ethanol buses and trucks. A European project named BioEthanol for Sustainable Transport (BEST) promoted the use of city buses equipped with commercial ethanol CI engines fuelled by commercial ethanol fuel (ED95 : composes of 95% hydrous ethanol and 5% commercial additives by volume) from 2006 to 2009 (Fenton and Carlsson, 2010). The project demonstrated that ethanol can be substituted for a significant percentage of the fossil fuels used for transport in Europe (Fenton and Carlsson, 2010; Birath, 2007) and Brazil (Velázquez, et al., 2009; Moreira, et al., 2008). In 2010-2011, a similar demonstration project was launched for public transportation in Thailand, further contributing to the development of sustainable fuels (Laoonual, 2013; Chollacoop, et al., 2013). Ethanol combustion in CI engines showed satisfied performance (Egeback, 1993; Birath, 2007; Velázquez, et al., 2009; Moreira, et al., 2008; Fenton and Carlsson, 2010) and promising reduction of particulate matter and NOx (Hardenberg and Schaefer, 1981; Nord, et al., 2004; Rodríguez-Fernández, et al., 2009; Saitoh and Uchida, 2004; Haupt and Nord, 2009; Haup, et al., 2004; Hansen, et al., 2004) compared with diesel fuel.

However, using ethanol in CI engines produces poor ignition due to difficulties in simultaneously achieving suitable concentration and temperature for self-ignition in a spray mixture formation (Saitoh and Uchida, 2007 and 2009). The main reasons of poor ignition quality are its properties. In comparison with conventional diesel fuels, ethanol has smaller stoichiometric air/fuel ratio and larger latent heat for evaporation, which require higher energy to evaporate. With poor quality of ignition, ethanol has longer ignition delay than that of diesel fuel. In case of long ignition delay, most of fuel is

injected before ignition start. It provides a large mixing between fuel and air leading to a rapid pressure rise when combustion occurs with high peak pressure. This produces audible knocking sound referred to diesel knock. In addition, as ignition start too late in expansion stroke, incomplete combustion, reduced power output and poor fuel conversion efficiency are occurred (Saitoh, 2009). Nevertheless, ethanol and hydrous ethanol with water content 10%v are auto-ignited approximately 900 K, but a temperature of 1100 K is required to generate sufficiently short ignition delay which produces suitable rate of pressure rise for diesel engine (Siebers, 1987). The typical CI engines are difficult to obtain a temperature of 1100 K. Therefore, to utilize ethanol in CI engines, the improvement of engine or fuel is required. Various techniques for the use of ethanol have been reviewed by Ecklund et al. (1984). They concluded that for displacement of diesel fuel shortages during short-term, ethanol-diesel solution and emulsion could best be employed, but these techniques are limited by the separation of fuel and small percentages of diesel replacement (less than 25%). In the moderate length shortages of diesel, dual fuel techniques including fumigation and pilot injection are better and easy to switch back to dedicated diesel engines. Ethanol percentage for fumigation and pilot injection techniques can be used up to 50% and 90%, respectively. If the total substitution of diesel fuel is interested, the use of spark assisted device or ignition improvers for ethanol is required for total replacement of diesel. From the view point of use, ignition improvers are a more practical solution with minor engine modifications, e.g. increasing compression ratio and injector nozzle hole, required to achieve viable engine output. Ignition improvers must be miscible with ethanol. The effective ignition improvers are thermally unstable, readily creating free radicals, which accelerate thermal decomposition and chain branching reaction of the main fuel stimulating the auto-ignition (Nord, et al., 2004). A number of ignition improvers were tested in unmodified diesel engines (Hardenberg and Schaefer, 1981; Schaefer and Hardenberg, 1981; Hardenberg and Ehnert, 1981). The results concluded that nitrate-based additives have a strong effect on the ignition of alcohol. Simonsen and Chomiak (1995) also concluded that nitrate ester as ignition improver with the trade name AVOCET is most efficiency improver. However, the use of nitrate-based improvers has some disadvantages including potential for increased corrosion; possibility of explosion; toxicity; wearing; and NO_x emission. Furthermore, this improver production had been stopped. For this reason, polyethylene glycol in the trade name BERAID is used to replace nitrate-based improver with various contents. In comparison of the use

of 7% BERAID (polyethylene glycol) and 2% AVOCET (nitrate ester), they showed the same ignition delay with no difference at the price. Unfortunately, the solubility of polyethylene glycol is a problem when the ambient temperature is approximate 0 ^{o}C. More recently, a commercial ethanol fuel (ED95) developed by SEKAB Biofuels & Chemical AB, has been used for the ethanol buses and heavy duty diesel engines. ED95 fuel consists of 95% hydrous ethanol and 5% commercial additive for ED95 (not nitrate-based additives), which contains the components to act as lubricant, corrosion inhibitor and ignition improver, i.e. Beraid 3555 (main component is glycerol ethoxylate) (Laoonual, 2013). The effect of the glycerol ethoxylate on ignition delay of ethanol was shown by Lif and Svennberg (1997). The ignition delay of hydrous ethanol fuel for CI engine is essentially shortened by glycerol ethoxylate. Beside the commercial ignition improvers, diethyl ether (DEE) and biodiesel are interesting, because they are renewable fuels and have suitable properties for diesel engines. Bailey et.al. (1997) has reviewed the possibility of diethyl ether (DEE) as a renewable diesel fuel. They concluded that DEE is a potential replacement fuel for compression ignition engines. But additional information is required on emission and performance of the use DEE as a neat fuel and blended fuel in diesel engines. Zhu et al. (2011) used biodiesel-ethanol blends as fuels for CI engine. They indicated that the biodiesel and biodiesel-ethanol blends have higher brake thermal efficiency in comparison with Euro V diesel fuel.

However, little is known about the effect of ignition improvers on emissions. The emissions from the ethanol CI engines should not be considerably affected by the additives. This is one of the requirements for an additive of ethanol used in diesel engines (Schaefer and Hardenberg, 1981). The change of injection characteristic of fuel (injection delay, injection rate and discharge coefficient) in CI engine is possible to change the quality of the fuel-air mixing process, which relies on the development of spray (Benajes, et. al., 2005) affecting combustion phenomena and emissions (Bower and Foster, 1990). Benajes, et. al. (2005) revealed that the different injection rate of diesel affects on spray penetration. The square type injection rate shows faster penetration than the ramp and boot type injection rate. Bower and Foster (1990) showed that KL factor, which represents soot concentration, was greatly sensitive to the injection rate, while flame temperature was insensitive to the injection rate.

From the literature, glycerol ethoxylate, biodiesel and DEE are expected to improve the ignition quality of ethanol, but the injection ad combustion characteristics of high blend ethanol using these ignition improvers have not been extensively studied, particularly ethanol injection using the common rail injection system that has high injection pressure. For this reason, this chapter shows the injection and combustion characteristics of hydrous ethanol with the promising ignition improvers and commercial additives under CI engine conditions. The effects of ignition improvers on injection characteristics, i.e. injection rate, injection delay and discharge coefficient, are investigated in an injection system using Zeuch method before combustion study to control the constant energy input and find the time of start of injection. Combustion characteristics, including ignition delay, combustion pressure, heat release rate, cumulative heat release, combustion efficiency and maximum rate of pressure rise, under CI engine conditions are investigated in the constant volume combustion chamber (CVCC) and the rapid compression and expansion machine (RCEM). CVCC is used to study the combustion characteristics with a wide range of the test condition, but RCEM is used to study combustion characteristics, flame temperature, KL factor and soot emission at more specific condition.

4.2 Methodology

4.2.1 Injection Characteristics

Injection characteristics including injection rate, injection delay and discharge coefficient are studied. Injection rate measurements are performed by Zeuch's measuring method (Bower and Foster, 1991; Marcic, 2006). With this method, the test fuel is injected into a constant volume chamber filled with test fuel at a certain pressure. The chamber pressure is increased in proportion to the injected fuel. Using bulk modulus of elasticity of the fuel and the conservation of the mass, injection rate can be estimated by equation (4.1).

$$\frac{dm}{dt} = \rho_f \frac{V}{K} \frac{dP}{dt} \tag{4.1}$$

where

$\frac{dm}{dt}$ Mass flow rate (kg/s)

ρ_f Fuel density (kg/m^3)

V Chamber volume (m^3)

K Modulus of compressibility (Pa)

$\frac{dP}{dt}$ Rate of pressure changed in chamber (Pa)

Figure 4.1 shows a typical fuel injection rate profile of ethanol, which is injected by a single hole injector from a common rail injection system, obtained by using equation (4.1). The injection rate curve can be divided into four stages, i.e. injection delay, needle opening (transitional zone), stabilized zone and needle closing (transitional zone). The injection delay is the period between start of energizing (SOE), i.e. supplying voltage for injector, and start of injection (SOI) where injection rate recover from the negative value. Injection rate shows the negative value just prior SOI, because the volume of system is changed due to needle lift yielding pressure of chamber decrease. The stabilized zone where the injector needle is completely opened is between needle opening and closing.

Discharge coefficient (Cd) is defined as the ratio of the measured mass flow rate to the theoretical mass flow rate computed from Bernoulli equation. This dimensionless parameter shows the efficiency of the nozzle fuel release (Payri, et al., 2012). The discharge coefficient of each fuel is estimated from equation (4.2).

$$C_d = \frac{\dot{m}_f}{\dot{m}_{th}} = \frac{\dot{m}_f}{A\sqrt{2\Delta P \rho_f}} \tag{4.2}$$

where

$\dot{m}_f$ Measured mass flow rate (kg/s)

$\dot{m}_{th}$ Theoretical mass flow rate (kg/s)

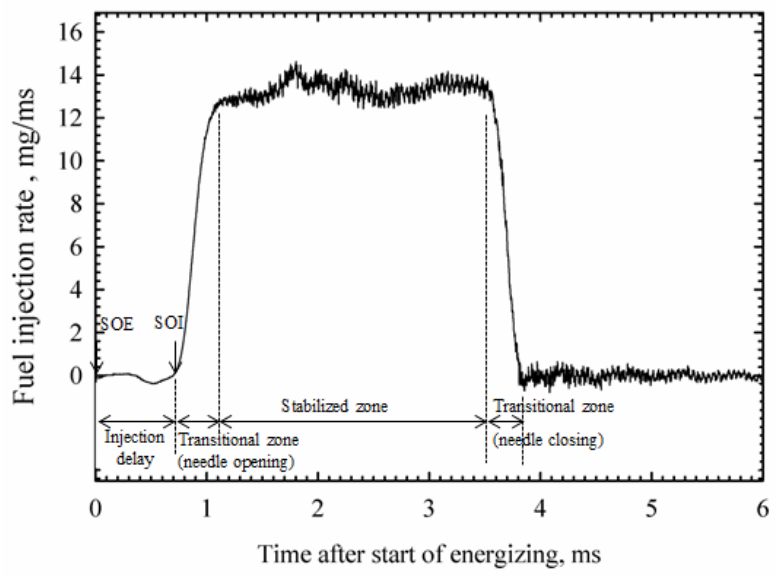

Figure 4.1 Typical fuel injection rate profile of ethanol at Pinj=900 bar injected by single hole injector using for common rail injection system.

4.2.2 Ignition Delay Determination

Ignition delay is the time interval between the start of injection (SOI) and the start of combustion (SOC). The start of combustion is more difficult to precisely determine and many approaches exist. Simonsen and Chomiak (1995) noted that all measurements are comparative. The methodology is applied consistently across all fuels tested. Previous works' definitions of the ignition delay and the start of combustion, with conditions and instrumentation is summarized in Table 4.1.

In this study, the start of combustion is defined as the pressure recovery point, shown in Figure 4.2. The calculation of the start of combustion was performed for each test and averaged.

The ignition delay for neat ethanol may also be estimated by the global expression for the ignition delay (in seconds), proposed by Curran, et al. (1992). This expression depends on the temperature and concentration of reactant and oxidizer, shown in the equation (4.3).

$$\tau = 10^{-14} exp\left(\frac{15500}{T}\right)[C_2H_5OH]^{-0.315}[O_2]^{-0.78}[Ar]^{+0.259} \quad (4.3)$$

where

τ Ignition delay (ms)
T Ambient gas temperature (K)
[ ] Substance concentration (mol/cc)

Notice that this expression can be used only for pure ethanol, obtained by experiment in a shock tube at the shock post-pressure range 2 atm to 4.5 atm and temperature range 1100 K to 1900 K.

Table 4.1 The definitions of the ignition delay and the start of combustion.

Investigator	Definitions of the ignition delay and the start of combustion	Fuel	Conditions				Measured ignition delay range (ms)
			Apparatus	P_g (MPa)	T_g (K)	P_{inj} (MPa)	
Sieber, et al. (1987)	Two definitions of ignition delay were referred to in the results: a) The pressure delay is defined as the time between injector opening and a combustion chamber pressure rise of 0.25 atm above the pressure that would have existed in the chamber had no fuel been injected. b) The luminous delay is defined as the time from injector opening until the first luminosity is sensed by the photodiode.	Ethanol and ethanol with 10% by volume of water	CVCC	2 to 7	900 to 1500	12 to 18	a) 1 to 30 b) 0.5 to 30
Lee, et al. (1993)	The ignition point is defined as the inflection point in the pressure rise during ignition.	Ethanol	RCM	3.01 to 3.39	750 to 1000	n.a.	1 to 10
Simonsen and Chomiak (1995)	a) The start of combustion was defined as the point at which the heat release rate exceeds 5 kJ/(kg °C.A.) (for single cylinder CI engine). b) The ignition delay is defined as the time required to reach a pressure increase of 1 bar above the initial pressure (for CVCV).	Ethanol with additives	a) Diesel engine (CR 16.9) b) CVCV	a) n.a. b) 4.5	a) n.a. b) 798	a) 23 b) 50	a) 0.18 to 0.62 b) 2 to 8.2
Allard, et al. (1996, 1997)	The ignition delay is defined as the time interval between the time of initial needle lift and the time of combustion pressure recovery point.	Diesel	CVCV	2.4 to 4.8	645 to 867	n.a.	3.8 to 6

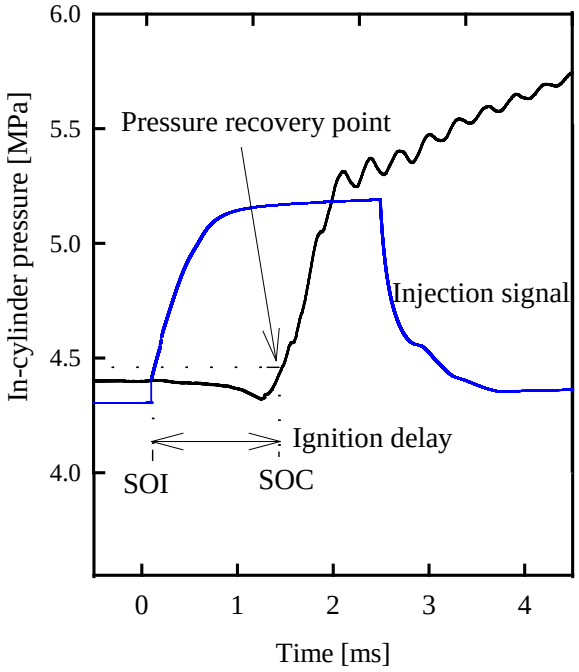

Figure 4.2 Determination of ignition delay time by pressure histories and injection signal.

4.2.3 Heat Release Rate

The constant volume combustion chamber (CVCC) was considered as a closed system. There have been no leakage from CVCC. Heat release rate can be determined from the first law of thermodynamics of the closed system (Heywood, 1988) shown in equation (4.4).

$$\frac{dQ}{dt} = \frac{\gamma}{\gamma-1} p \frac{dV}{dt} + \frac{1}{\gamma-1} V \frac{dp}{dt} \tag{4.4}$$

where

$\frac{dQ}{dt}$	Heat release rate (J/s)
V	In-cylinder volume (m^3)
P	In-cylinder pressure (Pa)
γ	Specific heat ratio
t	Time (s)

However, $\frac{dV}{dt}$ can be neglected due to volume is constant. Therefore, heat release rate for CVCC is obtained:

$$\frac{dQ}{dt} = \frac{1}{\gamma - 1} V \frac{dp}{dt} \tag{4.5}$$

4.2.4 Two-Color Method

Flame temperature and KL factor (optical thickness of soot) measured by two-color method has become a common diagnostic tool for the evaluation of engine designs and technologies. The principle of the two-color method has been well summarized (Matsui, et. al., 1979; Zhao and Ladommatos, 1998). Therefore, a brief overview of the technique will be provided. Two-color method is based on the emission of soot formed in the flame inside the combustion chamber. The principle of the method is the measurement of the thermalradiation from soot particle at two wavelengths on the emission spectrum. The monochromatic radiant intensity from non-black body of the flame can be expressed in equation (4.6).

$$I_{(\lambda,T)} = \varepsilon_\lambda \frac{C_1}{\pi \lambda^5} \; exp\left(-\frac{C_2}{\lambda T}\right) \tag{4.6}$$

As with the monochromatic radiant intensity, it can also be expressed in terms of the apparent temperature, T_a, as shown in equation (4.7).

$$I_{(\lambda,T)} = \frac{C_1}{\pi \lambda^5} \; exp\left(-\frac{C_2}{\lambda T_a}\right) \tag{4.7}$$

The modified equation for monochromatic emissivity of a soot cloud is given by equation (4.8) (Hottel and Broughton, 1932).

$$\varepsilon_\lambda = 1 - exp\left(-\frac{KL}{\lambda^\alpha}\right) \tag{4.8}$$

The monochromatic radiant intensity from equation (4.6) and (4.7) is equal. Replacing ε_λ by the right-hand side of equation (4.6), it is obtained:

$$1 - exp\left(-\frac{KL}{\lambda^\alpha}\right) = exp\left\{\left(-\frac{c_2}{\lambda}\left(\frac{1}{T_a} - \frac{1}{T}\right)\right)\right\}$$

$$KL \; = -\lambda^\alpha \ln\left[1 - exp\left\{-\frac{C_2}{\lambda}\left(\frac{1}{T_a} - \frac{1}{T}\right)\right\}\right] \tag{4.9}$$

where

ε	Emissivity
λ	Wavelength (nm)
K	Absorption coefficient
L	Path length
α	An empirical constant equal to 1.39 in the visible spectrum.
T	True temperature of the flame (K)
T_a	Apparent temperature of the flame (K)
$I_{(\lambda,T)}$	Monochromatic radiant intensity
C_1,C_2	First and second Planck constant

KL representing soot concentration can be assumed to be independent of wavelength for the small variations encountered when using this method. Therefore the measurement of two radiations at two distinct wavelengths enables solution for the variables KL and T, based on equation (4.9).

Although the combustion of ethanol in this work provides generally low luminosity of soot (because the oxygen content in ethanol contributes combustion), the luminosity is still useful and sufficient to find flame temperature and KL factor by two-color method.

4.3 Experiment Setup

4.3.1 Injection Rate Measurement

Injection rate was measured by a system using Zeuch method shown in Figure 4.3. It consists of common rail injection system, hand pump, constant volume chamber and data acquisition. To find injection rate, test fuel is filled into the constant volume chamber by hand pump until reach the desired pressure, i.e. the same pressure as in combustion test, measured by a static pressure transducer. Then test fuel is injected by the injection system, resulting in a steep pressure rise measured by a dynamic pressure transducer. Then injection rate can be calculated by replacing the measured dynamic pressure trace in equation (4.1). Then discharge coefficient (C_d) can be calculated by equation (4.2).

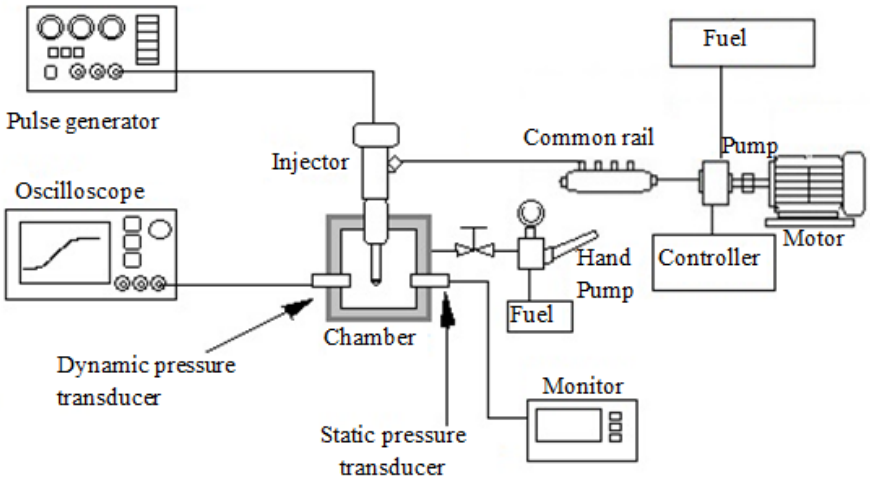

Figure 4.3 System for injection rate measurement using Zeuch method.

The combustion experiments can be devided into two parts. The first experiment was carried out in the constant volume combustion chamber (CVCC) with pre-combustion technique. The combustion characteristics, including ignition delay, heat release rate, combustion efficiency and maximum rate of pressure rise were investigated. The other experiment was performed in the rapid compression and expansion machine (RCEM). The combustion characteristics were also studied. In addition, flame visualization using the two-color method was applied to study flame temperature and soot formation. Then, soot emissions were measured after combustion.

4.3.2 The Experiment in CVCC

Figure 4.4 (a) shows schematic diagram for the experiment using CVCC. The equipment consist of CVCC, common rail injection system drived by motor, ignition system, gas system, data acquisition and controller. The important features of the CVCC are a very wide range of pressure and temperature conditions prior to injection with minimal quantities of test fuels, the possibility to simulate various levels of (simulated) EGR mass fraction (Baert, et al., 2009) and no effect of lubricant on HC the independent control of local wall temperature. The detail of measurement devices are shown in Chapter 3, section 3.5.4. A lean combustible gas consisting of 5.1% acetylene (C_2H_2), 33.75% O_2 and 61.7% N_2 at equivalence ratio 0.38 is used to create the CI engine conditions by pre-combustion technique. To avoid going into the explosion region during filling the gas, the order of filling is C_2H_2, N_2 and O_2. After pre-

combustion, oxygen content is remained 21%mol in the combustion product after pre-combustion (Baert, et al., 2009).

4.3.3 The Experiment in RCEM

The experiments were carried out in a rapid compression and expansion machine (RCEM) as shown in Figure 4.4 (b). The RCEM can simulate intake, compression, expansion and exhaust strokes of a single diesel cycle using an electrically controlled and hydraulically actuated driving system. The piston position can be detected by a displacement sensor. In this study the RCEM is only used to obtain high pressure and temperature at top dead center (TDC), where combustion occurs at the constant volume. The important features of the RCEM are accurate control of piston position at TDC, no effect of lubricant on HC and the independent control of local wall temperature. Tests can be performed over a wide range of operating conditions with easy access for optical diagnostics and minimal quantities of test fuels. The RCEM cylinder used as detailed in (Kobori and Kamimoto, 1995) has a 100 mm bore, stroke and clearance height of 150 mm and 20 mm respectively and compression ratio of 8.5. A flat piston is used to avoid turbulence in the combustion chamber during fuel injection. The synthetic air composed of 80% argon and 20% oxygen was prepared in a mixing tank at 180 ^{o}C, then entrained into the cylinder. Argon was used instead of nitrogen as it has a higher specific heat ratio. After synthetic air has been entrained into the cylinder it is compressed by piston from BDC to TDC within 30 ms. The piston is then held motionless at TDC for 150 ms to provide constant volume combustion chamber conditions. Gas pressure inside the combustion chamber is measured by piezoelectric pressure transducer (Kistler, 6125C01). Fuel is injected into the cylinder at constant pressure of 90 MPa via a single hole nozzle with diameter of 0.24 mm using a common rail system. Heat release rate is analyzed by equation (4.4) using the in-cylinder pressure. During combustion, the spray flame was imaged by high speed camera (NAC Memrecam GX-1), at 10000 frames per second and exposure time of 5 μs capturing an image of 476x464 pixels. The high speed camera is fit with a micro-Nikkor 55mm f/2.8 lens using aperture f/4 and an infrared filter (SIGMA KOKI-HAF-50S-15H). This filter transmits light in the visible region and absorbs the light in the infrared region, (i.e. 800 to 2000 nm), to allow study of flame temperature and KL factor the two - color method using equation (5.4). For two - color method, relationship between the photomultiplier output and apparent

temperature is calibrated by a blackbody furnace. Soot emission is measured by smoke meter (SOKKEN, model GSM3) after combustion.

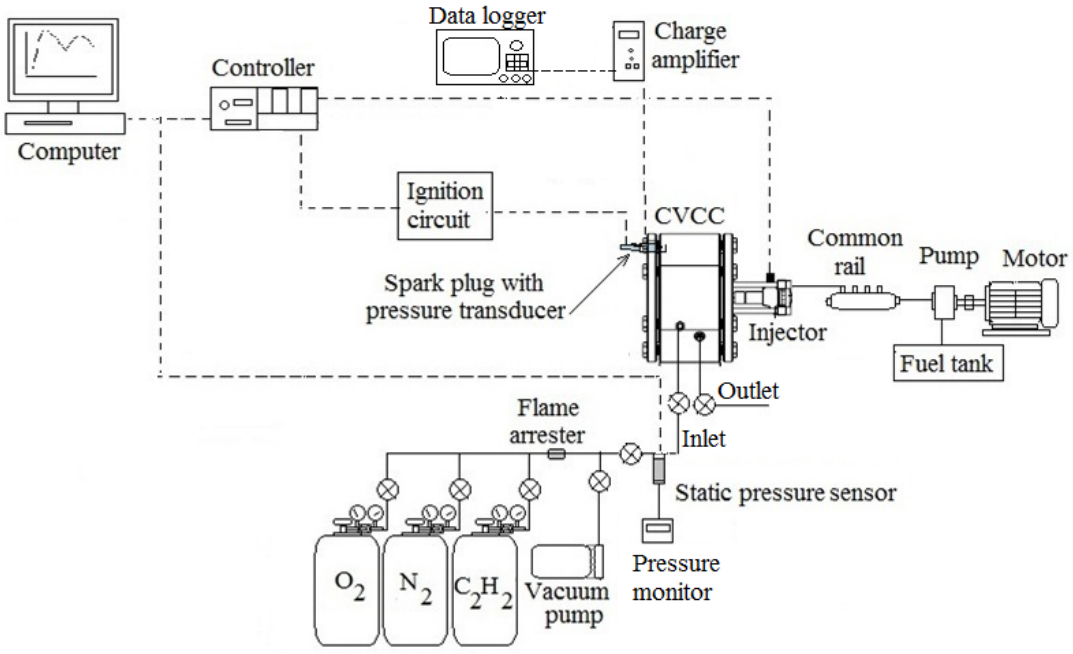

(a) System for combustion study using constant volume combustion chamber (CVCC)

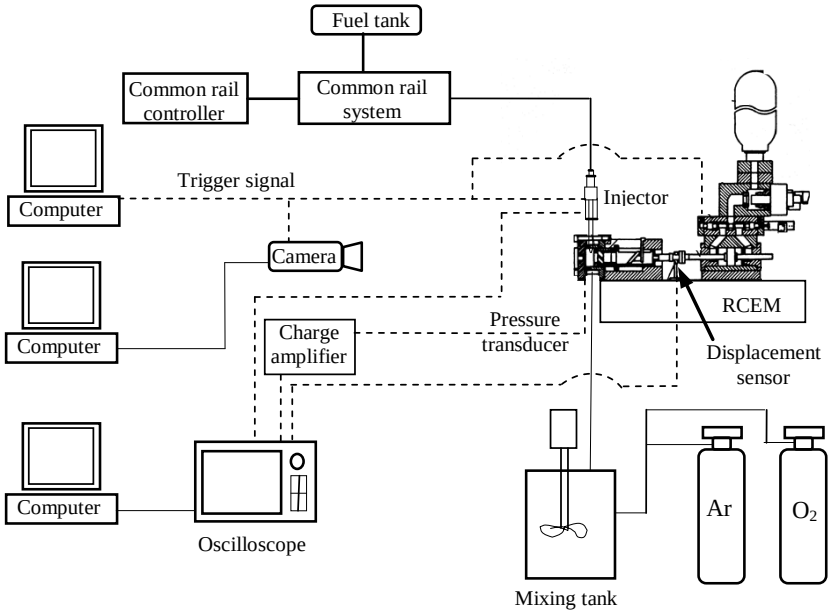

(b) Schematic diagram for combustion study using rapid compression and expansion machine (RCEM)

Figure 4.4 Schematic diagram of the combustion experiment.

4.3.4 Test fuels

The ignition improvers for hydrous ethanol are glycerol ethoxylate, biodiesel, diethyl ether and the commercial additive for ED95 produced by SEKAB Biofuels and Chemicals AB. Table 4.2 shows the components of the commercial additive for ED95. The commercial additive consists of denaturant, ignition improver, lubircant and corrosion inhibitor.

Table 4.2 Components of the commercial additive for ED95 (Laoonual, 2013).

Component Name	Function	Mixture by mass
95% Hydrous ethanol	Miscibility	40%-50%
Isobutanol	Denaturant	3%-6%
Beraid 3555	Ignition improver	40%-50%
Ethomeen O/12	Lubricity	7%-9%
Morpholine	Corrosion inhibitor	<0.2%

One of the scope of this work is that the lowest composition of alternative additives or ignition improvers is required. Therefore, the maximum composition of alternative additives is limited at 5% by mass in hydrous ethanol.

The eight fuels considered in this study are diesel; hydrous ethanol without ignition improver (Eh95); the ethanol dedicated for heavy duty vehicle (ED95: composed of 95% hydrous ethanol and 5% commercial additives by volume); hydrous ethanol containing 1% by weight of glycerol ethoxylate (1%GE); hydrous ethanol containing 3% by weight of glycerol ethoxylate (3%GE); hydrous ethanol containing 5% by weight of glycerol ethoxylate (5%GE); hydrous ethanol containing 5% by weight of biodiesel (5%BD); and hydrous ethanol containing 5% by weight of diethyl ether (5%DEE). Eh95 and ED95 are used to represent a low and high ignition quality of ethanol fuel for CI engines. Table 4.3shows the compositions of ethanol fuels. For hydrous ethanol without ignition improvers, 1% by weight of Lauric acid was added into hydrous ethanol to prevent injection system lubrication failure (Bika, et al., 2009). However, Lauric acid was not added to ED95, because ED95 already contains a lubricant. For each test fuel, results of combustion are averaged from 7 tests to analyze uncertainty and check repeatability.

Table 4.4 shows properties of diesel, ethanol and additives. The heat input of test fuels is kept constant at 937 J by varying the amount of injected fuel shown in Table 4.5.

Table 4.3 The compositions of test fuels used in this study.

Compositions, %wt \ Fuels		ED95	Eh95	1%G	3%G	5%G	5%BD	5%DEE
Ethanol		84.36	94.00	93.06	91.18	89.30	89.30	89.30
Water		4.44	5.00	4.95	4.85	4.75	4.75	4.75
Lauric acid		-	1.00	0.99	0.97	0.95	0.95	0.95
Additives	Commercial additive	11.20	-	-	-	-	-	-
	Glycerol ethoxylate	-	-	1.00	3.00	5.00	-	-
	Biodiesel	-	-	-	-	-	5.00	-
	DEE	-	-	-	-	-	-	5.00

Table 4.4 The properties of diesel, ethanol and ignition improvers.

Properties	Diesel [(a)]	Ethanol [(b)]	Biodiesel [(c)]	DEE [(d)]	Glycerol ethoxylate [(e)]
Formula	$C_nH_{2.8n}$	C_2H_5OH	$C_{18.74}H_{34.43}O_2$	$C_2H_5OC_2H_5$	$C_5H_{14}O_5$
Molecular weight (g/mol)	~170	46.00	291.62	74.00	154.00
Oxygen content (% by weigth)	0	34.80	10.97	21.62	48.78
Stoi. A/F ratio	14.5	9.01	13.80	11.13	5.35
Viscosity (cP)	2.38@40 °C	1.19@20 °C	3.50@37.8 °C	0.23@20 °C	364.2@21°C
Density (g/cc at 20 °C)	0.83-0.876	0.785	0.881	0.713	1.138
Cetane number	>52	<5.0	51.5	>125.0	n.a.
Vapor pressure (kPa) at 20°C	0.062	5.95	<0.267	58.6	n.a.
Heat of vaporization (kJ/kg)	270	854.8	n.a.	351.2	n.a.
Boiling temperature (°C)	160-366	78	182-338	35	200
Autoignition temperature (°C)	252	422	170	160	n.a.

Note: (a) Heywood, 1988; Saitoh and Uchida, 2007; Payri et. al., 2012; Hess, 2012.

(b) Bailey, et. al., 1997; Saitoh and Uchida, 2007, Petro Green Co., LTD, 2009.

(c) Bailey, et al., 1997; Sun, et al., 2010; Patum vetgetable oil Co., LTD, 2009.

(d) Bailey, et al., 1997; Zhang, et al., 2011, Sciencelab.com, Inc., 2013.

(e) Channiwala and Parikh, 2002; Sigma-Aldrich Corporation, 2011.

n.a.: not available

Table 4.5 Injection amount to maintain the constant energy input.

Test fuels	Injection amounts (mg)	Energy input (J)
Diesel	21.49	937
ED95	36.59	
Eh95	36.69	
1%GE	36.15	
3%GE	36.44	
5%GE	36.29	
5%BD	36.52	
5%DEE	36.56	

4.3.5 Experimental Conditions

To study combustion of ethanol under CI engine conditions, the required temperature to promote autoignition of hydrous ethanol without ignition improver is at least 900 K (Siebers and Edwards, 1987). This is the representative of polytropic compression with polytropic index (n) 1.35 from ambient conditions, i.e. air temperature of 25 ^{o}C and pressure of 1 atm, through compression ratios as high as 23:1. However, to obtain ignition delay and the rate of pressure rise during premixed combustion comparable with those for current diesel fuels when used in conventional diesel engines, in-cylinder temperatures of 1100 K is required for ethanol at injection (Siebers and Edwards, 1987). To achieve 1100 K at injection from ambient conditions using polytropic compression, the CI engine would require compression ratios in excess of 40:1, which is not practical in the typical CI engines. However, this condition is possible in CVCC with pre-combustion technique. Therefore, the target temperatures in this study are set as 900 and 1100 K.

Table 4.6 shows the experimental conditions for combustion characteristics of ethanol tested in CVCC. Gas temperature and injection pressure at the time of fuel injection are varied. Gas temperatures of 900 and 1100 K are used for the experiments. Effect of ambient gas pressure is not considered in this study, because the ignition delays of the alcohol fuels do not significant depend on gas pressure at any temperature (Siebers and Edwards, 1987). In experiments, fuels are injected into the CVCC with diferent pressure between 500- 900 bar via a six hole nozzle with diameter of 0.14 mm using a common rail injection system.

Table 4.6 The experimental conditions for CVCC.

Surrounding conditions	
Temperature : T_g	900 and 1100 K
Injection conditions	
Nozzle diameter	0.14 mm x 6 holes
Injection pressure	500, 700 and 900 bar
Injection duration	1.75-3.4 ms

Table 4.7 shows the experimental conditions for RCEM. At start of injection, mixture gas density, pressure and temperature are 21 kg/m^3, 4.4 MPa and 900 K, respectively. These experimental conditions represent polytropic compression of air from ambient conditions at compression ratio as high as 23 and engine speed 1000 rpm. A common rail fuel injection system and a single hole injector with hole diameter of 0.24 mm are used to inject fuel at constant pressure of 90 MPa. In this study, there are six fuels used in this study, i.e. Eh95, ED95, 1%GE, 5%GE, 5%BD and 5%DEE. ED95, commercial ethanol fuel for diesel engine, is used as a reference fuel.

Table 4.7 Experimental conditions for RCEM.

Surrounding conditions	
Temperature : T_g	900 K
Injection conditions	
Nozzle diameter	0.24 mm x 1 hole
Injection pressure	900 bar
Injection duration	3.05-3.30 ms

4.4 Results and Discussions

4.4.1 Injection Characteristics of Diesel and Hydrous Ethanol with Additives

Figure 4.5 (a), (b) and (c) show injection rate of test fuels injected by six hole injector against time after start of energizing at injection pressure of 500, 700 and 900 bar, respectively, at back pressure of 29 bar. The injection amount for each fuel is varied to maintain the constant energy input. For each fuel tested, the results are 10 measurement averages. The results show that in comparison of diesel and hydrous ethanol with additives at the same conditions, times for needle opening after start of energizing (injection delay) of Eh95 are shorter than that of diesel. It is expected that the difference in injection delay is caused by the different fuel viscosity. Corresponding to higher viscosity of diesel, additional time is required to raise the injector needle due to the viscous forces resisting needle movement (Payri, et al., 2012). However, diesel requires

less injection amount, because it has high energy content, resulting in shorter injection duration to get the same energy input. The results also show that injection delay is changed when ignition improvers were added into hydrous ethanol for all test conditions.

From Figure 4.5 (a), (b) and (c), it can be noticed that the injection rates of test fuels are the typical top hat or square. In the case of hydrous ethanol with ignition improvers, injection rates seemed to have two peaks, while diesel shows only one peak. When injection pressure is increased this characteristic is more obvious, but this characteristic cannot be observed in the case of diesel. It still shows only one peak. It is expected that the lower viscous force of hydrous ethanol allows the nozzle needle moved faster than that of diesel. In other words, the nozzle needle in the case of hydrous ethanol reaches the the fully opening position faster than that of diesel with higher momentum resulting in the higher injection rate at the initial phase of injection. However, the nozzle needle is unstable because of higher momentum at the fully opening position in the case of hydrous ethanol, giving the variation and second peak of injection rate. The other reasons for this characteristic were explained by Schmidt (1997), who also found many peaks of injection rate using multi-hole nozzle. He explained that the injection rate oscillations, which showed many peaks, came from a result of operating the injection system and poor needle seating or strong wave reflections in the injector. Schmidt (1997) also stated that these oscillations were a possible source of error and indicate poor injector performance. However, injection rate shapes can be varied from injector to injector as shown in previous works (Bower and Foster, 1991; Schmidt, 1997; Verhoeven, et. al., 1998; Marcic, 1999; Han, et. al., 2002; Phan, 2009). It depends on injection system and nozzle gemetry resulting in flow pattern in side nozzle.

For all injection pressures shown in Figure 4.5 (a) to (c), Eh95 shows the relatively high injection rate compared to those of the others. Glycerol ethoxylate at different composition, i.e. 1%, 3% and 5% by mass, and biodiesel at 5% by mass slightly change the value of injection rate, except 5% DEE shows drastically change in the injection rate at the fully opening position. It is believe that DEE at 5% by mass in hydruos ethanol enhances cavitation in the nozzle leading to the lower injection rate at the fully opening position.

Increasing injection pressure from 500 bar to 900 bar in Figure 4.5 (a) and (c) decreases not only injection delay but also injection duration, while injection rate is increased with increasing injection pressure for all fuels. The comparison between injection pressure of 900 bar and 500bar show that injection rates of test fuels at injection pressure of 900 bar are higher than that of injection pressure of 500 bar in the range of 21-26%, while injection delays of test fuels are decreased approximately 10-25% by injeciton pressure of 900 bar.

Figure 4.6 shows discharge coefficient (C_d) of test fuels. Discharge coefficients of diesle are in the range of 0.62 to 0.73, while discharge coefficients of hydrous ethanol that has high variation are in the range of 0.59 to 0.87.

In the case of diesel, increasing injection pressure from 500 bar to 700 bar increases C_d. Although increasing injection pressure increase flow velocity at the critical point such as at near a sharp inlet corner resulting in the separating flow and formation of a vena contracta at near inlet, but the decreased pressure at near inlet in nozzle is still higher than the vapor pressure of diesel. It is believe that no cavitating flow occurs in this case. Due to the theorical mass flow depends on fuel density, flow area and velocity (depends on the difference pressure between injection pressure and chamber pressure), the increasing injection pressure from 500 bar to 700 bar for diesel is possible to increase the measured flow rate when fuel density, flow area and chamber pressure are constant. However, increasing injection pressure from 700 bar to 900 bar, C_d of diesel slightly decreases. It is believe that the local pressure in nozzle at the critical point such as at near a sharp inlet corner falls below the vapor pressure of diesel leading to cavitation flow, becasue increasing the injection pressure results in the probability of presence of the cavitation (Sou, et. al., 2007). This phenomena was also observed by Payri, et. al., 2013. They found that C_d increases continuously with Reynolds number (which is the function of velocity depended on injection pressure) for non-cavitating conditions. However, C_d decreased when cavitating flow occurred.

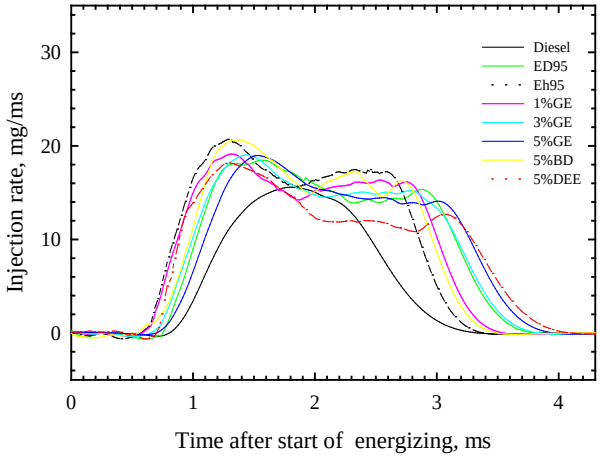

(a) P_{inj} = 500 bar

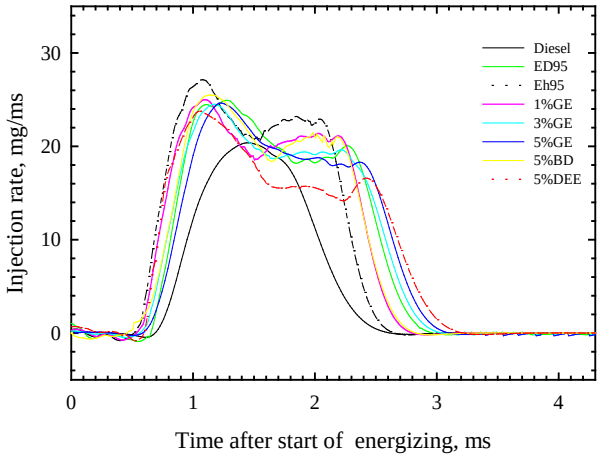

(b) P_{inj} = 700 bar

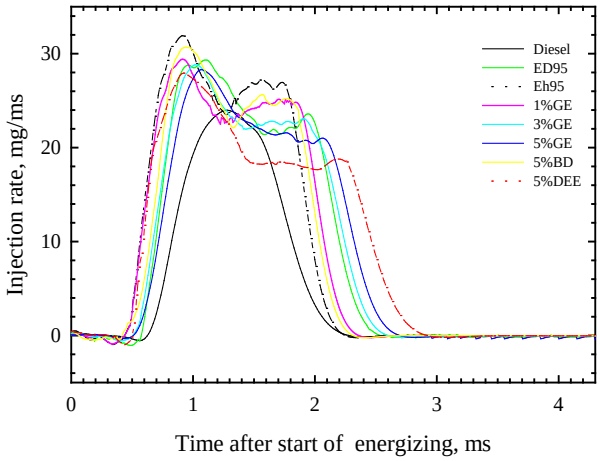

(c) P_{inj} = 900 bar

Figure 4.5 Injection rate of test fuels with different injection pressures.

For hydrous ethanol with additive, increasing the injection pressure decreases in C_d. This can be explained by the reason of existence of cavitation, because ethanol has high vapor pressure compared to diesel as shown in Table 4.4. It is possible that increasing pressure for hydrous ethanol with ignition improvers results in the low static pressure in nozzle leading to cavitating flow.

Figure 4.6 also shows that when ignition improvers are added into hydrous ethanol discharge coefficient are changed. This is probably affected by the vapor pressure and boiling temperature of ignition improvers. This explaination is reasonable especially in the case of 5%DEE. C_d of 5%DEE shows the lowest value, i.e. 0.59, at injection pressure of 900 bar. At this conditions, it is possible that high level of cavitation occurs in this case, because neat DEE has a relatively low boiling point temperature and high vapor pressure compared to ethanol.

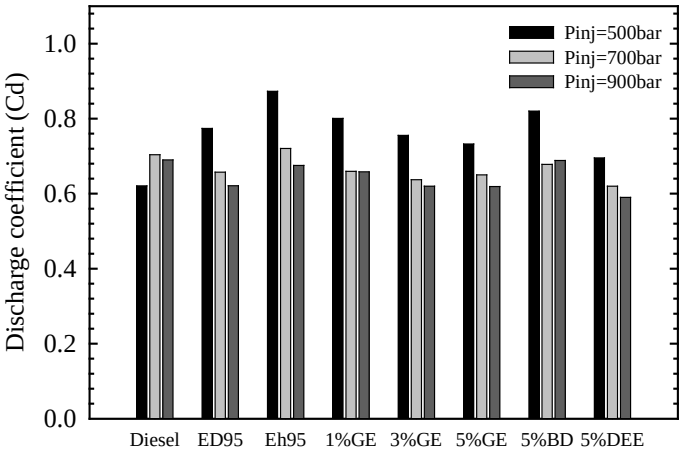

Figure 4.6 Discharge coefficient of test fuels.

4.4.2 Combustion Characteristics of Test Fuels in CVCC.

Figure 4.7 (a) and (b) shows the ignition delay with error bars indicating 95% confidence interval for test fuels at ambient gas temperature of 900 K and 1100 K, respectively. The results of combustion are averaged from 7 tests for each fuel. Test fuels were injected by the six hole injector. The ignition delay was derived from pressure curve as mentioned in the section 4.2.2. The results showed that at the same conditions, for ethanol fuels, Eh95 has the longest ignition delay, while ED95 (the commercial ethanol fuel) has the shortest ignition delay, but the ignition delay of ED95 is longer than that of diesel about of 40%. However, the ignition delay of ED95 is

considered acceptable for diesel engines as measured ignition delay time in the real diesel engines over a wide range of operating conditions are 0.6 ms to 3 ms for low-compression-ratio DI diesel engines, 0.4 ms to 1 ms for high-compression-ratio and turbocharged DI diesel engines and 0.6 ms to 1.5 ms for IDI diesel engines (Heywood, 1998). Therefore, ED95 can be used as a reference fuel for the ethanol with other ignition improvers used in CI engines.

Although neat biodiesel and diethyl ether (DEE) have high cetane number, which is represent the ignition quality of fuel, biodiesel and DEE at 5% by mass in hydrous ethanol show slightly improvement of the ignition delay of hydrous ethanol. Glycerol ethoxylate group shows promising results on ignition delay, especially 5% glycerol ethoxylate. The ignition delay in case of 5% glycerol ethoxylate is near to that of the commercial ethanol fuel ED95. The increase of injection pressure from 500 bar to 900 bar shorten igntion delay for all fuels in the range of 7-15% for gas temperature of 900 K and 8-25% for gas temperature of 1100 K. The reason of shortening ignition delay is the increase of injection pressure can enhance air-fuel mixing leading to shorter ignition delay. The increase of gas temperature from 900 K to 1100 K also decrease igntion delay for all fuels.

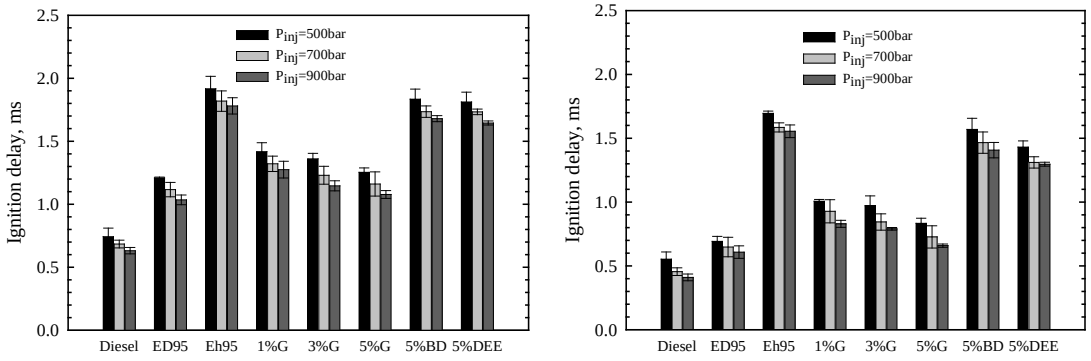

(a) Tg = 900 K (b) Tg = 1100 K

Figure 4.7 Ignition delay for test fuels.

Figure 4.8 (a) and (b) shows combustion efficiencies of hydrous ethanol with additives and diesel. Combustion efficiency is the ratio of total heat release due to combustion, i.e. cumulative heat release shown in Figure 4.9 and Figure 4.10, and the heat input of injection fuel.The results show that the value of combustion efficiencies are in the range

of 80-89% for all conditions. This means that the test fuels were injected into the cylinder with the similar heat input.

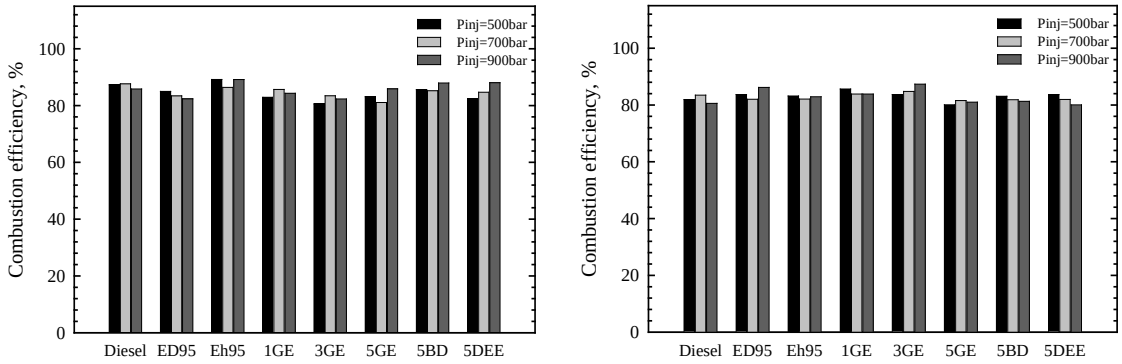

(a) T_g = 900 K (b) T_g = 1100 K

Figure 4.8 Combustion efficiency of test fuels.

Figure 4.9 and Figure 4.10 show pressure in the combustion chamber, heat release rate and cumulative heat release of test fuels at ambient gas temperature of 900 K and 1100 K, respectively. The results showed that at the same injection pressure and ambient gas temperature, the pressure rise of test fuels onset at different time. This means that different fuels have different ignition delay as discussed above. The longer ignition delay provides longer residence time for fuel-air mixing. It is possible to provide more of fuel-air mixing resulting in a rapid pressure rise when combustion starts. In addition, rate of heat release in premixed combustion phase is high. However, the phase of combustion in CVCC is quite difficult to distinguish. It seems to have only one phase of combustion, i.e. premixed combustion phase, for all test fuels, because the large volume of CVCC compared to the combustion chamber of real CI engines provide the sufficient air after start of combustion. In other words, air and fuel can be easily met in the larger volume of CVCC after start of combustion resulting to the main phase of combustion in CVCC is premixed combustion. This characteristic is the similar with the other work (Fujimoto, et al., 2005; Nguyen and Honnery, 2008).

The longest ignition delay occurs in case of Eh95 for all test conditions correspnding to the highest rate of heat release. Diesel shows the lowest heat release rate, because the shortest igntion delay in case of diesel allows less entrained air mixed with fuel resulting in the peak of heat release rate. In comparison between diesel and the commercial ethanol fuel ED95, it is shown that although ED95 is considered as a

commercial fuel for CI engines, which have been modified to use ethanol fuel, it still has different in ignition delay, pressure rise, heat release rate and combustion duration. ED95 is relatively long ignition delay, fast pressure rise, high heat release rate and long combustion duration. Therefore, it is better to use ED95 as a benchmark for the use of the ethanol in CI engines. In other words, the ethanol fuels that can be used for the CI engines should have combustion characteristics atleast as same as ED95.

At ambient temperature of 900 K (Figure 4.9), biodiesel and diethyl ether (DEE) at 5% by mass in hydrous ethanol can improve the combustion pressure and heat release rate of hydrous ethanol, but is still far from those of ED95. Glycerol ethoxylate (GE) at 1%, 3% and 5% by mass in hydrous ethanol shows that they can improve the pressure rise and heat release rate that is similar to those of ED95, especially for 5%GE. Pressure and heat release rate of 5%GE are very similar to those of ED95. However, the optimum of glycerol ethoxylate concentration for CI engines cannot be concluded from this work.

At ambient temperature of 1100 K (Figure 4.10), the results show the similar to those of ambient temperature of 900 K, but the difference in pressure and heat release rate between 1%GE, 3%GE and 5%GE decrease. Furthermore, they are near to those of ED95.

Increasing injection pressure increases heat release rate and reduces combustion duration for all fuels, because the increased injection pressure can induced more air into the spray. It is believed that a better mixing is enhanced.

Figure 4.11 (a) and (b) show the maximum rate of pressure rise at ambient gas temperature of 900 K and 1100 K, respectively. The maximum rate of pressure rise is an important parameter for the application of alternative fuels in diesel engines (Siebers and Edwards, 1987), because the rapid pressure rise can increase the engine wear and combustion noise, commonly referred to as diesel knocking (Heywood, 1988; Simonsen and Chomiak, 1995). The maximum rate of pressure rise can be obtained by the calculation of pressure change in the recorded time interval. The results show that Eh95 is the highest maximum rate-of-pressure-rise, which is two times higher than that of diesel and significantly higher than that of the commercial ethanol fuel ED95 at ambient gas temperature of 900K, and is much higher than that of diesel and ED95 at ambient gas temperature of 1100K for all injection pressure.The maximum rate of pressure rise

of ED95 is relatively higher than that of diesel. Glycerol ethoxylate at 1%, 3% and 5% by mass in hydrous ethanol can reduce the maximum rate of pressure rise of hydrous ethanol, while 5% by mass of biodiesel and diethylether in hysdrous ethanol shows some effect on the maximum rate of pressure rise of hydrous ethanol. It can be noticed that the level of maximum rate of pressure rise corresponds with the ignition delay times at the same conditions. In other words, the longer ignition delay time provides the higher the maxumum rate of pressure rise for fuel combustion.

The increasing ambient gas temperature from 900 K to 1100K shows the reduction of the maximum rate of pressure rise. It can be explained that shorter ignition delay allow less entrain air into fuel spray which decrease fuel-air mixing leading to a slower pressure rise.

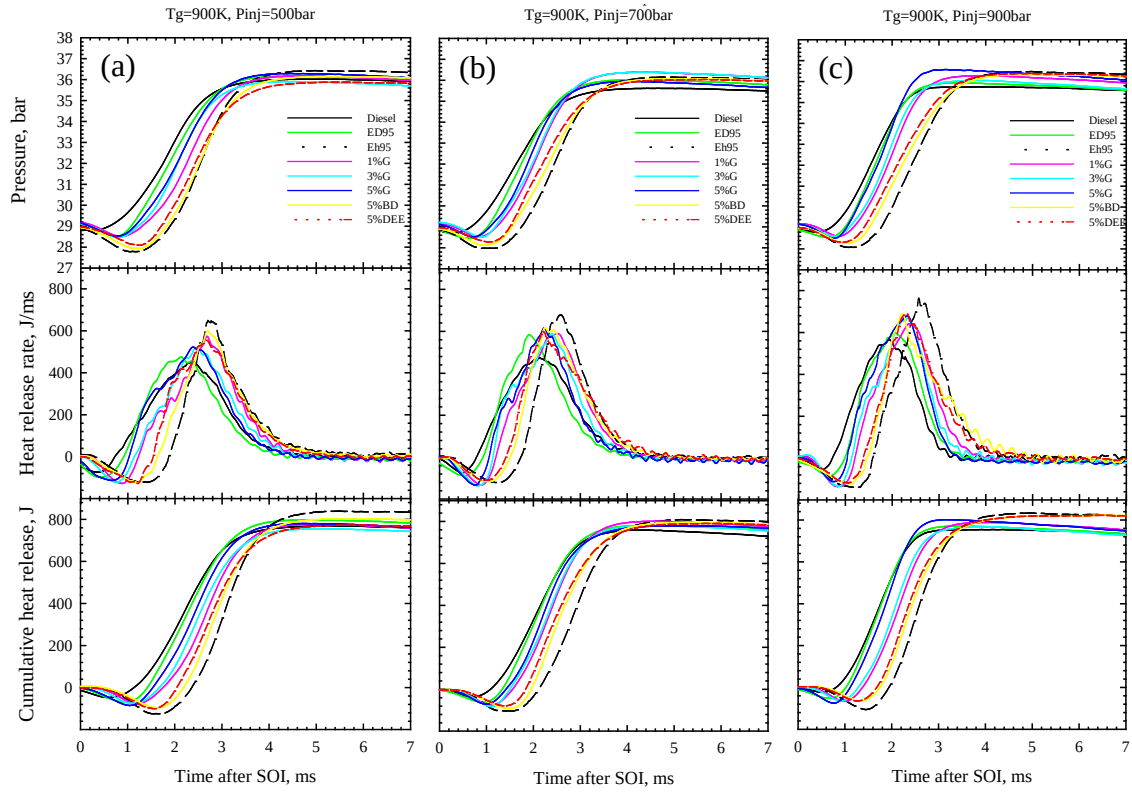

Figure 4.9 Pressure, heat release rate and cumulative heat release of test fuels at ambient gas temperature (T_g) of 900K.
(a) P_{inj}= 500 bar (b) P_{inj}= 700 bar and (c) P_{inj}= 900 bar

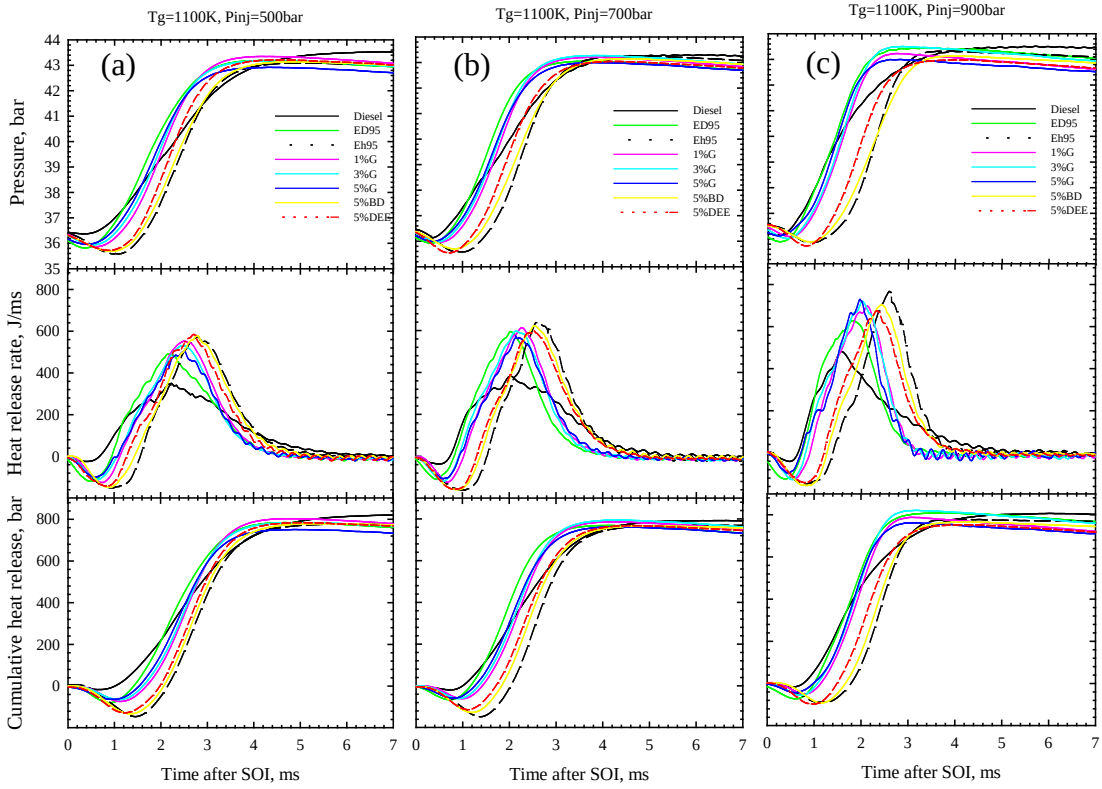

Figure 4.10 Pressure, heat release rate and cumulative heat release of test fuels at ambient gas temperature (T_g) of 1100K.
(a) P_{inj}= 500 bar (b) P_{inj}= 700 bar and (c) P_{inj}= 900 bar

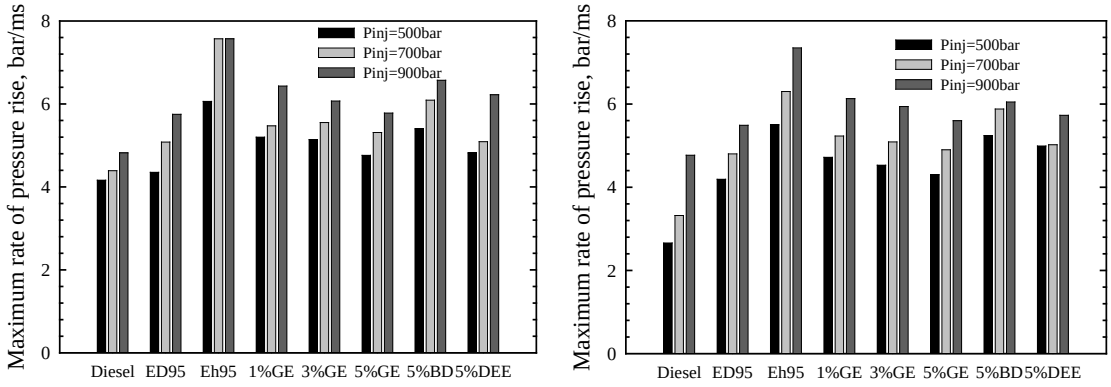

(a) T_g= 900 K (b) T_g= 1100 K

Figure 4.11 Maximum rate of pressure rise.

Figure 4.12 shows the relation between ignition delay and the maximum rate of pressure rise tested in CVCC. Corresponding to ignition delay, the maximum rate of pressure rise increases when ignition dealy increases. The effect of injection pressure on maximum rate of pressure rise is clearly observed. Increasing injection pressure drastically increases the maximum rate of pressure rise, but slightly shortens ignition

delay as discuss above. Increasing temperature shows the similar maximum rate of pressure rise for all fuels.

Figure 4.13 shows the relation between ignition delay and the maximum rate of heat release tested in CVCC. The longer ignition delay results in the higher maximum heat release rate. Increasing injection pressure drastically increases the maximum rate of heat release rate.

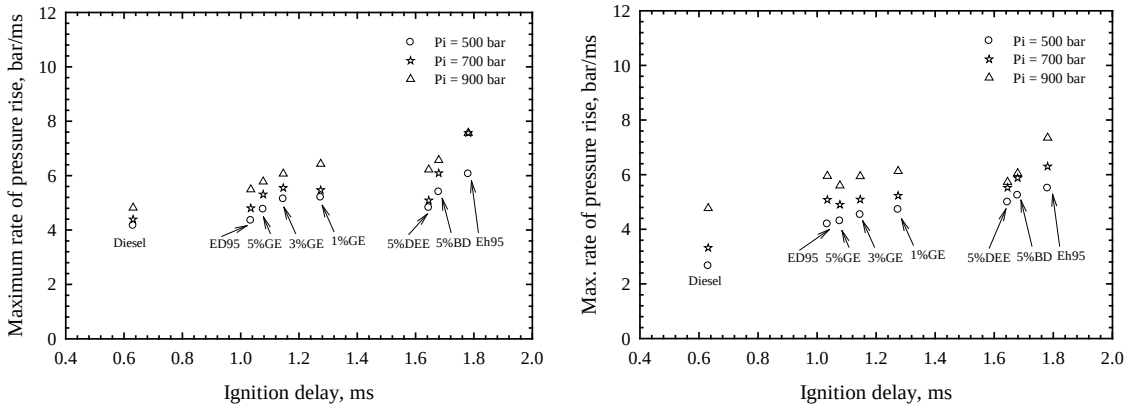

(a) Tg = 900 K (b) Tg = 1100 K

Figure 4.12 The relation between ignition delay and the maximum rate of pressure rise tested in CVCC.

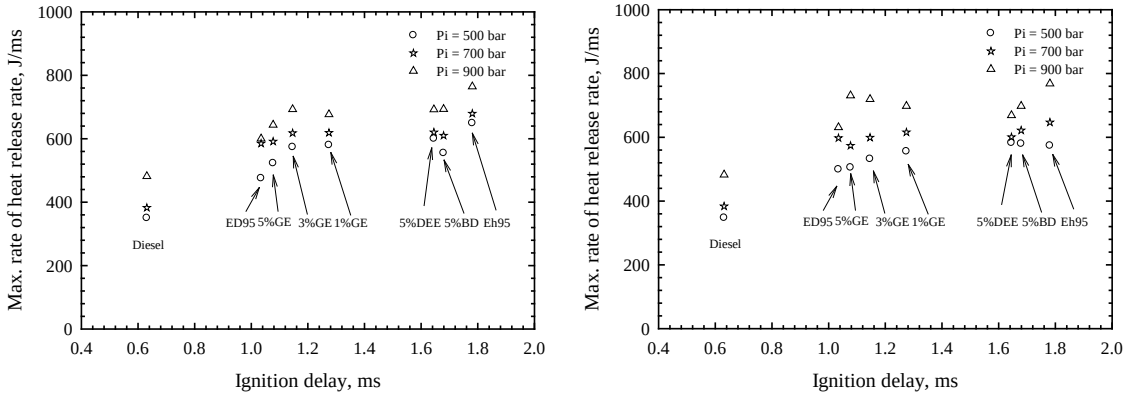

(a) Tg = 900 K (b) Tg = 1100 K

Figure 4.13 The relation between ignition delay and the maximum rate of heat release tested in CVCC.

4.4.3 Combustion Characteristics of Test Fuels in RCEM

Figure 4.14 shows the average ignition delay with error bars indicating 95% confidence interval for test fuels. Test fuels were injected by the single hole injector. Eh95, ED95, 1%GE, 5%GE, 5%BD, 5% DEE and diesel, are 1.33 ms ± 0.09 ms, 0.91 ms ± 0.07 ms, 1.06 ms ± 0.12 ms, 0.79 ms ± 0.08 ms, 1.32 ms ± 0.09 ms, 1.29 ms ± 0.07 ms and 0.52 ms ± 0.03 ms (Tsuda, 2007), respectively. Uncertainty analysis for tested fuels revealed that the results are scattered within 5% to 11%, indicating that the pressure recovery point provided repeatability of the ignition delay. As a further reference, calculation using the global expression for ignition delay for pure ethanol (Curran, et.al., 1992) at experimental conditions gives a value of 1.97 ms. Comparison of the calculated ignition delay for pure ethanol against Eh95 shows that the calculated value is higher than experimental measurements. In fact, the ignition delay for pure ethanol should be lower than that of Eh95 (hydrous ethanol with 5% by weight water), as hydrous ethanol requires higher activation energy to commence combustion. This variation can be attributed to the difference in operating conditions. Original operating conditions used to reach the global expression for pure ethanol are in the pressure range 2 atm to 4.5 atm and temperature range 1100 K to 1900 K, whilst the mentioned calculation uses operating conditions outside these ranges, (i.e. pressure and temperature are 40 atm and temperature 900 K respectively).

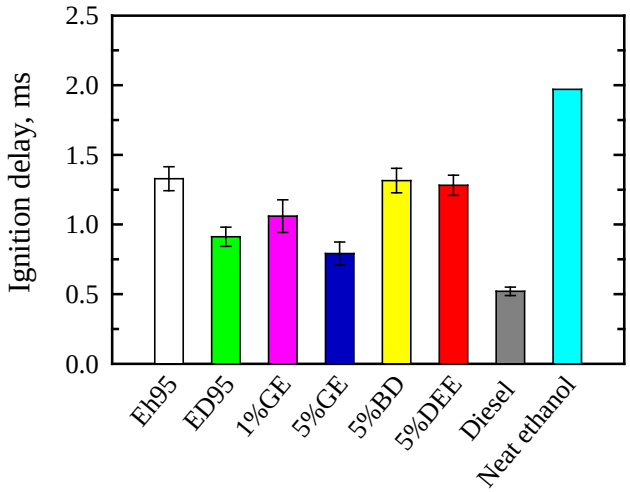

Figure 4.14 Ignition delay of test fuels compared with diesel (Tsuda, 2007) and neat ethanol (Curran, et. al., 1992).

Representative of low and high ignition quality ethanol fuel for diesel engines, Eh95 and ED95 exhibited a drastic difference in ignition delay. The ignition delay for ED95 is much shorter than that of Eh95. However, ED95 is longer than that of diesel fuel by approximately 75%. Nevertheless, the 0.91 ms ignition delay for ED95 is considered acceptable for diesel engines as measured ignition delay time in the real diesel engines over a wide range of operating conditions are 0.6 ms to 3 ms for low-compression-ratio DI diesel engines, 0.4 ms to 1 ms for high-compression-ratio and turbocharged DI diesel engines and 0.6 ms to 1.5 ms for IDI diesel engines (Heywood, 1988).

1%GE and 5%GE showed promising results and can be considered as fuel for diesel engines. Both 1%GE and 5%GE significantly improved ignition quality of the hydrous ethanol. This may be explained due to the number of attack sites for creation of radicals, (i.e. chain length), increased yielding a shorter ignition delay (Heywood, 1988; Simonsen and Chomiak, 1995). Another explanation supposes that ignition improvers are thermally unstable, thus thermal composition occurs yielding free radicals. These Radicals might accelerate the reactions leading to auto-ignition of the fuel (Al-Rubaie, et, al., 1991). Ignition delay of 5%GE is slightly shorter than ED95, while 1%GE is longer than ED95.

Ignition delays of 5%BD and 5% DEE are similar to that of Eh95. So despite neat DEE and biodiesel having much higher molecular weight and higher cetane number than ethanol, addition of biodiesel and DEE at 5% by weight has little effect on the ignition delay. Ignition delays are slightly reduced, explainable by the dependency of local mixture stoichiometry on the oxygen content of fuels. Lower oxygen content might occur and influence mixture stoichiometry yielding on ignition delay. Yet in pursuit of renewable and sustainable fuels DEE and biodiesel remain interesting ignition improvers at higher concentrations.

In-cylinder pressure, heat release rate and cumulative heat release for all fuels tested are shown in Figure 4.15 (a), (b) and (c), respectively. 5%GE behaves near identical to ED95. However, 1%GE, 5BD, 5% DEE and Eh95 are yield diverse data compared to ED95. As shown in Figure 4.15 (a), the peak in-cylinder pressures for all tested fuels are similar due to injection at equal calorific value. Results illustrate that Eh95 exhibited the most rapid pressure rise and highest heat release rate. 5%GE and ED95 showed contrary results. Heat release rate and cumulative heat release of 1%GE are

intermediate between those of ED95 and Eh95. Using 5%GE, the observed heat release rate and cumulative heat release are near identical to those of ED95. Heat release rate and cumulative heat release for 5%BD and 5% DEE are similar to those for Eh95. Heat release in premixed combustion phase accounts for 57.2% of the total heat release for Eh95, 55% for 5%BD and 5% DEE, 47.6% for 1% GE, 25.9% for ED95, and 25.5% for 5%GE.

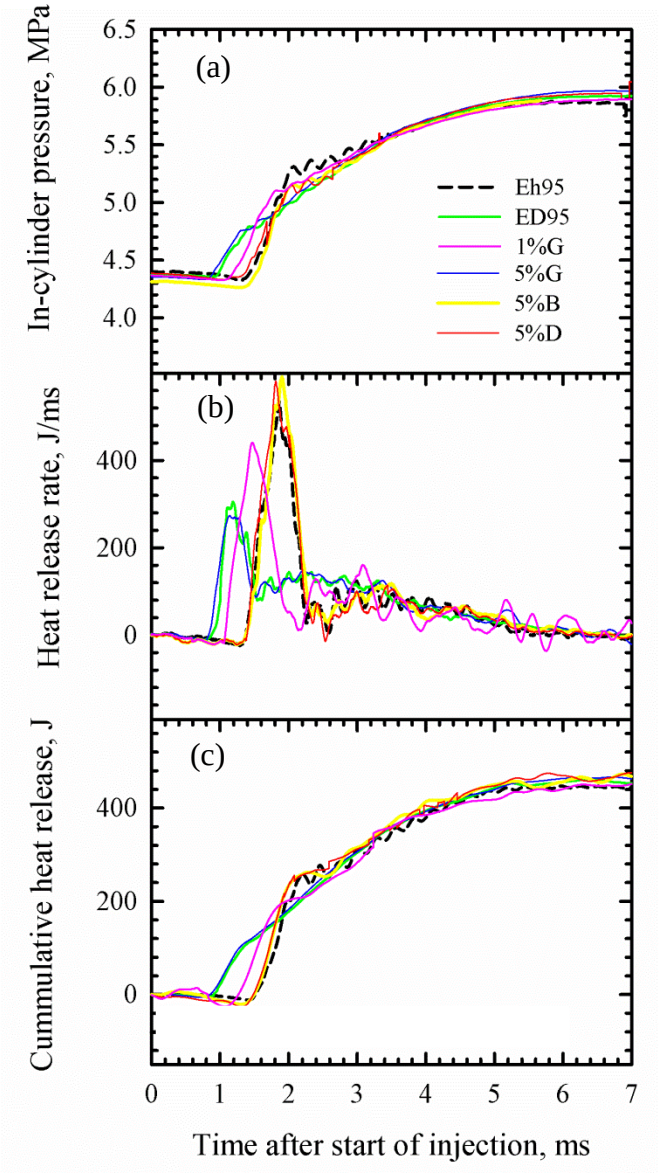

Figure 4.15 Combustion characteristics of test fuels in RCEM. (a) In-cylinder pressure, (b) heat release rate and (c) cumulative heat release for test fuels.

Figure 4.16 shows combustion efficiencies of hydrous ethanol with additives and diesel. Combustion efficiency is the ratio of total heat release due to combustion, and the heat input of injection fuel.The results show that the value of combustion efficiencies are similar value. This may be argued that the test fuels, which have the different heat content, were injected into the cylinder with the similar heat input.

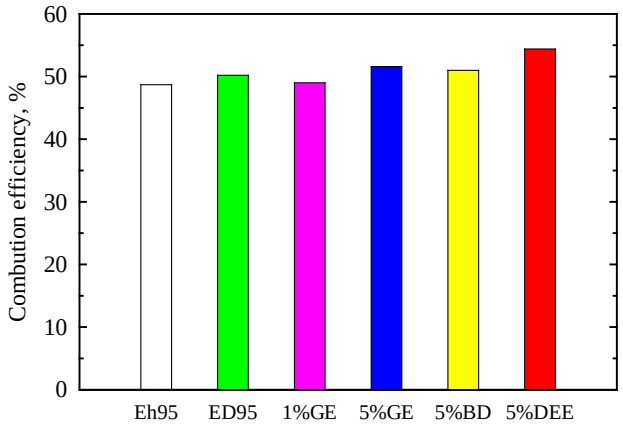

Figure 4.16 Combustion efficiency of test fuels in RCEM.

Maximum rate of pressure rise for test fuels are shown in Figure 4.17. This parameter is also an important parameter for the application of alternative fuels in diesel engines (Siebers and Edward, 1987). Results show that Eh95 gives the highest maximum rate of pressure rise (1.04 MPa/ms). The maximum rate of pressure rise for 5%BD, 5% DEE, 1%GE, 5%GE and ED95 are 0.91, 0.80, 0.67, 0.58 and 0.59 MPa/ms respectively. This sequence corresponds with measured ignition delay times. The maximum rate of pressure rise depends on the ignition delay. When a longer ignition delay occurs, fuel and air have more time to mix prior to the start of combustion. Increased air and fuel mixing leads to a more rapid pressure rise and high heat release rate in premixed combustion phase. Rapid pressure rise can increase the engine wear and combustion noise, commonly referred to as diesel knocking (Heywood, 1998; Simonsen and Chomiak, 1995).

In RCEM, it also shows that the longer ignition delay has the higher maximum rate of pressure rise and higher heat release rate, and increasing injection pressure increases the maximum rate of pressure rise and heat release rate as shown in Figure 4.18 and Figure 4.19.

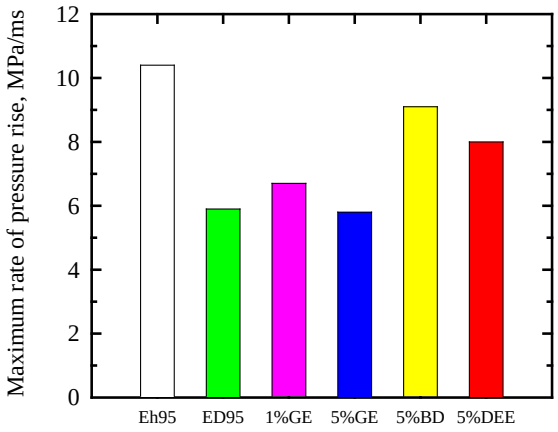

Figure 4.17 Maximum rate of pressure rise for test fuels.

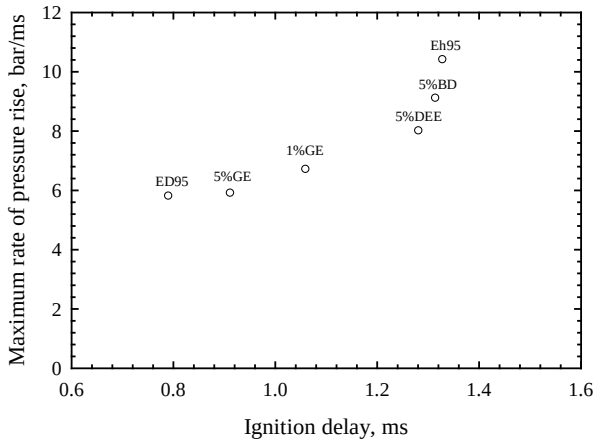

Figure 4.18 The relation between ignition delay and the maximum rate of pressure rise tested in RCEM.

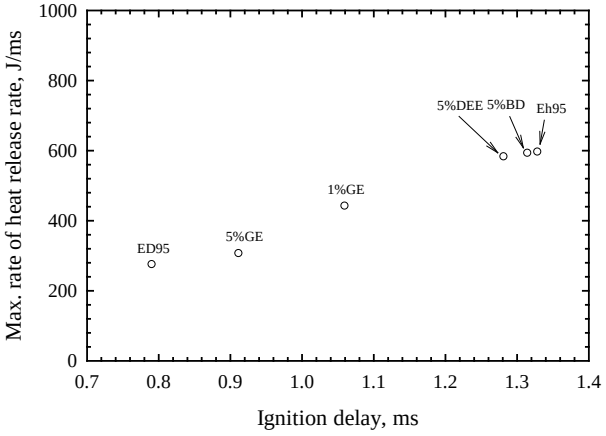

Figure 4.19 The relation between ignition delay and the maximum heat release rate tested in RCEM.

4.4.4 Comparison between the Combustion Characteristics in CVCC and RCEM

This section shows the comparison combustion characteristics of test fuels performed in CVCC and RCEM at the same injection pressure (900 bar) and ambient gas temperature (900 K).

Figure 4.20 shows the comparison of the ignition delay in the constant volume combustion chamber (CVCC) and the rapid compression and expansion machine (RCEM). It is noticed that the different injectors were used. Fuel tests in RCEM were injected by the single hole injector with nozzle hole diameter of 0.24 mm, while fuel tests in CVCC were injected by the six hole injector with nozzle hole diameter of 0.14 mm. However, the relative comparison can be made. Ignition delays for all fuels testing in CVCC are higher than those in RCEM in the range of 13-36%. The difference of the ignition delays between two apparatus probably comes from the difference of the hole diameter and number of nozzle used in both appartus resulting in spray formation and mixing process.

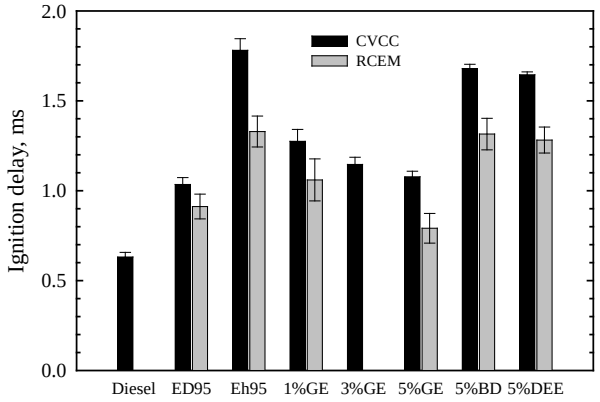

Figure 4.20 Comparison of the ignition delay tested in CVCC and RCEM at Tg = 900 K and Pinj = 900 bar.

Figure 4.21 shows the comparison of pressure, heat release rate and cumulative heat release tested in CVCC and RCEM. Pressure rises of test fuels in CVCC are more steep than that in RCEM resulting in the differences of heat release rate and cumulative heat release. The increasing pressures in CVCC, i.e. the pressure differnce between pressure after combustion and pressure at injection, are about an half of those in RCEM. The difference of the increasing pressures in CVCC and RCEM can be explained by their

volumes. In other words, volume of RCEM (157.08 cc) that is appromimately 55% smaller than that of CVCC (353.43 cc) allows higher increasing pressure. However, both apparatus produce the coressponding results as explained in previous sections.

Heat release rates and cumulative heat release for both apparatus are also different corresponding to the pressure. There are two phase of combustion, i.e. premixed and mixing-controlled combustion phases, as same as the typical direct injection CI engines, but heat release rates in CVCC are difficult to notice the mixing-controlled combustion phase. It seemed that only premixed combustion phase, resulting in the maximum value of heat release rate, occurs in the case of CVCC. This characteristic is similar to the other works (Nguyen and Honnery, 2008; Fujiomoto, et al., 2005) that use CVCC for combustion study.

Figure 4.22 shows the comparison of combustion efficiency of fuels tested in CVCC and RCEM. The combustion efficiency of fuels tested in CVCC are approximately 35% higher than that in RCEM. It is possible that there is abudant air to supply the mixing process in CVCC leading to more complete combustion and higher combustion efficiency. In other words, fuel and air can easily find to each other. In addition, it is possible that heat transfer in case of RCEM is higher than that of CVCC, because flame contact to the wall of the smaller volume of RCEM resulting in higher heat transfer.

Figure 4.23 shows the comparison of the maximum rate of pressure rise tested in CVCC and RCEM at the same condition. As expected,The maximum pressure rise rates in RCEM are higher than those of CVCC. It can be explained with the same reasons of the difference in pressure. The small volume of RCEM allows the higher maximum rate of pressure rise.

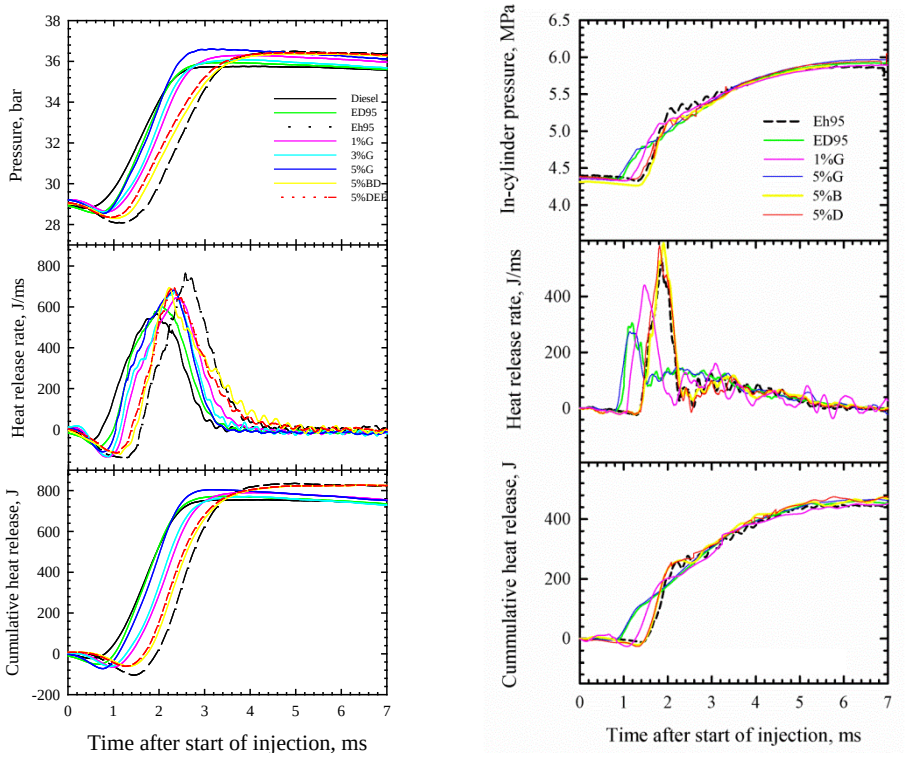

(a) CVCC (b) RCEM

Figure 4.21 Comparison of combustion pressure, heat release rate and cumulative heat release tested in CVCC and RCEM at Tg = 900 K and Pinj = 900 bar.

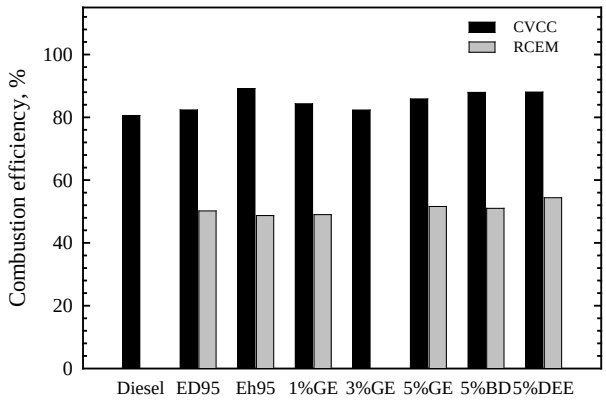

Figure 4.22 Comparison of combustion efficiency in CVCC and RCEM at Tg = 900 K and Pinj = 900 bar.

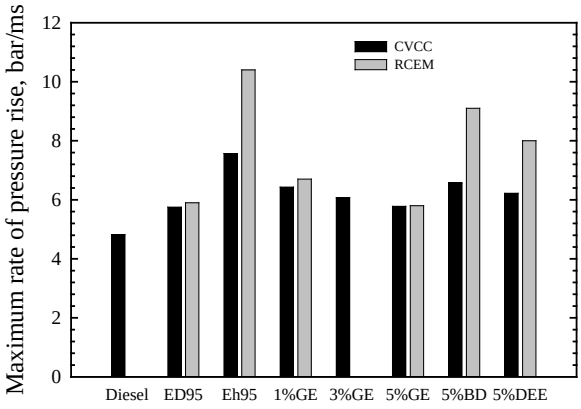

Figure 4.23 Comparison of the maximum rate of pressure rise tested in CVCC and RCEM at Tg = 900 K and Pinj = 900 bar.

From the comparison of CVCC and RCEM at Tg = 900 K and Pinj = 900 bar, it was found that the longer ignition delay increases the maximum rate of pressure rise and maximum heat release rate. The maximum rates of pressure rise in RCEM are higher than those of CVCC, while the maximum heat release rates in RCEM are lower than those of the CVCC for the same fuels as shown in Figure 4.24 and Figure 4.25. The reason of the difference come from the difference of volume as discussed above.

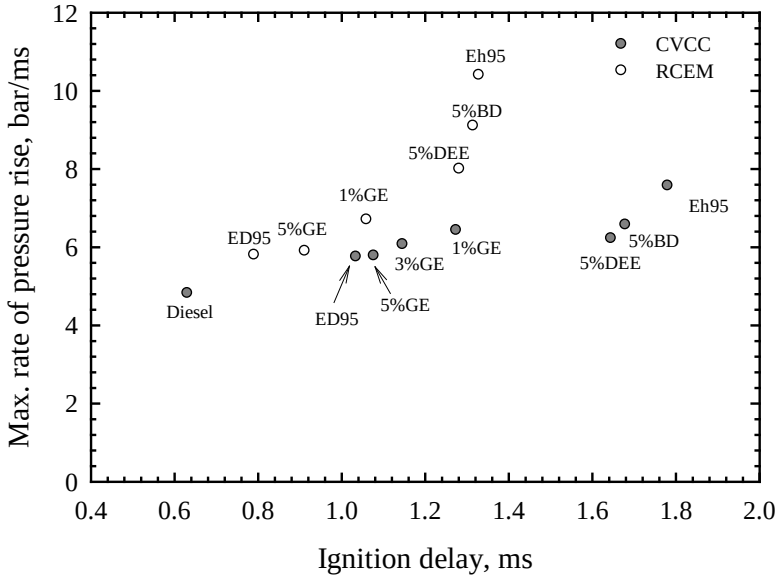

Figure 4.24 Comparison of relation between ignition delay and maximum rate of pressure rise tested in CVCC and RCEM at Tg = 900 K and Pinj = 900 bar.

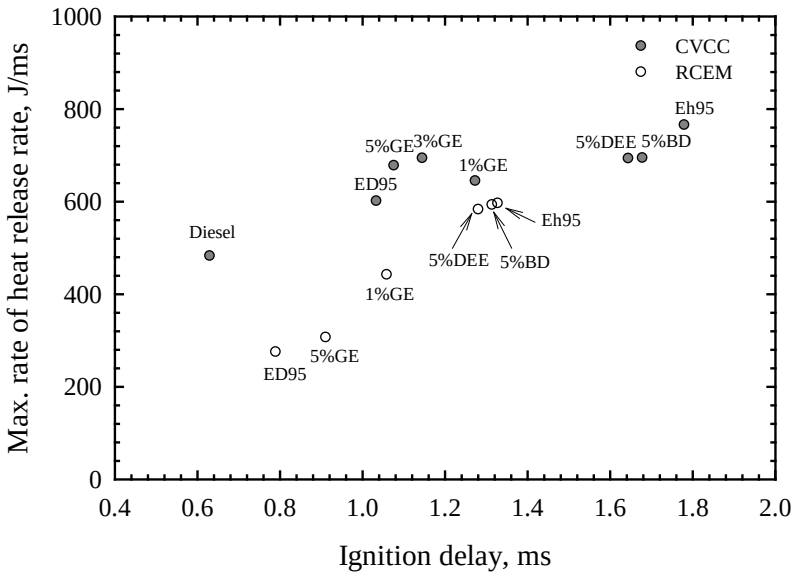

Figure 4.25 Comparison of relation between ignition delay and the maximum heat release rate tested in CVCC and RCEM at Tg = 900 K and Pinj = 900 bar.

4.4.5 Flame Visualization using Two Color Method

Flame Visualization using Two Color Method was performed in the RCEM. The effect of ignition improvers on combustion characteristics in RCEM, i.e. ignition delay, heat release rate and rate of pressure rise, are revealed in the previous section. The results show that combustion characteristics of the 5%GE are only near identical to those of ED95, while 1%GE show the effective on ignition delay, but it is still diferent in pressure rise and heat release rate. 5% biodiesel and 5%DEE has insignificant effect on hydrous combustion of ethanol compared to the commercial additive for ED95. Therefore, Eh95 (poor ignition quality), ED95 (commercial ethanol fuel for CI engine) and 5%GE (ethanol fuel that behaves near identical combustion characteristics to ED95) are only studied by visualization and two-color method.

Figure 4.26 shows the corresponding typical images of flame temperature contour obtained by two-color method during combustion duration. The range of the flame temperature is between 1600 K to 2000 K. A flame temperature of below 1600 K was designated blue, and a flame temperature of above 2000 K was designated red. In the images, the single hole injector position is located in the upper center. The similar flame shape can be noticed for all fuels. The spray combustion shows non-uniform and non-axisymmetric temperature inside spray flame. The latest first apparent flame temperature is in the case of Eh95 because of the longest ignition delay. The maximum flame temperature is shown in the middle of flame temperature images. The flame temperatures of 5%GE and ED95 are higher than that of Eh95, because the higher soot radiation is resulted by the earlier and longer diffusion combustion of 5%GE and ED95 as shown in Figure 5. The higher temperature could increase the NO_x formation. Unfortunately, NO_x could not be measured in these experiments because no nitrogen presented in the synthetic air and test fuels.

Figure 4.27 shows the corresponding flame temperature distribution of test fuels obtained from the average of temperature in the flame area of ten images. Each image is captured at every 0.1 ms. Flame temperature curves for all fuels show the same trend. There are two peaks of temperature distribution. The first peak of flame temperature occurs during fuel injection event. The second peak occurs just after the end of the fuel injection which is nearly identical to the level of the first peak. Afterward, the flame

temperature gradually decreased till end of combustion. The overall highest flame temperature is produced in case of 5%GE that is slightly larger than that of ED95 and Eh95 about of 0.9% and 0.7%, respectively. This showed that there is no significant difference between the flame temperatures of test fuels.

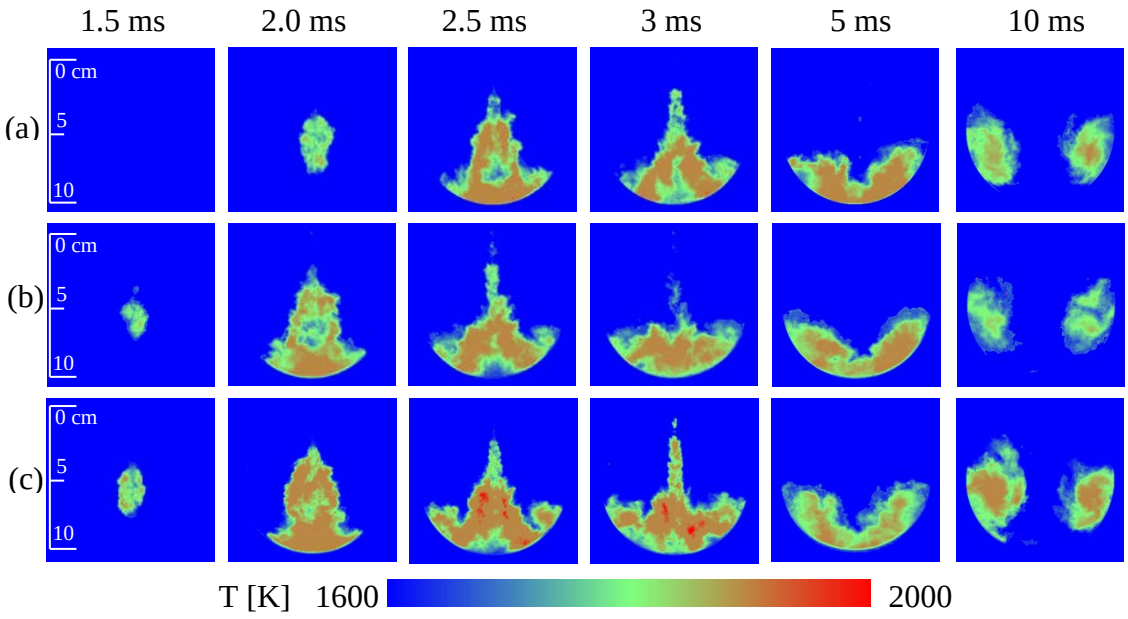

Figure 4.26 Flame temperature contour of test fuels.

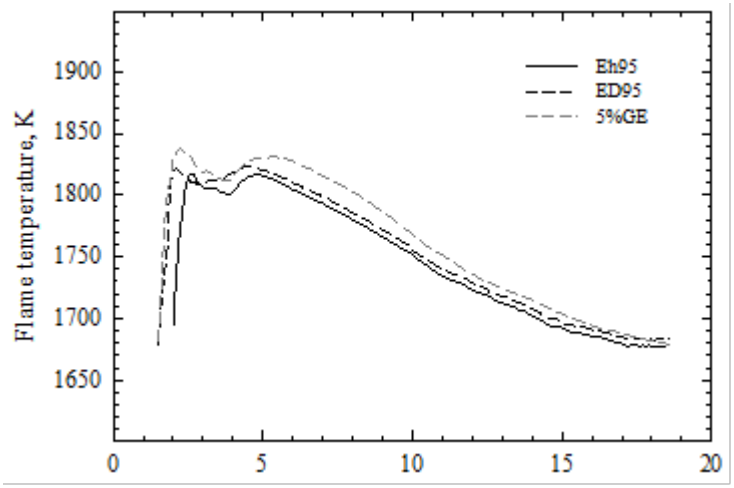

Figure 4.27 The corresponding flame temperature distribution of test fuels.

Figure 4.28 depicts the KL factors, which is a parameter that is approximately proportional to soot amount in the optical path, images and distributions over the combustion duration. In the images of KL factor, the high value occurs inside flame at high temperature zone. KL factor of ED95 illustrates more homogeneous distribution and higher value than that of Eh95a and 5%GE. This means that soot in case of ED95 is mainly generated at entire spray during fuel injection, while soot in case of Eh95 and 5%GE is mainly produced at the tip and center of spray.

Figure 4.29 shows the corresponding variation of KL factor during the combustion process. KL history can be used to interpret soot formation and oxidation during the process. There are two peaks of KL factor as well as flame temperature history, but the timing of soot generation is mostly in late combustion phase of test fuels. The histories of KL factor are quite similar shape for all fuels, but ED95 shows slightly higher KL factor than the others at initial period, but 5%GE shows the highest value in the late of combustion. This illustrates that soot is probably formed in the later stage for 5%GE which different from ED95 and Eh95. The order of magnitude of KL factor from ethanol combustion is also much lower than those of diesel combustion presented in the other studies (Matsu, et. al., 1979; Svensson, et. al., 2005; Kosaka and Arai, 2011). The reason for the difference is the oxygen concentration in ethanol enhanced more complete combustion.

Figure 4.30 shows average soot concentration measured from combustion of hydrous ethanol with ignition improvers. It illustrates that average soot from ethanol combustion is between 0.6 to 0.8 mg/m3 with high variation, which is significantly lower than that of diesel (60-100 mg/ m3) (Tsuda, 2007). Corresponding to KL factor, the combustion of ED95 shows the highest soot In comparison with Eh95, soot in case of ED95 and 5%GE is slightly higher due to the longer diffusion combustion phase of ED95 and 5%GE, where the fuel and oxygen are difficult to obtain the complete combustion resulting in higher soot.

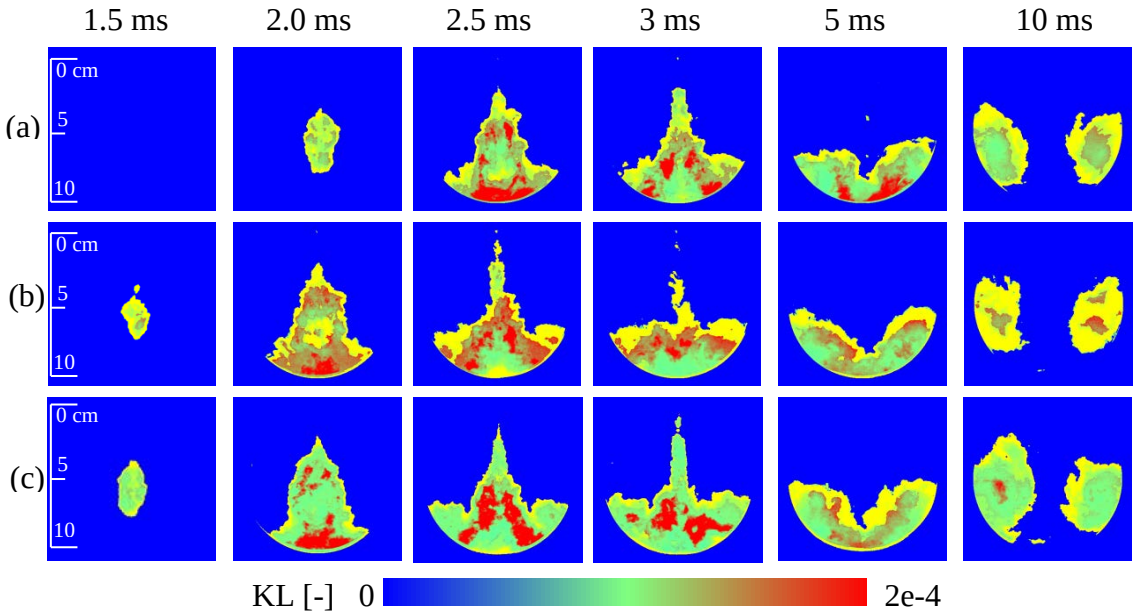

Figure 4.28 KL factor images of test fuels.

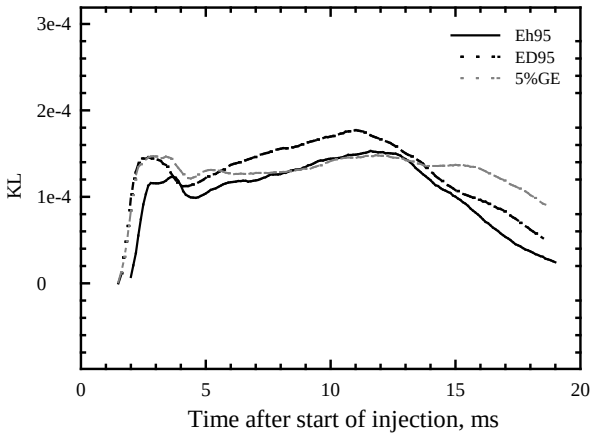

Figure 4.29 The corresponding KL factor distribution of test fuels.

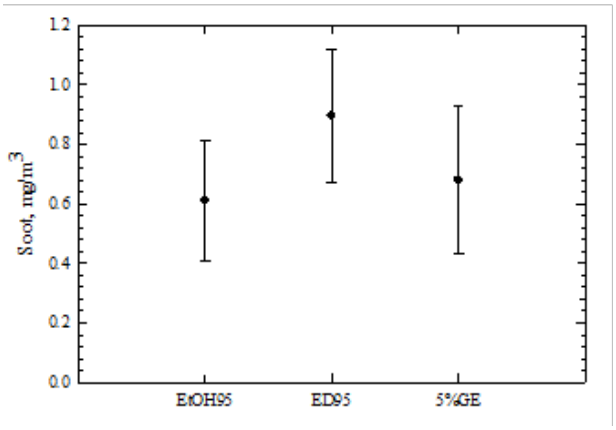

Figure 4.30 Soot measured from combustion of test fuels.

4.5 Summary

The effect of ignition improvers on injection and combustion characteristics of hydrous ethanol under CI engine condition was investigated in this chapter These results are relevant to modern CI engine design and provide extended data and analysis on injection and combustion characteristics of ethanol. The main conclusions are shown below:

- The ignition improvers change not only injection delay but also the maximum injection rate and discharge coefficient of hydrous ethanol. To maintain the energy input as same as diesel, the change of injection duration is required.
- Although ED95 is really used as a commercial ethanol fuel for CI engines. ED95 still has different ignition delay, pressure rise and heat release rate compared with those of diesel. However, the value of ignition delay of ED95 is acceptable for high compression-ratio CI engines, with performance within the typical ignition delay time range of 0.4 ms to 1 ms (Heywood).
- Biodiesel and diethyl ether (DEE) at 5% by mass in hydrous ethanol slightly improve the ignition delay, combustion pressure, heat release rate of hydrous ethanol and rate of pressure rise. The effective of these igntion improvers is still far from those of ED95.
- Glycerol ethoxylate (GE) at 1%, 3% and 5% by mass in hydrous ethanol shows the promissing results. However, only the 5%GE has the ignition delay, heat release rate and maximum rate of pressure rise near identical to those of the commercial ethanol ED95.
- The commercial additive for ED95 and glycerol ethoxylate at 5% by mass show a minor effect on soot emissions, KL factor and flame temperature. The differences of flame temperature between Eh95, ED95 and 5%GE are less than 1% during the combustion.
- Increasing injection pressure shortens igntion delay of hydrous ethanol, but increases the maximum rate of pressure rise and heat release rate. Increasing the maximum rate of pressure rise and heat release rate probably increase the engine wear and combustion noise.
- Increasing ambient gas temperature can also shorten ignition delay of hydrous ethanol with the decrease in the maximum rate-of-pressure-rise.

CHAPTER 5
CONCLUSIONS AND SUGGESTIONS

5.1 Conclusions

5.1.1 Performance and Emissions of a Small SI Engine Generator Set Fuelled by Hydrous Ethanol with High Water Contents up to 40%

Hydrous ethanol with high water content (up to 40% by volume) can be used in a small SI engine generator at constant load and engine speed. However, increasing water content from 20% to 40% by volume, the overall efficiency and NO_x emission gradually decreased by approximately 5% and 80%, respectively, but on the other hand break specific fuel consumption (BSFC), CO, HC, formaldehyde and acetaldehyde emissions increased by about 75%, 58%, 267%, 150% and 275% respectively. All emissions were measured just before the catalytic coverter. However, the increased emissions from increasing the water content were substantially reduced by the catalytic converter leading to meet the EPA limit model year 2011. Therefore, the direct use of hydrous ethanol in SI engines is considered an alternative fuel to improve the energy balance of ethanol production.

5.1.2 Design of Constant Volume Combustion Chamber (CVCC) with Pre-Combustion Technique for Simulation of CI Engine Conditions

The cylindrical-shaped constant volume combustion chamber (CVCC) with the tangential inlet has been selected through the systematic design. With this feature, the homogineity of premixed charge before premixed combustion is enhanced with no mixing fan. CVCC diameter of 100 mm and depth of 45 mm have been selected to be able to study the spray combustion and free spray of diesel, biodiesel and ethanol without impinging on the walls. The CVCC can be used to simulated a wide range of conditions prior injection of CI engines that has compression ratio over 28:1 with error less than 4%. From strength analysis, the maximum pressure operating in CVCC is up to 100 bar.Wall thickness of stainless steel CVCC and quartz window should be greater than 13.4 mm and 61.3 mm, respectively.

5.1.3 Combustion Characteristics of Hydrous Ethanol with Ignition Improvers under CI Engine Conditions

The ignition improvers, including the commercial additive for ED95; glycerol ethoxylate at 1%, 3% and 5% by mass; biodiesel 5% by mass; and diethyl ether 5% by mass, change injection characteristics of hydrous ethanol. The longer injection delay and lower injection rate occur in the case of hydrous ethanol blended with ignition improvers compared with hydrous ethanol without ignition improvers. Increasing injection pressure of test fuels increases injection rate and decreases injection delay. To maintain the constant energy input as same as diesel at the same injection pressure, the change of injection duration is required.

In comparison with diesel, ED95 shows the different ignition delay resulting in different pressure rise and heat release rate. However, the ignition delay of ED95 is acceptable for high compression-ratio CI engines which requires the igntion delay in the range of 0.4 ms to 1 ms (Heywood, 1988).

Under the same test condition, Biodiesel and diethyl ether (DEE) at 5% by mass in hydrous ethanol slightly affect on combustion characteristics. Glycerol ethoxylate (GE) at 1%, 3% and 5% by mass can shorten ignition delay of hydrous ethanol leading to change in pressure rise and rate of heat release, but only 5%GE shows the combustion characteristics near identical to those of the commercial ethanol ED95. Although the commercial additive and glycerol ethoxylate at 5% by mass change injection charateristics and significantly improve combustion characteristics of hydrous ethanol, they show insignificant effect on soot emissions, KL factor and flame temperature which is correlated to NO_x. Therefore, 5%GE is supposed to be use for CI engine providing the same combustion characteristics as the commercial ethanol (ED95) with slight effect on emissions.

Increasing injection pressure can shorten ignition delay of test fuels, but it also increases the maximum rate of pressure rise that probably increase the engine wear and combustion noise. Increasing ambient gas temperature can also shorten ignition delay of hydrous ethanol with the decrease in the maximum rate-of-pressure-rise. For the CI engines, increasing ambient gas temperature is suitable for improving combustion of ethanol.

These results are relevant to modern CI engine design and provide extended data and analysis on injection and combustion characteristics of ethanol.

5.2 Suggestions

5.2.1 Performance and Emissions of a Small SI Engine Generator Set Fuelled by Hydrous Ethanol with High Water Contents up to 40%

- To confirm that hydrous ethanol with high water content (up to 40% by volume) is suitable for SI engine generators, an assessment of the engine wear, engine durability, visual investigation of several critical engine components, engine oil and fuel filter clogging, engine oil contamination, engine oil change frequency, material and lubricant compatibility should be studied in the next step with more development and research.
- The catalytic converter is recommended when hydrous ethanol with high water content is used for the SI engine operating at constant engine speed and load, because the catalytic converter can reduce the regulated and unregulated emissions in all conditions tested.

5.2.2 Design of Constant Volume Combustion Chamber (CVCC) with Pre-Combustion Technique for Simulation of CI Engine Conditions

- The lubrication of injector and pump; injector tribology; injector durability; and material compatibility of injector should be studied, because there are a number of injector broken during the experiment.
- Measurement device should not be connected to CVCC directly. Adapters or plugs are convenient for removing devices.
- The products of the combustion tend to foul the spark plug. A cleasing system with no removing window or spark plug is preferable for experiment.
- Electronic control for filling process can reduce complexity of the experiment and human error.

5.2.3 Combustion Characteristics of Hydrous Ethanol with Ignition Improvers under CI Engine Conditions

The data tested should be used to shift the operating from the basic study to the real engines. Suggestions for this topic show below.

- To maintain energy input of hydrous ethanol with ignition improvers as same as the typical diesel, the larger nozzle hole diameter, higher injection pressure, and longer injection duration are required to increase injection amount of ethanol.
- Higher concentration of biodesel and diethyl ether is possible to improve ignition and combustion of hydrous ethanol as same as the commercail additive for ED95.
- Although increasing injection pressure can shorten ignition delay, increasing injection pressure should be used carefully, because it also increase the maximum rate of pressure rise that is a cause of engine wear and knocking.
- Increasing gas temperature is recommended to improve combustion of hydrous ethanol. High temperature prior injection can be achieved by using EGR, air preheating and increasing compression ratio.

REFERENCES

Agarwal, A.K., 2006, “Biofuels (Alcohols and Biodiesel) Applications as Fuels for Internal Combustion Engines”, **Progress in Energy and Combustion Science,** Vol. 33, pp. 233–271.

Allard, L.N., Webster, G.D., Hole, N.J., Ryan III, T.W., Ott, D. and Fairbridge, C.W., 1996, “Diesel Fuel Ignition Quality as Determined in the Ignition Quality Tester (IQT)”, **SAE**, No. 961182, pp. 955-959.

Allard, L.N., Hole, N.J., Webster, G.D., Ryan III, T.W., Ott, D., Beregszazy, A., Fairbridge, C.W., Cooley, J., Mitchell, K., Richardson, E.K., Elliot, N.G. and Rickeard, D.J., 1997, “Diesel Fuel Ignition Quality as Determined in the Ignition Quality Tester (IQT)-part II”, **SAE**, No. 971636, pp. 554-563.

Al-Rubaie, M.A.R., Griffiths, J.F. and Sheppard, C.G.W., 1991, “Some Observation on the Effectiveness of Additives for Reducing the Ignition Delay Period of Diesel Fuels”, **International Fuels and Lubricants Meeting and Exposition**, 7-10 October, Toronto, Canada.

AK Steel Corporation, 2007, **Specification of Stainless Steel 304/304** [Online], Available: http://www.aksteel.com/pdf/markets_products/stainless/austenitic/304_304L_Data_Sheet.pdf [2012, April 03].

Baert, R., Frijters, P., Somers, B., Luijten, C. and de Boer, W., 2009, “Design and Operation of a High Pressure, High Temperature Cell for HD Diesel Spray Diagnostics: Guidelines and Results”, **SAE 2009 World Congress**, 20-23 April, Detroit, Michigan, USA.

Bailey, B., Eberhardt, J., Goguen, S. and Erwin, J., 1997, “Diethyl Ether (DEE) as a Renewable Diesel Fuel”, **SAE**, No. 972978, pp. 1-7.

Beggs, D.H. and Brill, J.P., 1973, “A Study of Two-Phase Flow in Inclined Pipes”, **Journal of PetroleumTechnology**, Vol. 25 (5), pp. 607-617.

Benajes, J., Payri, R., Molina, S. and Soare, V., 2005, “Investigation of the Influence of Injection Rate Shaping on the Spray Characteristics in a Diesel Common Rail System Equipped with a Piston Amplifier”, **Journal of Fluids Engineering**, Vol. 127, 1102-1110.

Bika, A.S., Franklin, L.M. and Kittelson, D.B., 2009, “Hydrogen as a Combustion Modifier of Ethanol in Compression Ignition Engines”, **SAE 2009 Powertrains, Fuels & Lubricants Meeting,** 2-4 November, San Antonio, Texas, USA.

Birath, K., 2007, **Experiences from Introduction of Ethanol Buses and Ethanol Fuel Stations**. Report no. D 2.1 and D 2.2.

Boons, M., Van Den Bulk, R. and King, T., 2008, “The Impact of E85 Use on Lubricant Performance”, **2008 SAE International Powertrains, Fuels and Lubricants Congress,** 23-25 June, Shanghai, China.

Bower, G.R. and Foster, D.E. , 1991, “A Comparison of the Bosch and Zuech Rate of Injection Meters”, **International Congress and Exposition**, 25 February-1 March, Detroit, Michigan, USA.

Channiwala, S.A. and Parikh, P.P., 2002, “A Unified Correlation for Estimating HHV of Solid, Liquid and Gaseous Fuels”, **Fuel**, Vol. 81(8), pp. 1051-1063.

Chatterjee, D., Deutschmann, O. and Warnatz, J., 2001, “Detailed Surface Reaction Mechanism in a Three-Way Catalyst**”, Faraday Discuss,** Vol. 119, pp. 371–384.

Chen, R.H., Chiang, L.B., Wu, M.H. and Lin, T.H., 2009, “Gasoline Displacement and NO_x Reduction in an SI Engine by Aqueous Alcohol Injection”, **Fuel,** Vol. 89, pp. 604–610.

Cherry, M., Morrisset, R. and Bec, N., 1992, “Extending Lean Limit with Mass-Timed Compression Ignition Using a Catalytic Plasma Torch”, **Future Transportation Technology Conference & Exposition,** 10-13 August, Costa Mesa, California, USA.

Chollacoop, N., Saisirirat, P., Sukkasi, S., Tongroon, M., Fukuda, T., Fukuda, A. and Nivitchanyong, S., 2013, “Potential of Greenhouse Gas Emission Reduction in Thai Road Transport by Ethanol Bus Technology”, **Applied Energy,** Vol. 102, pp. 112–123.

Clemente, R.C., Werninghaus, E., Coelho, E.P.D. and Ferraz, L.A.S., 2001, “Development of an Internal Combustion Alcohol Fueled Engine”, **SAE,** No. 2001–01-3917.

Costa, R.C. and Sodre, J.R., 2009, “Hydrous Ethanol vs. Gasoline–Ethanol Blend: Engine Performance and Emissions”, **Fuel,** Vol. 89, pp. 287–93.

Curran, H.J., Dunphy, M.P. and Simmie, J.M., 1992, “Shock Tube Ignition of Ethanol, Isobutene and MTBE: Experiments and Modeling”, **Proceedings of the Combustion Institute,** Vol. 24(1), pp.769-776.

da Silva, R.D., Cataluña, R., de Menezes, D.W., Samios, D. and Piatnicki, C.M.S., 2005, “Effect of Additives on the Antiknock Properties and Reid Vapor Pressure of Gasoline”, **Fuel,** Vol. 84, pp. 951–959.

Department of Alternative Energy Development and Efficiency (DEDE), 2012, **The Renewable and Alternative Energy Development Plan for 25 Percent in 10 Years (AEDP 2012-2021)** [Online], Available: http://www.dede.go.th/dede/images/stories/dede_aedp_2012_2021.pdf [2014, June 1].

Ecklund, E., Bechtold, R., Timbario, T. and McCallum, P., 1984, “State-of-the-Art Report on the Use of Alcohols in Diesel Engines”, **SAE**, No. 840118.

Egeback, KL., 1993, “Experiences from the Use of Ethanol for Heavy Duty Compression Ignition Engines”, **SAE,** No. 931630.

Fenton, P. and Carlsson, H., 2009, **BioEthanol for Sustainable Transport Results and Recommendations from the European BEST Project**, LenandersGrafiska AB, pp. 8-21.

Fujiomoto, H.G., Higashi, K., Yamashita, T. and Senda, J., 2005, "Effects of Ambient Temperature and Oxygen Concentration on Soot Behavior in Diesel Flame", **SAE,** No. 2005-24-007.

Han, J.S., Lu, P.H., Xie, X.B., Lai, M,C. and Henein, N.A., 2002, "Investigation of Diesel Spray Primary Break-up and Development for Different Nozzle Geometries", **SAE**, No. 2002-01-2775.

Hansen, A.C., Lyne, P.W.L. and Zhang, Q., 2001, "Ethanol-Diesel Blends: a Step Towards a Bio-Based Fuel for Diesel Engines", **ASAE Annual International Meeting**, Paper no. 01-6048, 30 July -1 August 2004, California.

Hara, T. and Tanoue, K., 2006, "Laminar Flame Speeds of Ethanol, n-Heptane, Iso-Octane Air Mixtures", **FISITA 2006 World Automotive Congress**, 22–27 October 2006, Yokohama.

Hardenberg, H. and Ehnert, E., 1981, "Ignition Quality Determination Problems with Alternative Fuels for Compression Ignition Engines", **SAE**, No. 811212.

Hardenberg, H.O. and Schaefer, A.J., 1981, "The Use of Ethanol as a Fuel for Compression Ignition Engines", **SAE**, No. 811211,.

Haupt, D., Nord, K., Egebäck, K.E. and Ahlvik, P., 2004, "Hydrocarbons and Aldehydes from a Diesel Engine Running on Ethanol and Equipped with EGR, Catalyst and DPF", **SAE,** No. 2004-01-1882.

Haupt, D., Nord, K., Tingvall, B., Ahlvik, P., Egebäck, K.E., Andersson, S. and Blomquist, M., 2004, "Investigating the Potential to Obtain Low Emissions from a Diesel Engine Running on Ethanol and Equipped with EGR, Catalyst and DPF", **SAE,** No. 2004-01-1884.

Haupt, D. and Nord, K., 2009, "Aftertreatment Strategy for Reducing Emissions from an Ethanol Fueled CI Engine", **SAE**, No. 2009-01-1949.

He, B.Q., Wang, J.X., Hao, J.M., Yan, X.G. and Xiao, J.H., 2002, "A Study on Emission Characteristics of an EFI Engine with Ethanol Blended Gasoline Fuels", **Atmospheric Environment**, Vol. 37, pp.949–957.

Hess, 2012**, Diesel Safety Data Sheet** [Online], Available: http://www.hess.com/docs /us-safety-data-sheets/dieselfuel_alltypes_includingultralowsulfur_diesel(ulsd).pdf? sfvrsn=2 [2014, July 20].

Heidaryan, E., Salarabadi, A. and Moghadasi, J., 2010, "A Novel Correlation Approach for Prediction of Natural Gas Compressibility Factor", **Journal of Natural Gas Chemistry**, Vol. 19 (2), pp. 189–192.

Heilig, A., Kaiser, M. and Dinkelacker, F., 2011, "Spray Analysis and Comparison of Diesel and Diodiesel-Methanol Blends", **ILASS – Europe 2011, 24th European Conference on Liquid Atomization and Spray Systems,** 5-7 September 2011, Estoril, Portugal.

Heywood, J.B., 1988, Internal Combustion Engine Fundamental, McGraw-Hill, New York.

Hottel, H.C. and Broughton, F.P., 1932, "Determination of True Temperature and Total Radiation from Luminous Gas Flames", **Journal of Industrial and Engineering Chemistry**, Vol. 4(2), pp. 166-175.

Hu, C., Jian-Xin, W., Shi-Jin, S., Xin-Liang, A. and Wen-Miao, C., 2006, "Effects of Ethanol in Ester-Ethanol-Diesel Blended Fuels on Spray Behavior and PM Emission", **SAE,** No. 2006-01-0236.

International Energy Agency (IEA), 2014, **Biofuel** [Online], Available: http://www.iea.org/topics/biofuels/ [2014, May 21].

International Energy Agency (IEA), 2013, **CO_2 Emissions From Fuel Combustion Highlights** [Online], Available: http://www.iea.org/publications/freepublications/publication/KeyWorld2013.pdf [2014, May 21].

International Energy Agency (IEA), 2013, **Energy Technology Perspective 2010** [Online], Available: https://www.iea.org/publications/freepublications/publication/etp2010.pdf [2014, May 21].

International Energy Agency (IEA), 2013, **2013 Key World Energy Statistics** [Online], Available: http://www.iea.org/publications/freepublications/publication/KeyWorld2013.pdf [2014, May 21].

Jeuland, N., Montagne, X. and Gautrot, X., 2004, "Potentiality of Ethanol as a Fuel for Dedicated Engine", **Oil Gas Sci Techno – Revue d'IFP Energies,** Vol. 59, pp. 559–570.

Kašpar, J., Fornasiero, P. and Hickey, N., 2003, "Automotive Catalytic Converters: Current Status and Some Perspectives", **Catalysis Today,** Vol. 77, pp. 419–449.

Kobori, S. and Kamimoto, T., 1995, "Development of a Rapid Compression-Expansion Machine Simulating Diesel Combustion", **SAE**, No. 952514.

Koop, J. and Deutschmann, O., 2009, "Detailed Surface Reaction Mechanism for Pt-Catalyzed Abatement of Automotive Exhaust Gases", **Applied Catalysis B,** Vol. 91, pp. 47–58.

Kwon, S.I., Arai, M. and Hiroyasu, H., 1990, "Effects of Cylinder Temperature and Pressure on Ignition Delay in Direct Injection Diesel Engine", **Bulletin of the Mechanical Engineering Scientific Journal**, Vo1. 18, No.1.

Ladisch, M.R. and Dyck, K., 1979, "Dehydration of Ethanol: New Approach Gives Positive Energy Balance", **Science**, Vol. 205, pp. 898-900.

Laoonual, Y., 2013, “Ethanol Fuel Technology for Substitution of Diesel Part 1”, **Automotive Navigator Magazine**, Vol. Jul/Sep 2013, p. 26.

Laoonual, Y., 2013, “Ethanol Fuel Technology for Substitution of Diesel Part 2”, **Automotive Navigator Magazine**, Vol. Oct/Dec 2013, p. 28.

Leclercq, L., Robyns, B. and Grave, J.M., 2003, “Control Based on Fuzzy Logic of a Flywheel Energy Storage System Associated with Wind and Diesel Generators”, **Mathematics and Computers in Simulation,** Vol. 63, pp. 271–280.

Lee, D., Hochgreb, S. and Keck, J.C., 1993, “Autoignition of Alcohols and Ethers in a Rapid Compression Machine”, **SAE**, No. 932755.

Lee, S.W., Park, S. and Daisho, Y., 2004, “An Experimental Study of the Effects of Combustion Systems and Fuel Properties on the Performance of a Diesel Engine”, **Proceedings of the Institution of Mechanical Engineers, Part D: Journal of Automobile Engineering**, vol. 218, pp. 1317-1323.

Lee, W.J., Liu, Y.C., Mwangi, F.K., Chen, W.H., Lin, S.L., Fukushima, Y., Liao, C.N. and Wang, L.C., 2011, “Assessment of Energy Performance and Air Pollutant Emissions in a Diesel Engine Generator Fueled with Water-Containing Ethanol–Biodiesel–Diesel Blend of Fuels”, **Energy,** Vol. 36, pp. 5591–5599.

Li, J., Gong, C.M., Su, Y., Dou, H.L. and Liu, X.J., 2010, “Effect of Injection and Ignition Timings on Performance and Emissions from a Spark-Ignition Engine Fueled with Methanol”, **Fuel,** Vol. 89, pp. 3919–3925.

Li, L., Liu, Z., Wang, H., Deng, B., Xiao, Z., Wang, Z., Gong, C. and Su, Y., 2003, “Combustion and Emission of Ethanol Fuel (E100) in Small SI Engine”, **SAE,** No. 2003–01-3262.

Lif, A. and Svennberg, S., 1997, **Ethanol Fuel and the Use of an Ignition Improver**, US. Patent, No. 5,628,805.

Kosaka, H. and Arai, T., 2011, “Simultaneous Measurements of Temperatures of Flame and Wall Surface in a Combustion Chamber of Diesel Engine”, **SAE**, No. 2011-01-2047.

Mack, J.H., Aceves, S.M. and Dibble, R.W., 2009, “Demonstrating Direct Use of Wet Ethanol in a Homogeneous Charge Compression Ignition (HCCI) Engine”, **Energy,** Vol. 34, pp. 782–787.

Magnusson, R., Nilsson, C. and Andersson, B., 2002, “Emissions of Aldehydes and Ketones from a Two-Stroke Engine using Ethanol and Ethanol-Blended Gasoline as Fuel”, **Environmental Science & Technology,** Vol. 36, pp. 1658–1664.

Magnusson, R. and Nilsson, C., 2011, “The Influence of Oxygenated Fuels on Emissions of Aldehydes and Ketones from a Two-Stroke Spark Ignition Engine”, **Fuel,** Vol. 90, pp.1145–1154.

Marcic, M., 1999, “A New Method for Measuring Fuel-Injection Rate”, **Flow Measurement and Instrumentation**, Vol. 10, pp.159–165.

Marcic, M., 2006, “Sensor for Injection Rate Measurements”, **Sensors**, Vol. 6, pp. 1367-1382.

Marinov, N.M., 1999, “A Detailed Chemical Kinetic Model for High Temperature Ethanol Oxidation”, **International Journal of Chemical Kinetics,** Vol. 31, pp. 183–220.

Martinez-Frias, J., Aceves, S.M. and Flowers, D.L., 2007, “Improving Ethanol Life Cycle Energy Efficiency by Direct Utilization of Wet Ethanol in HCCI Engines”, **Transactions of the American Society of Mechanical Engineers,** Vol. 129, pp. 332–337.

Matsui, Y., Kamimoto, T. and Matsuoka, S., 1979, “A Study on the Time and Space Resolved Measurement of Flame Temperature and Soot Concentration in a DI Diesel Engine by the Two-Colour Method”, **SAE**, No. 790491.

Moreira, J.R., dos Santos, S.M.A., Coelho, S.T., Velázquez, S.M.S.G., Melo, E.H. and Elmadjian, P.H.B., 2008, “Bioethanol for Sustainable Transport - BEST Project”, **SAE,** No. 2008-36-0216.

Mott, R.L., 2008, **Applied Strength of Materials**, Prentice Hall, New Jersey.

National Renewable Energy Laboratory and National Ethanol Vehicle Coalition, 2006, “Handbook for Handling, Storing, and Dispensing E85”, **Energy Efficiency and Renewable Energy,** p.11.

Nguyen, D. and Honnery, D., 2008, “Combustion of Bio-Oil Ethanol Blends at Elevated Pressure”, **Fuel**, Vol. 87 (2), pp. 232–243.

Nguyen, D.N., Ishida, H. and Shioji, M., 2010, “Ignition Delay and Combustion Characteristics of Gaseous Fuel Jets”, **Journal of Engineering for Gas Turbines and Power**, vol. 132, pp. 1-8.

Nilaphai, O., Bavornsethanan, S., Kaewtatip, P. and Laoonual, Y., 2012, “Preliminary Evaluation of Fuel Economy of the First ED95 Ethanol Bus in Thailand” (in Thai), **The 26th conference on mechanical engineering network of thailand (ME-NETT),** 24-27 October 2012, Chiangrai, Thailand.

Niven, R.K., 2005, “Ethanol in Gasoline: Environmental Impacts and Sustainability Review Article”, **Renew Sustain Energy,** Vol. 9, pp. 535–555.

Nord, K., Haupt, D., Ahlvik, P. and Egebäck, K.E., 2004, “Particulate emissions from an Ethanol Fueled Heavy-Duty Diesel Engine Equipped with EGR, Catalyst and DPF”, **SAE**, No. 2004-01-1987.

Olberding, J., Beyerlein, D.C.S., Steciak, J. and Cherry, M., 2005, “Dynamometer Testing of an Ethanol-Water Fueled Transit Van”, **SAE,** No. 2005-01-3706.

Oren, D., Wahiduzzaman, S. and Ferguson, C, 1984, “A Diesel Combustion Bomb: Proof of Concept”, **SAE,** No. 841358.

Organisation for Economic Co-operation and Development-Food and Agriculture Organization of the United Nations (OECD-FAO), 2011, **OECD-FAO Agricultural Outlook 2011–2020** [Online], Available: http://dx.doi.org/10.1787/agr_outlook-2011-en [2012, August 04].

Patum vetgetable oil Co., LTD, 2009, **Biodiesel Material Safety Data Sheet**, Bangkok.

Payri, R., García, A., Domenech, V., Durrett, R. and Plazas, A.H., 2012, “An Experimental Study of Gasoline Effects on Injection Rate, Momentum Flux and Spray Characteristics using a Common Rail Diesel Injection System”, **Fuel**, Vol. 97, pp. 390–399.

Payri, R., Salvador, F.J., Gimeno, J. and Venegas, O., 2013, “Study of Cavitation Phenomenon using Different Fuels in a Transparent Nozzle by Hydraulic Characterization and Visualization”, **Experimental Thermal and Fluid Science**, Vol. 44, pp. 235–244.

Pepermans, G., Driesen, J., Haeseldonckx, D., Belmans, R. and D’haeseleer, W., 2005, “Distributed Generation: Definition, Benefits and Issues”, **Energy Policy,** Vol. 33, pp. 787–798.

Petro Green Co., LTD, 2009, **Ethanol Material Safety Data Sheet**, Bangkok.

Phan, A., 2009, **Development of a Rate of Injection Bench and constant Volume Combustion Chamber for Diesel Spray Diagnostics**, Master thesis, Mechanical Engineering, Iowa State University.

Poulopoulos, S.G., Samaras, D.P. and Philippopoulos, C.J., 2001, “Regulated and Unregulated Emissions from an Internal Combustion Engine Operating on Ethanol Containing Fuels”, **Atmospheric Environment,** Vol. 35, pp. 4399–4406.

Rodríguez-Fernández, J., Tsolakis, A., Theinnoi, K., Snowball, J., Sawtell, A. and York, A.P.E., 2009, “Engine Performance and Emissions from Dual Fuelled Engine with In-Cylinder Injected Diesel Fuels and In-Port Injected Bioethanol”, **SAE**, No.2009-01-1853.

Saitoh, H. and Uchida, K., 2004, “Effect of Hot EGR on Combustion and Emission Characteristics in a Diesel Type Alcohol Engine”, **Proceeding of 24th CIMAC World Congress on Combustion Engine Technology**, 7-11 June 2004, Kyoto.

Saitoh, H. and Uchida, K., 2007, “Difference of Spray Mixture Formation Between Gas-Oil and Ethanol in the Constant Volume Electrical Heating Chamber”, **SAE**, No. 2007-01-3617.

Saitoh, H. and Uchida, K., 2009, “On the Main Factors Governing Auto-Ignition Phenomenon of Alcohol Spray – A Study from the View Point of Fuel Properties”, **SAE**, 2009-01-1931.

Sanjari, E. and Lay, N.J., 2012, “An Accurate Empirical Correlation for Predicting Natural Gas Compressibility Factors”, **Journal of Natural Gas Chemistry**, Vol. 21(2), pp. 184–188.

Schaefer, A.J. and Hardenberg, H.O., 1981, “Ignition Improvers for Ethanol Fuels”, **SAE**, No. 810249.

Schifter, I., Diaz, L., Rodriguez, R., Gómez, J.P. and Gonzalez, U., 2011, “Combustion and Emissions Behavior for Ethanol–Gasoline Blends in a Single Cylinder Engine”, **Fuel,** Vol. 90, pp. 3586–3592.

Schmidt, D.P., 1997, **Cavitation in Diesel Fuel Injector Nozzles**, Dissertation, Department of Mechanical Engineering, University of Wisconsin – Madison.

Sciencelab.com, Inc., 2013, **Ethyl Ester Material Safety Data Sheet**, Texas.

Sigma-Aldrich Corporation, 2011, **Specification of Glycerol Ethoxylate**, Missouri.

Siebers, D. and Edwards, C., 1987, "Autoignition of Methanol and Ethanol Sprays under Diesel Engine Conditions", **SAE,** No. 870588.

Siebers, D. and Higgins, B., 2001, "Flame Lift-Off on Direct Injection Diesel Sprays Under Quiescent Conditions", **SAE**, No. 2001-01-0530.

Simonsen, H. and Chomiak, J., 1995, "Testing and Evaluation of Ignition Improvers for Ethanol in a DI Diesel Engine", **SAE**, No. 952512.

Shapouri, H., Duffield, J.A. and Graboski, M.S., 1995, "Estimating the Net Energy Balance of Corn Ethanol", **USDA Economic Research Service Report,** No. AER-721.

Shapouri, H., Duffield, J.A. and Wang, M., 2003, "The Energy Balance of Corn Ethanol Revisited", **Transactions of the American Society of Agricultural Engineers,** Vol. 46, pp. 959–968.

Sou, A., Hosokawa, S., Tomiyama, A., 2007, "Effects of Cavitation in a Nozzle on Liquid Jet Atomization", **International Journal of Heat and Mass Transfer**, Vol. 50, pp. 3575–3582

State of California Air Resources Board, 2005, **California Exhaust EmissionStandards and Test Procedures for 2005 and Later Small Off-Road Engines** [Online], Available: http://www.arb.ca.gov/msprog/OFFROAD/sore/sorectp/sorectp.html [2010, May 10].

Sun, J., Caton, J.A. and Jacobs, T.J., 2010, "Oxides of Nitrogen Emissions from Biodiesel-Fuelled Diesel Engines", **Progress in Energy and Combustion Science**, Vol. 36(6), pp. 677-695.

Svensson, K., Mackrory, A., Richards, M. and Tree, D., 2005, “Calibration of an RGB, CCD Camera and Interpretation of Its Two-Color Images for KL and Temperature”, **SAE**, No. 2005-01-0648.

Tosoh Corporation, 2011, **Specification of Fused Silica Quartz** [Online], Available: http://www.tosoh.com/our-products/advanced-materials/silica-glass [2012, April 03].

Turner, D., Xu, H., Cracknell, R.F., Natarajan, V. and Chen, X., 2011, “Combustion Performance of Bio-Ethanol at Various Blend Ratios in a Gasoline Direct Injection Engine”, **Fuel,** Vol. 90, pp. 1999–2006.

Tsuda, S., 2007, **A Study on Effect of Heterogeneity of Oxygen Concentration and Temperature Distributions in Combustion Chamber on Emissions and Combustion of Diesel Engine,** Master Thesis (in Japanese), Department of Mechanical and Aerospace Engineering, Tokyo Institute of Technology, Tokyo.

U.S. Environmental Protection Agency, 2007, **Integrated Risk Information System (IRIS) on Acetaldehyde and Formaldehyde** [Online], Available: http://www.epa.gov [2010, May 10].

U.S. Environmental Protection Agency, 2010, **Nonroad Spark-Ignition Engines 19 kW and below – Exhaust Emission Standards** [Online], Available: http://www.epa.gov/otaq/standards/nonroad/smallsi-exhaust.html [2010, May 10].

Velázquez, S., Apolinário, S.M., Melo, E.H., Elmajian, P.H.B., Janssen, R. and Hofer, A., 2009, **Report on Experiences of Ethanol Buses and Fuel Stations in São Paulo. Final report**, Report no. D2.07.

Verhoeven, D., Vanhemelryck, J. and Baritaud, T., 1998, “Macroscopic and Ignition Characteristics of High-Pressure Sprays of Single-Component Fuels”, **SAE**, No. 981069.

Vongsoasup, S., 2014, **Alternative Fuel Policy for Thai Transportation** [Online], Available: http://www.thaiauto.or.th/2012/Automotive-Summit2014/doc/Program_files/PPT/221/Mrs.%20Sirinthorn%20Vongsoasup.pdf [2014, June 21].

Wagner, T. and Wyszyhki, M.L., 1996, "Aldehydes and Ketones in Engine Exhaust Emissions – a Review", **IMechE,** Vol. 104, pp.109–122.

Wakuri, Y., Fujii, M., Amitani, T. and Tsuneya, R., 1960, "Study on the Phenomena of Fuel Spray in a Diesel Engine", **Bulletin of JSME**, vol. 3 (9), pp. 123-130.

Yates, A., Bell, A. and Swarts, A., 2010, "Insights Relating to the Autoignition Characteristics of Alcohol Fuels", **Fuel**, Vol. 89, pp. 83-93.

Zhang, N., Huang, Z., Wang, X. and Zheng, B., 2011, "A Comparative Study of Two Kinds of Biodiesels and Biodiesel-DEE Blends in a Common Rail Diesel Engine", **SAE**, No. 2011-01-0640.

Zhao, H. and Ladommatos, N., 1998, "Diesel Engine Temperatures and Soot Particle Densities Measured by the Two-Colour Method in Diesel Engines", **Progress in Energy and Combustion Science**, Vol. 24, pp. 221-155.

Zhao, H. and Ladommatos, N., 1998, "Optical Diagnostics for In-Cylinder Mixture Formation Measurements in IC Engines", **Progress in Energy and Combustion Science**, Vol. 24, pp. 297–336.

Zhu, L., Cheung, C.S., Zhang, W.G. and Huang, Z., 2011, "Combustion, Performance and Emission Characteristics of a DI Diesel Engine Fueled with Ethanol-Biodiesel Blends Fuel", **Fuel**, Vol. 90(5), pp. 1743-1750.

APPENDIX A

Constant Volume Combustion Chamber

Appendix A.1 shows all drawing of CVCC parts. Figure A.1 and Fugure A.2 show the CVCC assembly and miscellaneous devices. The geometry and dimension of all parts are obtained from design as shown in Chapter 3. The difference between Figure A.1 and Figure A.2 is the combustion chamber head. There are two types of combustion chamber head, i.e. steel head (Figure A.1) and window head (Figure A.2). However, the steel head is only used in this work. Figure A.3 to Figure A.6 show all details of CVCC. The dimension of all figure is shown in millimeter. Figure A.7 shows the drawing of head for injector. The injector cooling system is at the center of head. The injector is connected to this head in the experiments. Figure A.8 shows water jacket which is a part of the head for injector. The injector clamp is shown in Figure A.9. The base or support of CVCC is shown in Figure A.10. There is a small cylinder chamber at the center of the support. This small chamber is used for gas released from the explosion of rupture disc. Figure A.11 shows the steel head using in this work. Figure A.12 shows the head for window. Unfortunately, it do not use in this study. Figure A.13 show the window clamp. This is used to lock the window. Quartz window is shown in Figure A.14.

Appendix A.2 shows wiring diagram of electronic devices

Appendix A.3 shows the ARDUINO code used to control spark plug and injector in combustion experiment.

Appendix A.4 shows temperature of pre-combsution which is calculated from pressure using equation (3.10).

Appendix A.5 shows the calculation of the compressibility of the production gas compressibility factor (Z)

A.1 CVCC Drawing

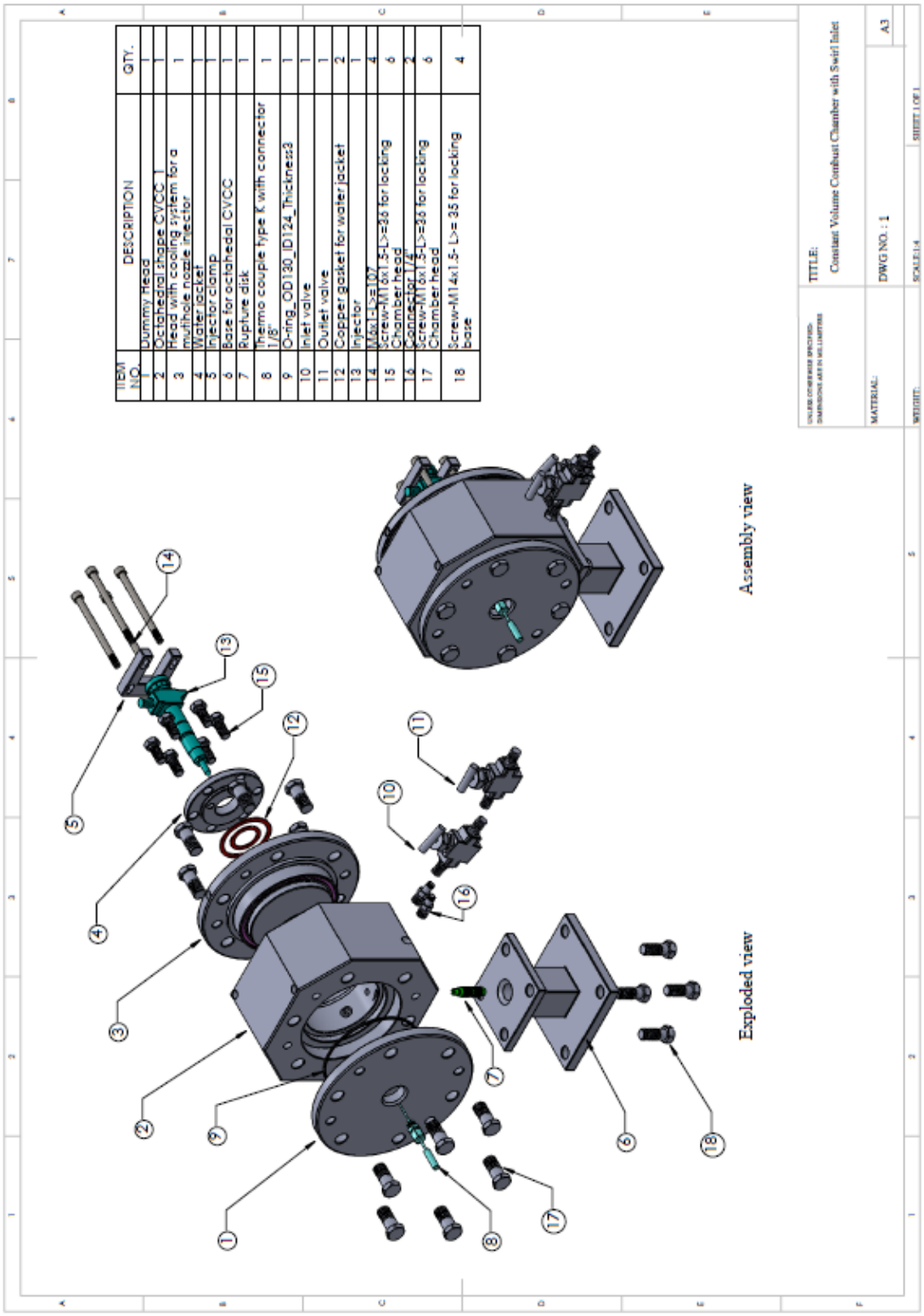

Figure A.1 CVCC with steel head (File: Assembly_CVCC1).

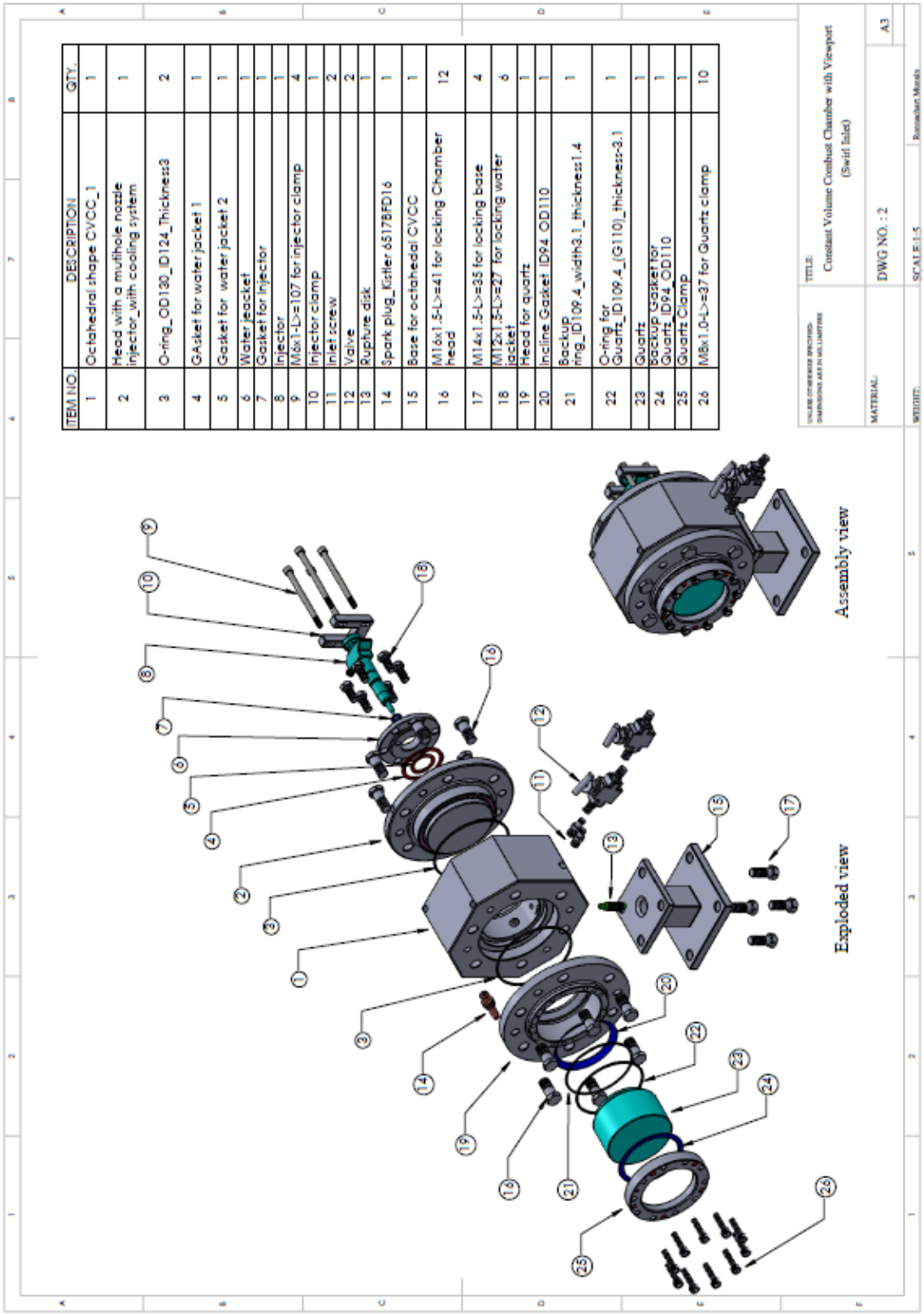

Figure A.2 CVCC with window head (File: Assembly_CVCC2).

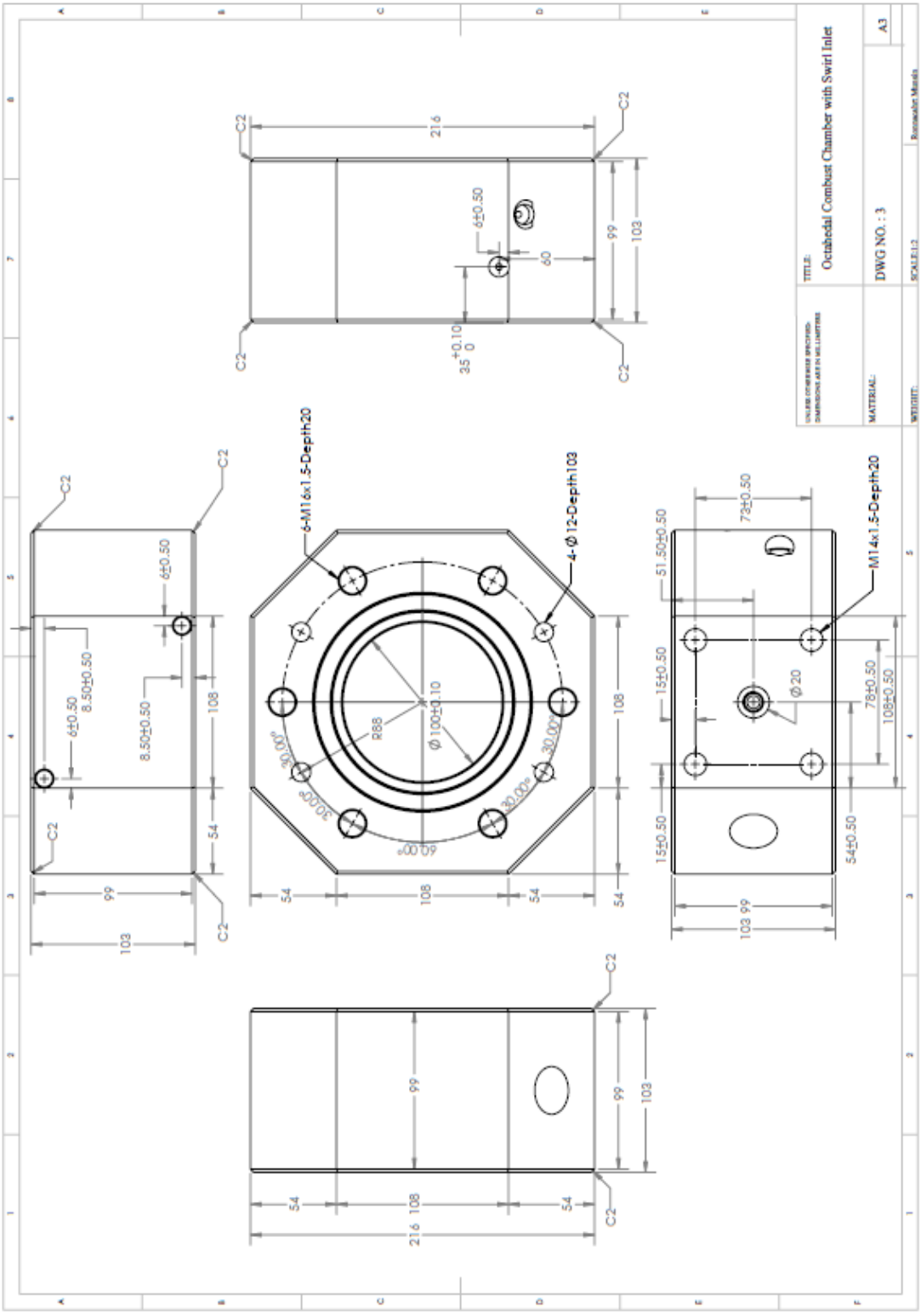

Figure A.3 Drawing of CVCC-1 (File: CVCC_section1).

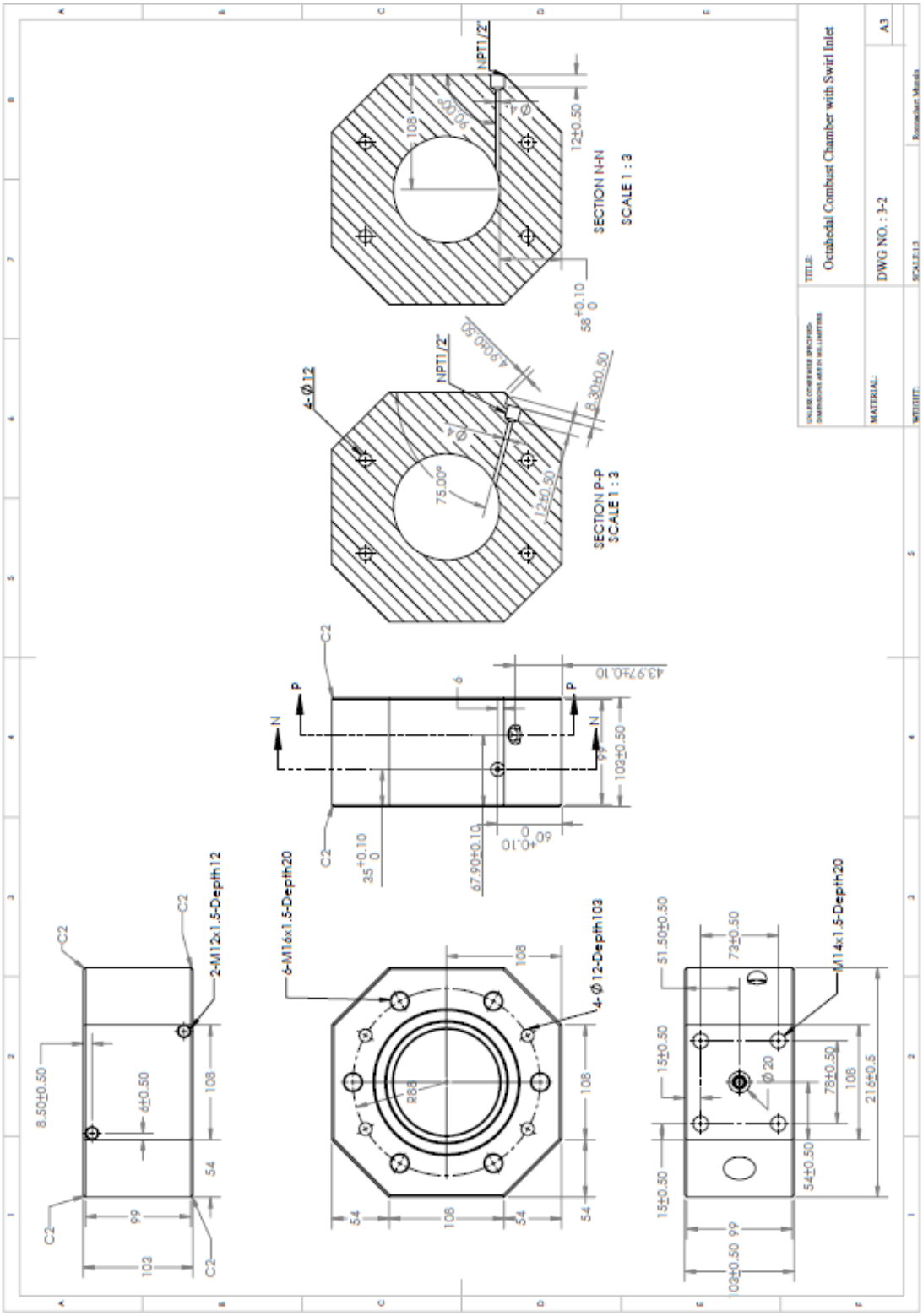

Figure A.4 Drawing of CVCC-2 (File: CVCC_section2).

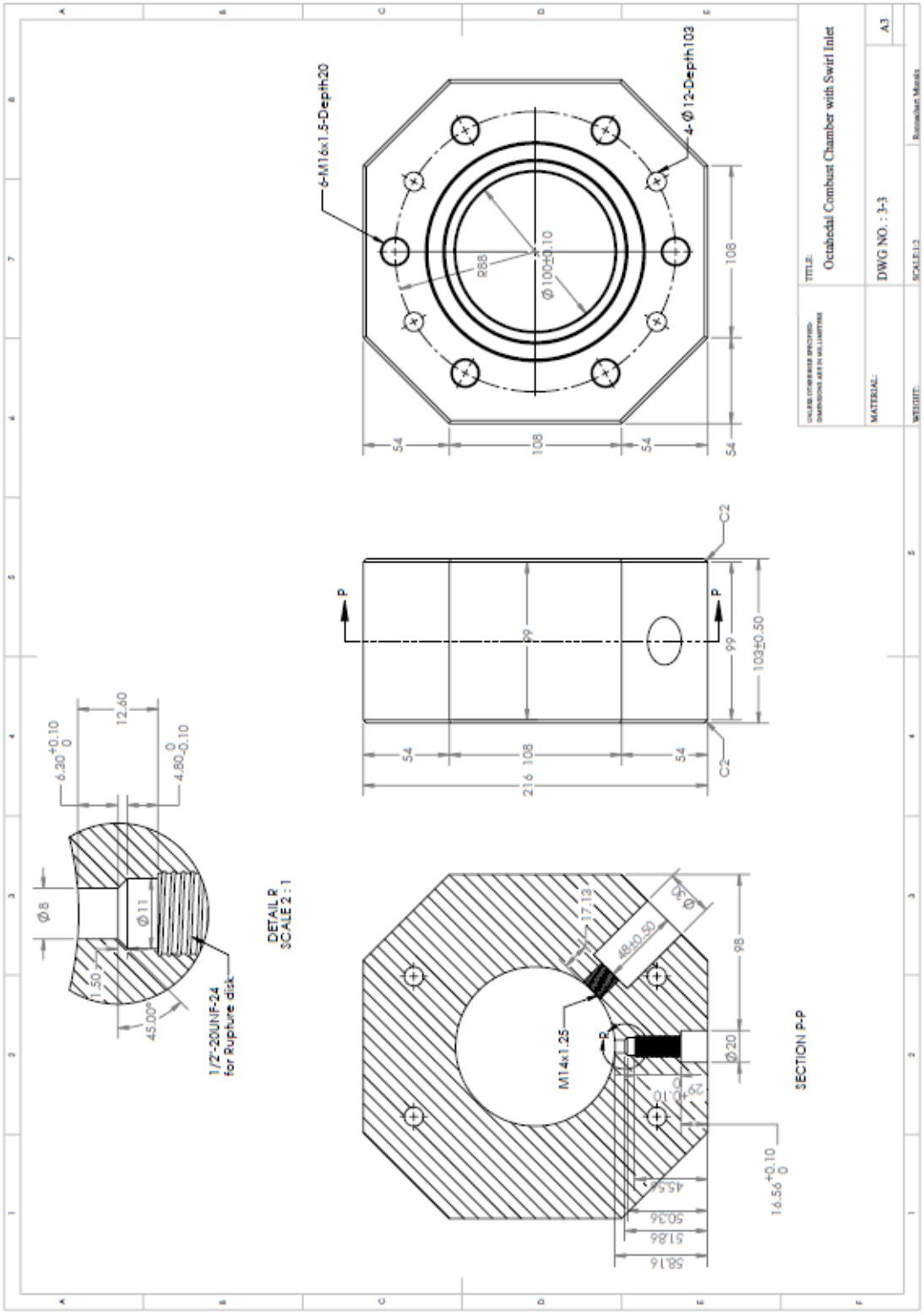

Figure A.5 Drawing of CVCC-3 (File: CVCC_section3).

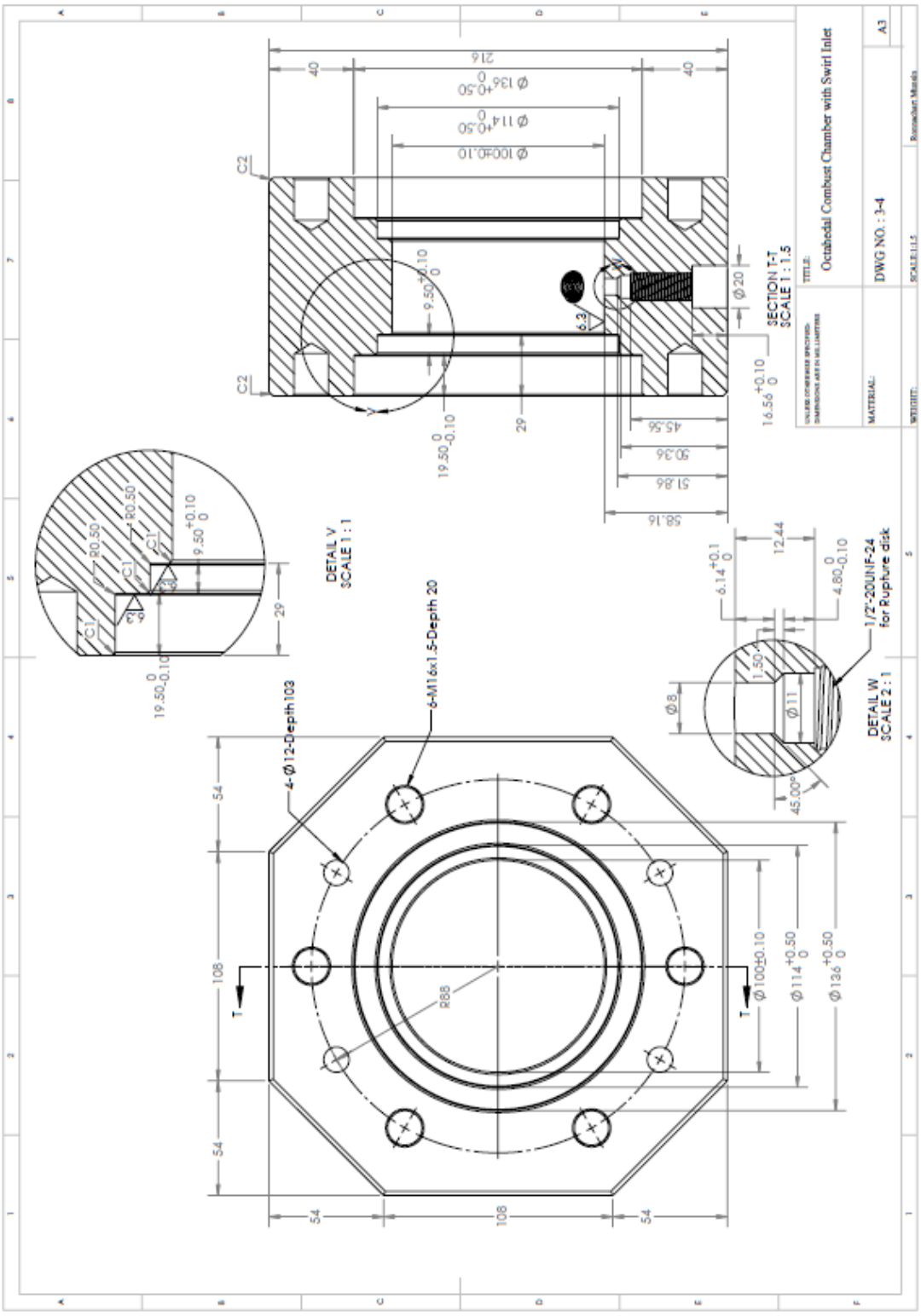

Figure A.6 Drawing of CVCC-4 (File: CVCC_section4).

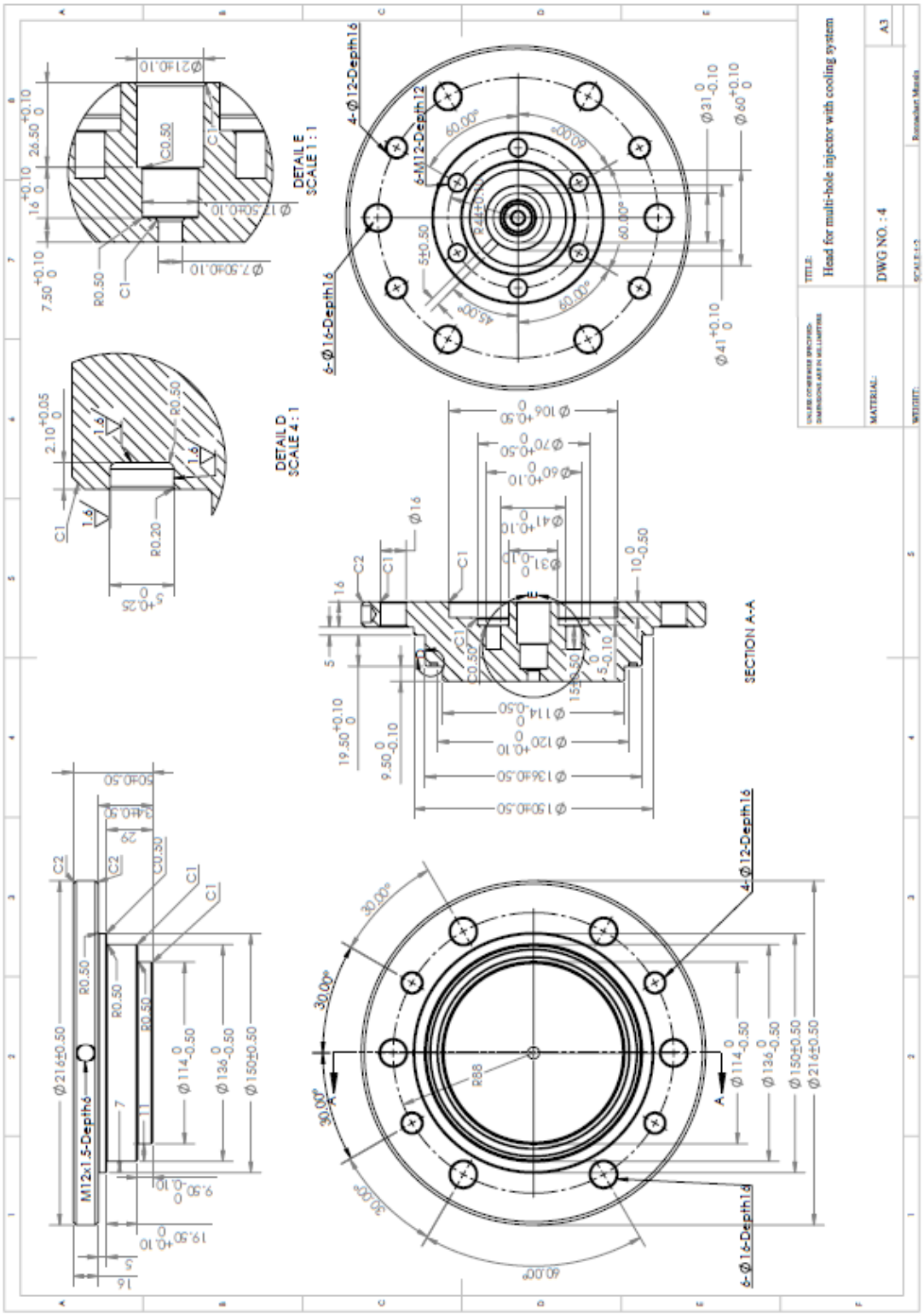

Figure A.7 Head for injector (File: Head for injector).

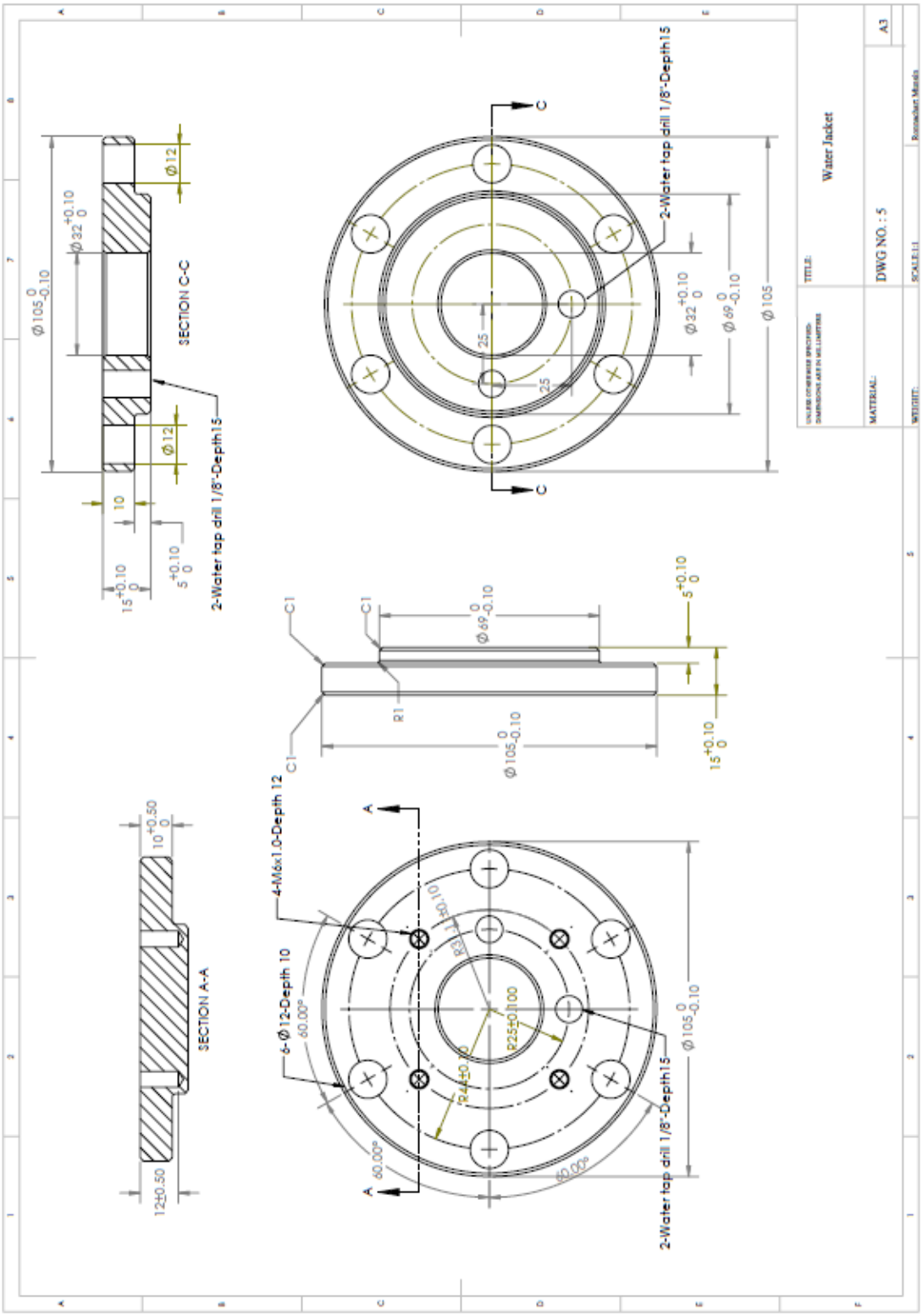

Figure A.8 Water jacket (File: Water jacket).

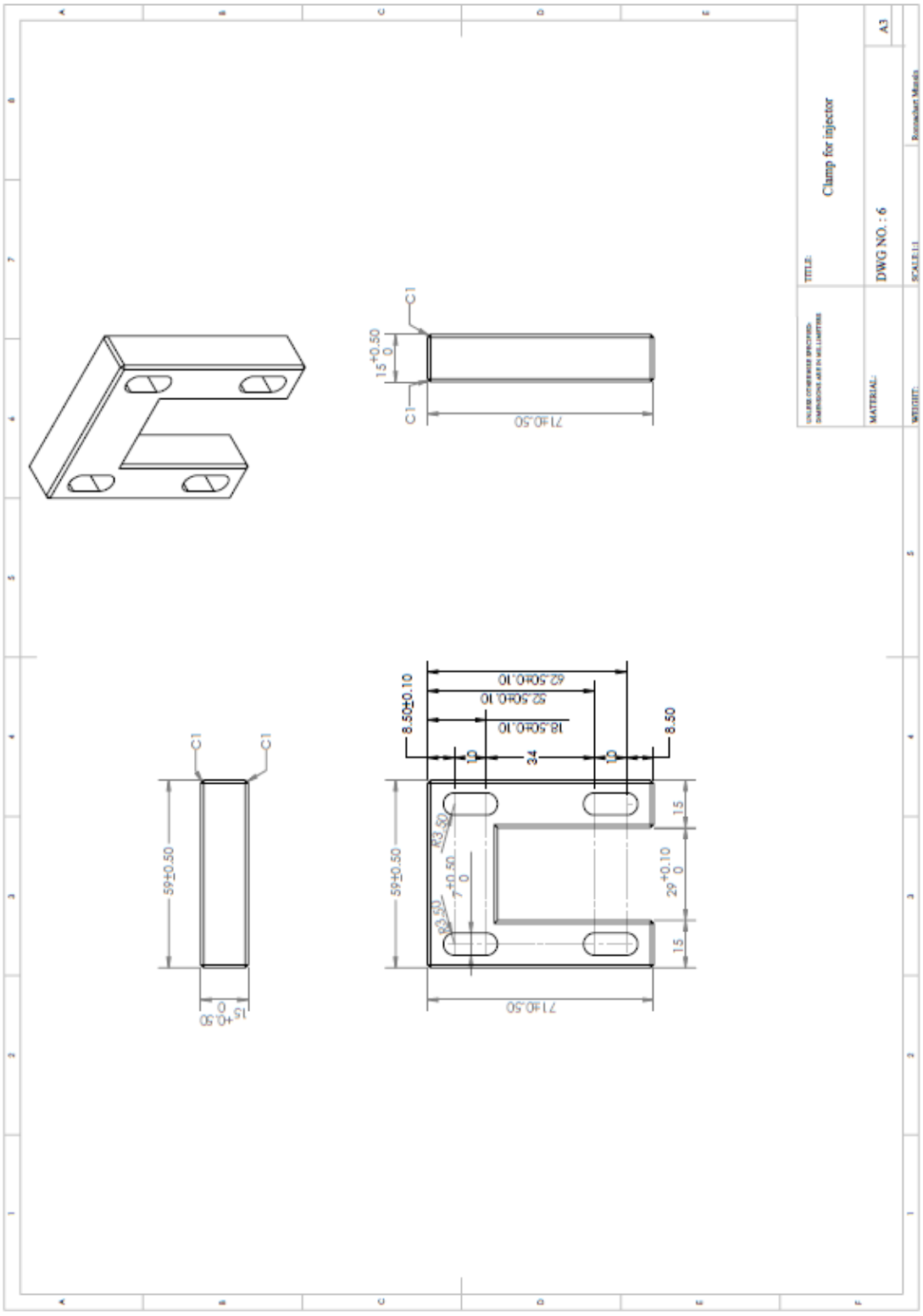

Figure A.9 Injector clamp (File: Injector clamp).

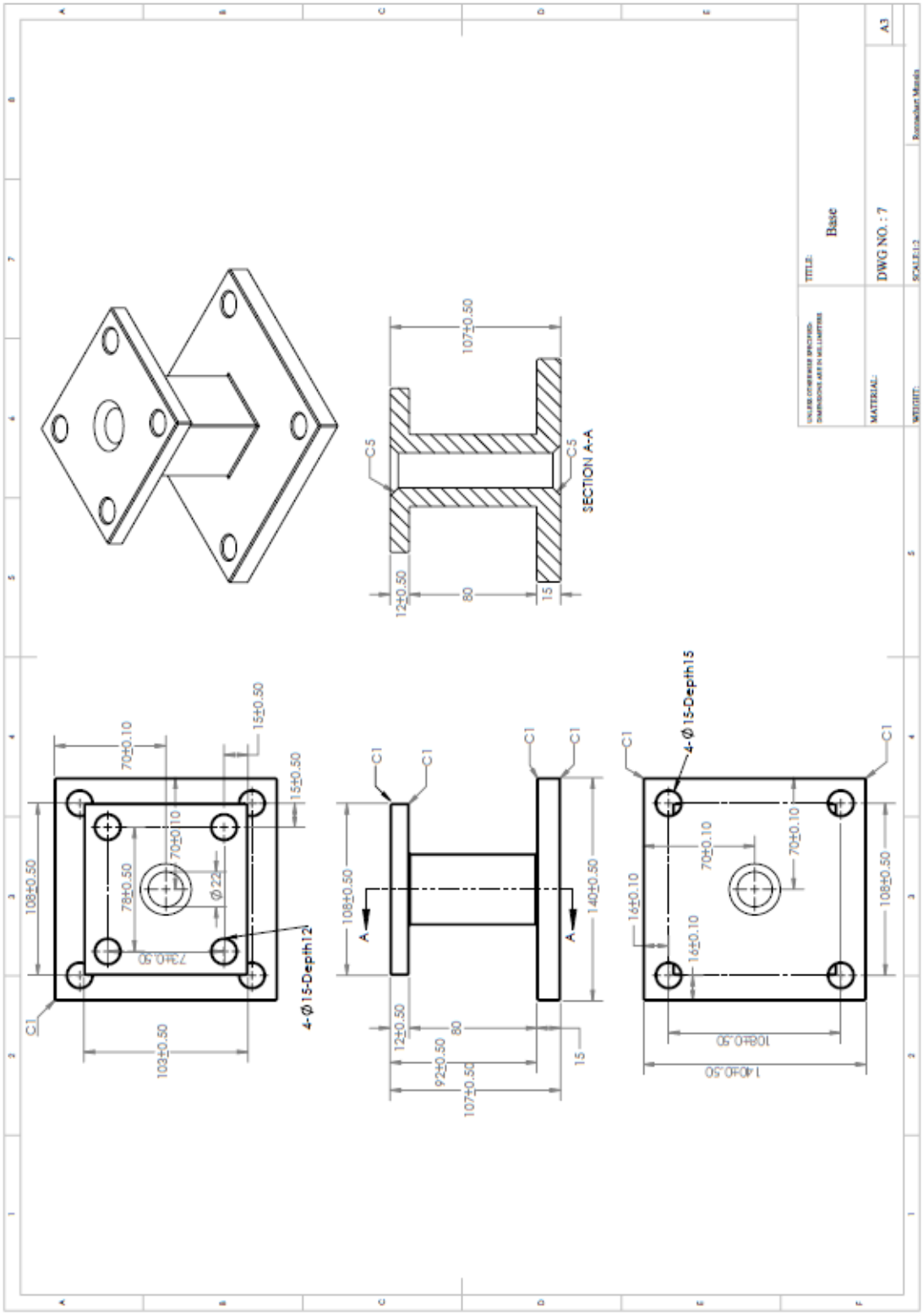

Figure A.10 Base (File: Base).

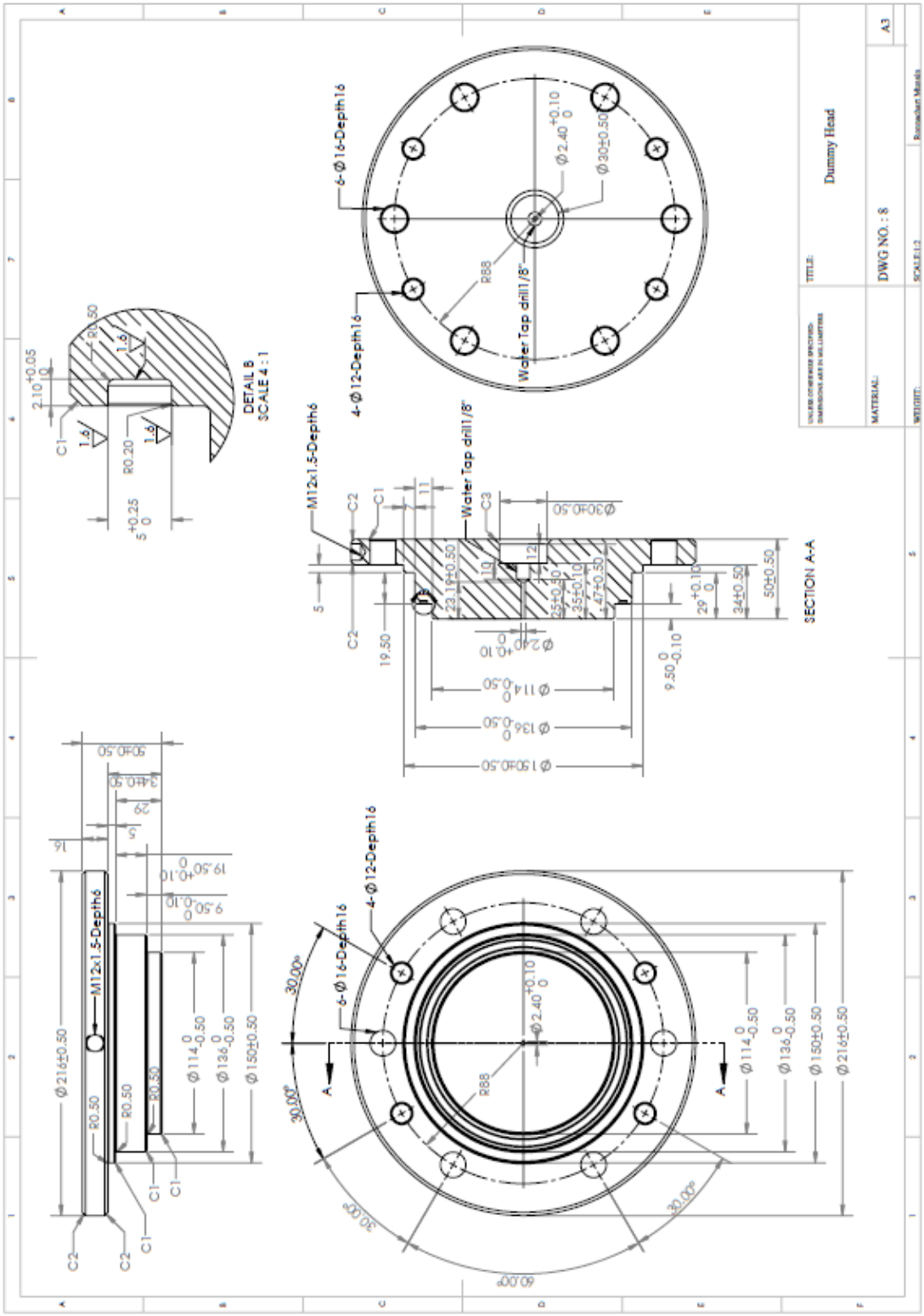

Figure A.11 Steel head (File: Steel head).

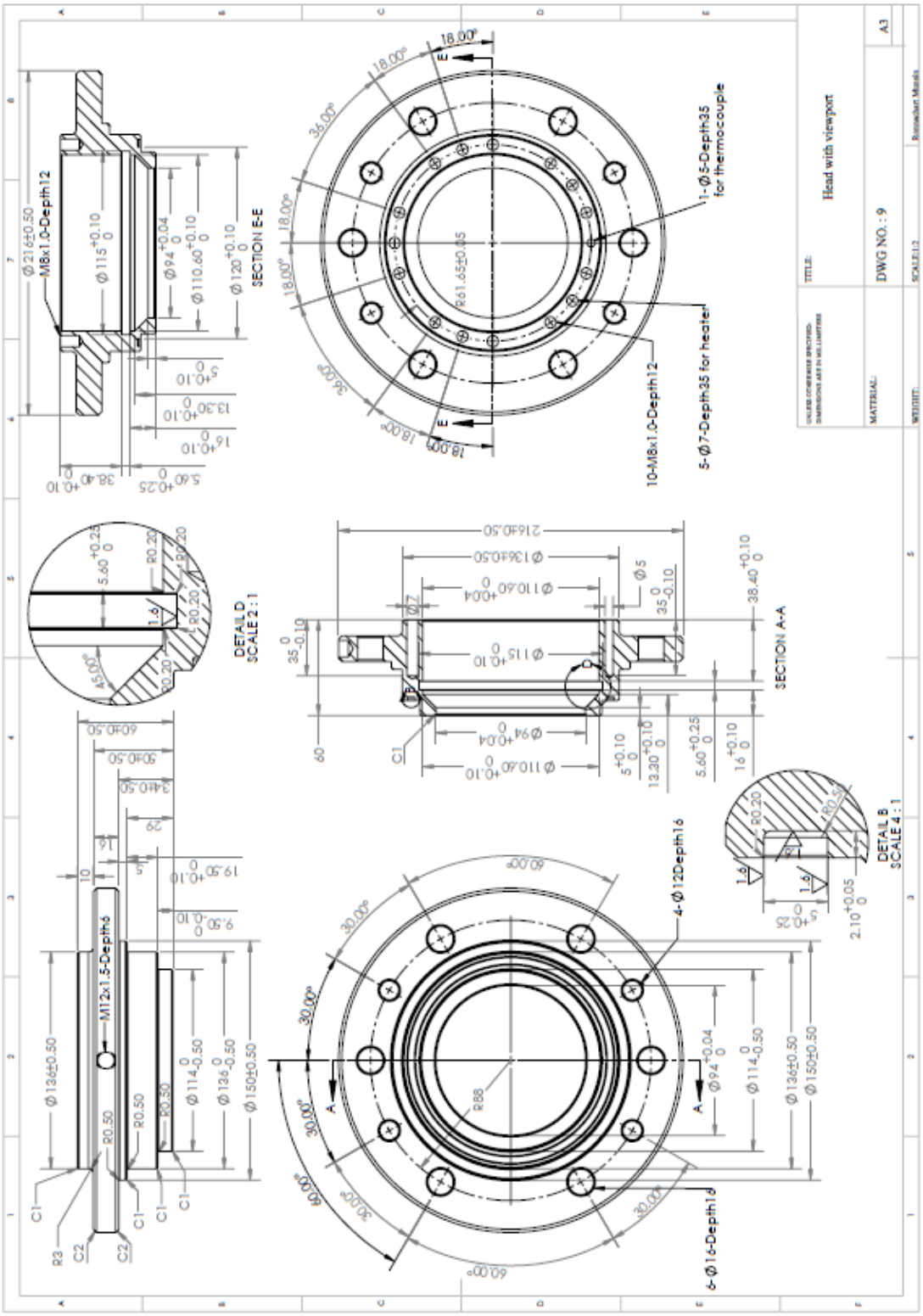

Figure A.12 Head for window (File: Head for window).

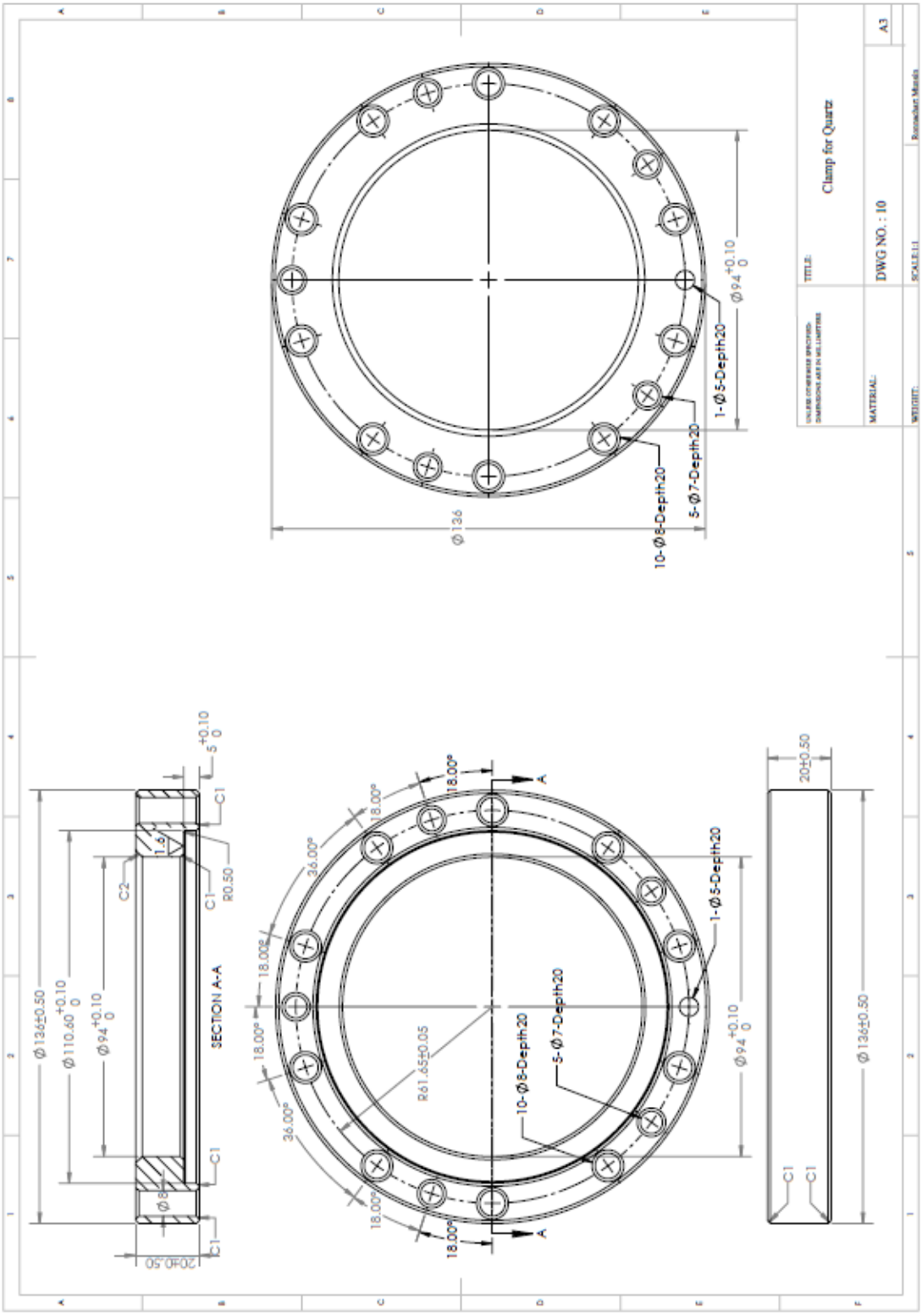

Figure A.13 Window clamp (File: Window clamp).

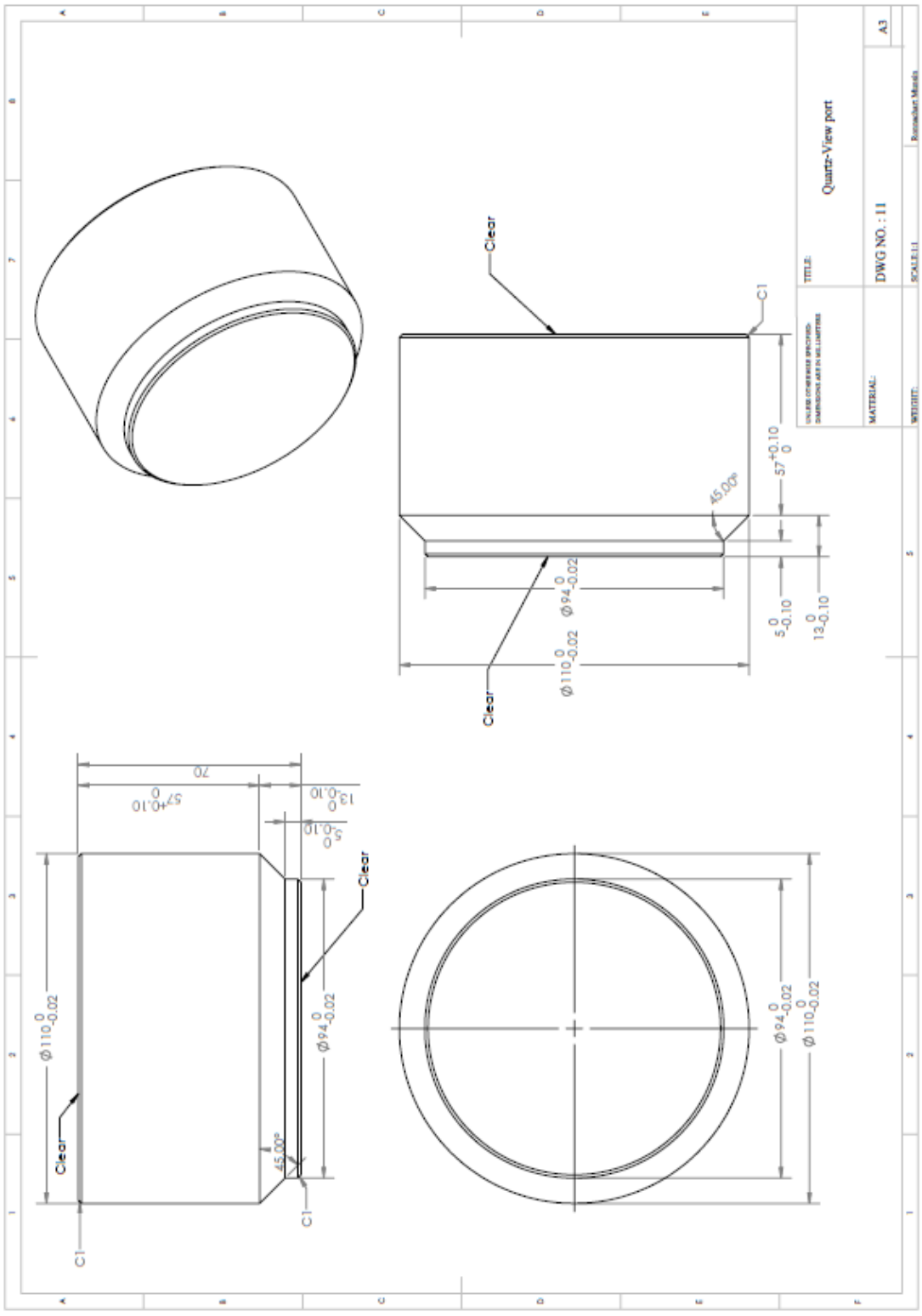

Figure A.14 Quartz window (File: Quartz window).

A.2 Wiring Diagram of Electronic Devices

Figure A.15 shows a wiring diagram of electronic devices that used for triggering a spark plug and an injector. Voltage regulator from 12 V to 5 V (IC 7805) is used for supplying voltage for the opto (PC817). PC817 is used to protect micro controller from back voltage that could be damage the micro controller. With these devices, the signal from micro controller can trigger the spark plug and electronic driving unit (EDU) through the PC817.

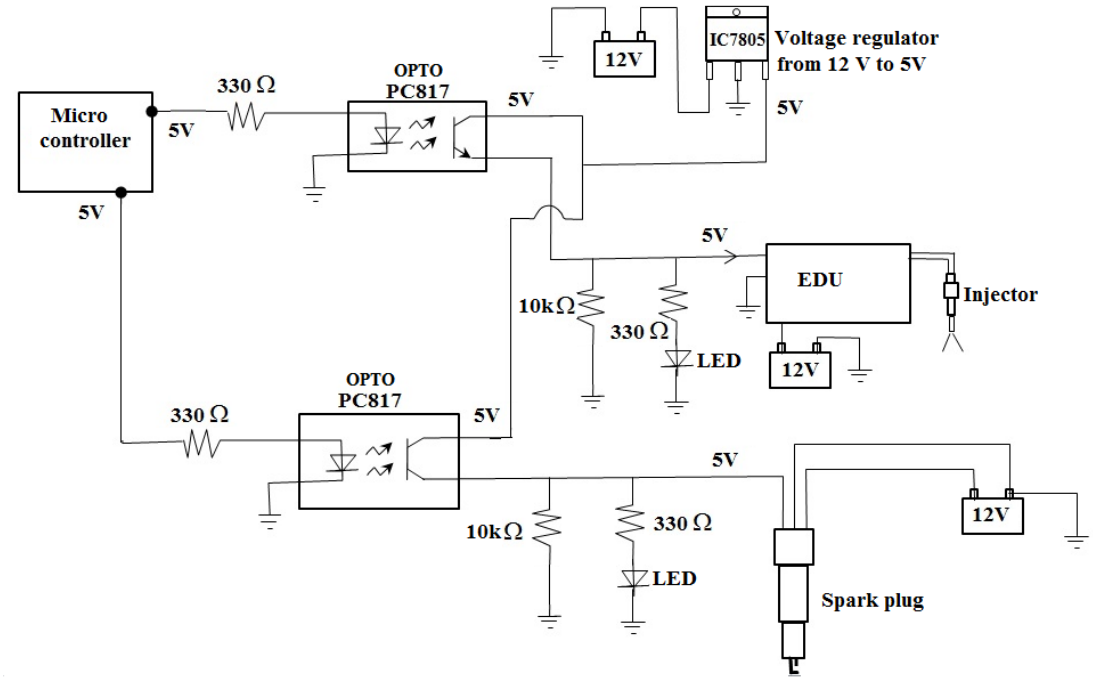

Figure A.15 Wiring diagram of electronic devices.

A.3 Programming for Injection and Combustion

Figure A.16 shows spark plug and injection signal used for programming. The micro controller with ARDUINO software is programmed following this sequence. After triggering, spark plug signal is sent to igntion coil for charging. Then, after dwell time, injection signal is generated from micro controller.

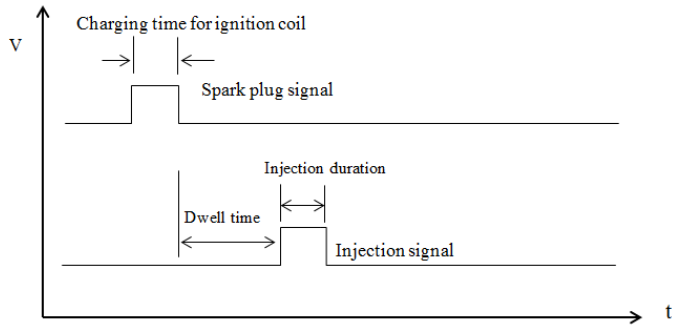

Figure A.16 Spark plug and injection signal used for programming.

The ARDUINO code used to control spark plug and injector in combustion experiment shown below.

```
#define sparkplug 8
#define injector 10
#define swt 0
int sw;
void setup()
{
  pinMode (swt,INPUT);
  pinMode (sparkplug,OUTPUT);
  pinMode (injector,OUTPUT);
}

void loop()
{
sw=digitalRead(swt);
   if(sw==0)
   {
     delay(50); // delay for switch
     digitalWrite(sparkplug,HIGH);  // sparkplug 8
     delay(3);   //This delay is the charging time for ignition coil of sparkplug in the unit of millisecond. Normally, it is in the range of 3-6ms.
     digitalWrite(sparkplug,LOW);
     delay(497);  //This delay is dwell time from spark plug LOW. This dwell time depends on cooling curve of pre-combustion of premixed gas. Dwell time of 497 ms is
```

used for temperature of 1100K, while Dwell time of 747 ms is used for temperature of 900K.

```
    digitalWrite(injector,HIGH); // Start of injection (SOI).
    delayMicroseconds(1350);  // This delay is the injection duration in the unit of microsecond.The maximum value for this command is 16383us. However, in case of time over 1000us, the command "delay" should be used.
    digitalWrite(injector,LOW); // End of injection (EOI).
  }
  else
  {
  }
}
```

A.4 Temperature of Pre-Combustion Gas

A lean combustible gas consisting of 5.1% C_2H_2, 33.75% O_2 and 61.7% N_2 at equivalence ratio 0.38 is used for making the diesel engine like-conditions by pre-combustion technique. With this technique, the high pressure and temperature products after pre-combustion are similar to the compressed air at TDC of diesel engine. Oxygen content is remained 21%mol after combustion (Baert, et al., 2009).

Figure A.17 shows pressure history during precombustion period of combustible gas consisted with different initial total pressure. It is clear that increasing initial total pressure of combustible gas increases the maximum pressure approximately 6-7 times.

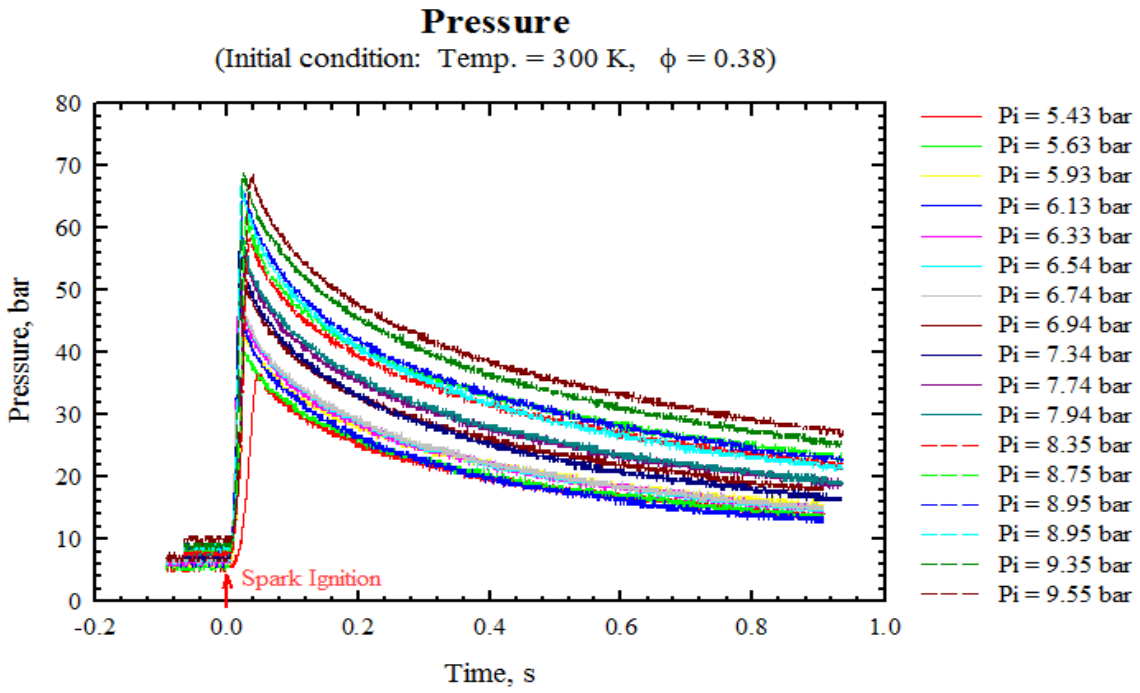

Figure A.17 Cooling curve during precombustion period at different initial total pressure.

Product gas temperature can be calculated from this pressure using the assumptions as shown in Chapter 3, section 3.5.4.

Figure A.18 shows bulk temperature of pre-combustiom at different initial total pressure calculated from pressure data in Figure A.17. Maximum temperature is slightly higher when initial pressure increase. Temperature history for the different initial pressure shows the similar trend. The target temperatures are 900 K abd 1100 K. Test fuels will be injected at these temperature. However, the cooling process should be at least

halfway before injection (Baert, et al., 2009). From Figure A.18, the cooling curve of temperature in case of initial pressure of 9.35 bar is selected to meet target temperature at leat halfway before injection. Therefore, the initial total pressure of 9.35 bar is used consistently for all experiments.

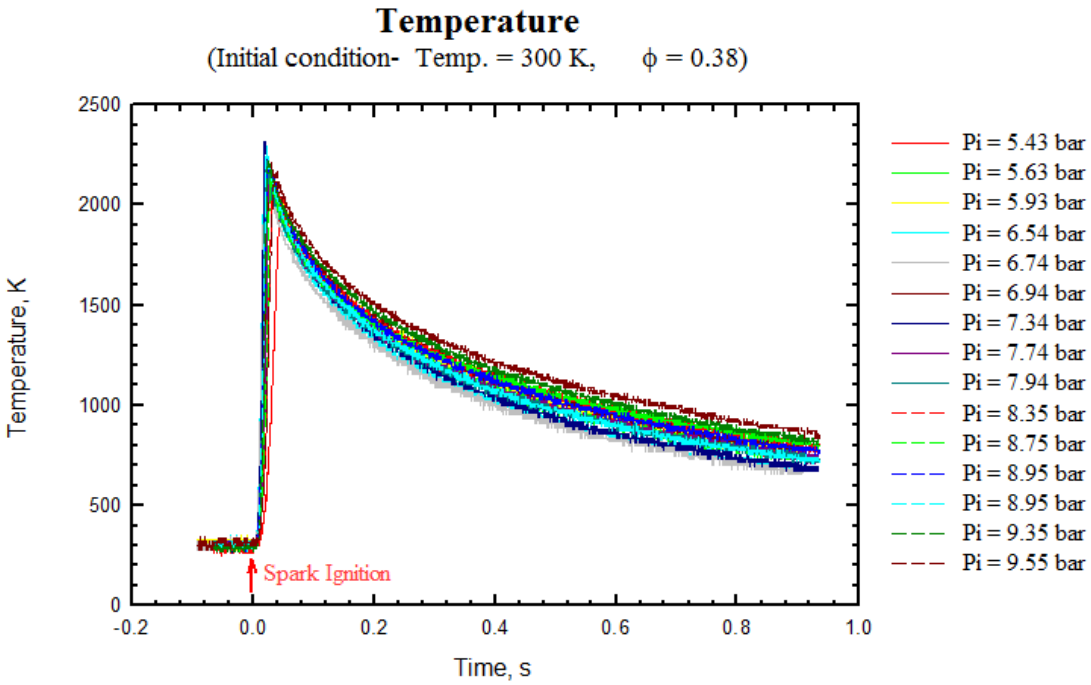

Figure A.18 Bulk temperature of pre-combustion at different initial total pressure.

A.5 The Calculation of the Compressibility of the Production Gas Compressibility Factor (Z)

This section provides the calculation of the compressibility factor of production gas. The gas compressibility factor is an essential thermodynamic property which is required for analyzing pressure and temperature behavior of various mixtures. The gas compressibility factor is considered at the production gas temperature of 800 to 1400 K where it covers the desired condition (900 K and 1100K) at start of fuel injection.

The empirial correlations used for the compressibility factor calculation, which is a function of reduced pressure (P_r) and temperature (T_r), are shown below.

(a) Heidaryan-Moghadasi-Rahimi model (Heidaryan, et al., 2010)

$$Z = ln\left(\frac{A_1+A_3 ln(P_r)+\frac{A_5}{T_r}+A_7\left(ln(P_r)\right)^2+\frac{A_9}{T_r^2}+\frac{A_{11}}{T_r}\ln(P_r)}{1+A_2\ln(P_r)+\frac{A_4}{T_r}+A_6(\ln(P_r))^2+\frac{A_8}{T_r^2}+\frac{A_{10}}{T_r}\ln(P_r)}\right) \quad \text{(A.1)}$$

Where

Z	Compressibility factor
P_r	Reduced pressure ($\frac{P}{P_{critical}}$)
T_r	Reduced temperature ($\frac{T}{T_{critical}}$)

The values of constant coefficients (A_1-A_{11}) used in equation (A.2) are provided in Table A.1.

Table A.1 Optimal coefficients of Heidaryan–Moghadasi–Rahimi model (Heidaryan, et al., 2010).

Coefficient	Value [$0.2 \le P_{pr} \le 3.0$]	Value [$3.0 < P_{pr} \le 15.0$]
A_1	$2.827793 \times 10^{+00}$	$3.252838 \times 10^{+00}$
A_2	$-4.688191 \times 10^{-01}$	$-1.306424 \times 10^{-01}$
A_3	$-1.262288 \times 10^{+00}$	$-6.449194 \times 10^{-01}$
A_4	$-1.536524 \times 10^{+00}$	$-1.518028 \times 10^{+00}$
A_5	$-4.535045 \times 10^{+00}$	$-5.391019 \times 10^{+00}$
A_6	6.895104×10^{-02}	$-1.379588 \times 10^{-02}$
A_7	1.903869×10^{-01}	6.600633×10^{-02}
A_8	6.200089×10^{-01}	6.120783×10^{-01}
A_9	$1.838479 \times 10^{+00}$	$2.317431 \times 10^{+00}$
A_{10}	4.052367×10^{-01}	1.632223×10^{-01}
A_{11}	$1.073574 \times 10^{+00}$	5.660595×10^{-01}

(b) Sanjari and Nemati Lay model (Sanjari and Nemati Lay, 2012)

$$Z = 1 + A_1 P_r + A_2 P_r^2 + \frac{A_3 P_r^{A_4}}{T_r^{A_5}} + \frac{A_6 P_r^{(A_4+1)}}{T_r^{A_7}} + \frac{A_8 P_r^{(A_4+2)}}{T_r^{(A_7+1)}} \quad \text{(A.2)}$$

The constant coefficients used in equation (A.2) are in Table A.2.

Table A.2 Tuned coefficients for Sanjari and Nemati Lay (2012) model (Sanjari and Nemati Lay, 2012).

Coefficient	Value [$0.01 < P_{pr} < 3.00$]	Value [$3.00 < P_{pr} < 15.00$]
A_1	0.007698	0.015642
A_2	0.003839	0.000701
A_3	−0.467212	2.341511
A_4	1.018801	−0.657903
A_5	3.805723	8.902112
A_6	−0.087361	−1.136000
A_7	7.138305	3.543614
A_8	0.083440	0.134041

With these models and the correlation of real gas (PV=zmRT), the comprssibility and temperature could be calculated.

Figure A.19 shows the comparison of gas temperature and compressibility factor using the different models. The compressibility factor and temperature calculated from equation A.1 and A.2 are compared with those of ideal gas law. Gas temperature increase linearly with the increase of gas pressure for all models. For pressure of 25-45 bar, the calculated temperature using ideal gas law are approximately 800 to 1400 K, while the temperature calculated from Heidaryan-Moghadasi-Rahimi model (Heidaryan, et al., 2010) and Sanjari and Nemati Lay model (Sanjari and Nemati Lay, 2012) differ from ideal gas about of 1.2- 2.7% and 0.4-1%,respectively.

The compressibility factors in the range of pressure of 25-45 bar are 1.013-1.027 and 1.004-1.009 for Heidaryan-Moghadasi-Rahimi model and Sanjari and Nemati Lay model, respectively. Increase of pressure shows the insignificant difference in the compressibility compared with each model. In addition, they are near to unity (in the case of ideal gas law).

It is clear that at the considered pressure range, the difference of the calculated temperature and compressibility factor of ideal gas and real gas calculation is very small. Therefore, to reduce the calculation time and complexity of temperature of

produciton gas, the effect of compressibility factor on gas temperature could be neglected.

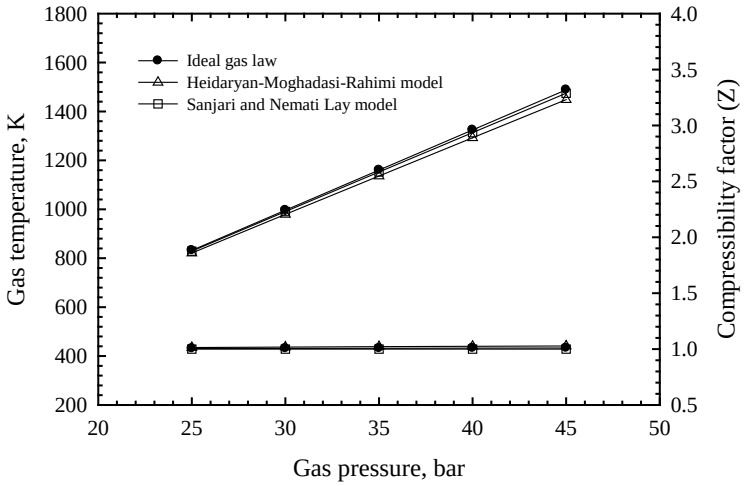

Figure A.19 Comparison of gas temperature and compressibility factor using the different models.

BIOGRAPHY

NAME Mr. Ronnchart Munsin

DATE OF BIRTH April 3, 1981

EDUCATIONAL BACKGROUND

HIGH SCHOOL Assumption College Lampang, 1998

BACHELOR'S DEGREE Bachelor of Engineering (Agricultural Engineering) Maejo University, 2003

MASTER'S DEGREE Master of Engineering (Mechanical Engineering) Chiangmai University, 2008

DOCTORAL DEGREE Doctor of Engineering (Mechanical Engineering) King Mongkut's University of Technology Thonburi, 2014

SCHOLARSHIP The Royal Golden Jubilee Ph.D. Program (Grant No. PHD/0083/2551)

PUBLICATIONS Munsin, R., Laoonual, Y., Jugjai, S. and Imai, Y., 2013, "An experimental study on performance and emissions of a small SI engine generator set fuelled by hydrous ethanol with high water contents up to 40%", **Fuel**, Vol. 106, pp. 586–592.

CONFEFRENCE Munsin, R., Laoonual, Y., Bavornsethanan, S. and Jugjai, S., 2010, "An Experimental Study on Aldehyde Emissions of a Hydrous Ethanol Fuelled Small SI Engine Generator Set", **The 1st TSME International Conference on Mechanical Engineering**, October 20-22, Ubon Ratchathani, Thailand.

Munsin, R., Laoonual, Y., Jugjai, S., Matsuki, M. and Kosaka, H., 2011, "Investigation of Effects of Ignition Improver on Ignition Delay Time of Ethanol Combustion

with Rapid Compression-Expansion Machine", **The 2nd TSME International Conference on Mechanical Engineering**, October 19-21, Krabi, Thailand.

Munsin, R., Laoonual, Y., Jugjai, S., Matsuki, M. and Kosaka, H., 2012, "Investigation of Effects of Ignition Improver on Ignition Delay Time of Ethanol Combustion with Rapid Compression and Expansion Machine", **SAE World Congress**, Apr 24-26, Michican, USA.

Munsin, R., Laoonual, Y., Jugjai, S., Matsuki, M. and Kosaka, H., 2012, "The Visualization of Flame Temperature History from Combustion of Dedicated Hydrous Ethanol under CI Engine Condition". **International Conference of Automotive Technology of Young Engineers (ICATYE)**, March 8, Tokyo, Japan.

Munsin, R., Laoonual, Y., Jugjai, S., Matsuki, M. and Kosaka, H., 2012, "The Visualization of Flame Temperature History from Combustion of Dedicated Hydrous Ethanol under CI Engine Condition", **The 8th International Conference on Automotive Engineering (ICAE-8)**, April 2-5, Bangkok, Thailand.

Munsin, R., Chung Lim Shing, B., Phunpheeranurak, K., Phongphankasem, T., Laoonual,Y., Jugjai, S. and Chanchaona, S., 2013, "Design of Constant Volume Combustion Chamber (CVCC) with Pre-Combustion Technique for Simulation of CI Engine Conditions", **The 4th TSME International Conference on Mechanical Engineering**, October 16-18, Chonburi, Thailand.

SEMINAR

Munsin, R., Laoonual, Y., Jugjai, S., Matsuki, M. and Kosaka, H., 2012, “Investigation of Effects of Ignition Improvers on Ignition Delay Time of Ethanol Combustion”, **Young Researcher Workshop on Automotive Energy and Environment**, February 15, Bangkok, Thailand.

Munsin, R., Laoonual, Y., Jugjai, S., Matsuki, M. and Kosaka, H., 2013, “Effects of Ignition Improver on Ignition Delay Time of Ethanol Combustion”, **The Royal golden Jubilee-Ph.D. Congress XIV**, April 5, Pattaya, Thailand.

Munsin, R., Laoonual, Y. and Jugjai, S., 2014, “Combustion Characteristics of Hydrous Ethanol with Ignition Improvers under CI Engine-like Conditions using Constant Volume Combustion Chamber”, **TRF Seminar Series in Basic Research: CIII - Advanced Research in Mechanical Engineering**, June 27, Bangkok, Thailand.